Préparation et caractérisation de nouveaux amphiphiles fonctionnalisés par des oligo-et polysaccharides

Alexandre Gonçalves Dal -Bó

UNIVERSITÉ DE GRENOBLE

THÈSE

Pour obtenir le grade de

DOCTEUR DE L'UNIVERSITÉ DE GRENOBLE

Spécialité : **PHYSICO-CHIMIE POLYMÈRES**

Arrêté ministériel : 7 août 2006

Présentée par

ALEXANDRE GONÇALVES DAL-BÓ

Thèse dirigée par **Dr. Redouane Borsali, Cermav,** et
Thèse dirigée par **Pr. Valdir Soldi , UFSC** et
codirigée par **Cr. Sébastien Fort Cermav**

préparée au sein du **University of Santa Catarina (UFSC) and at the Center for Development of Plant Macromolecules(Cermav)**

dans **Program in Chemistry of the Federal University of Santa Catarina and Joseph Fourier University - Grenoble Doctoral School of Chemistry and Life Sciences**

Préparation et caractérisation de nouveaux amphiphiles fonctionnalisés par oligo-et polysaccharides

Thèse soutenue publiquement le **25/04/2011**,
devant le jury composé de :

Français, Jean-Jacque Robin
Professeur, Institut Charles Gerhardt Montpellier (Rapporteur)
Français, Dr. Redouane Borsali
Directeur de Recherches, (Cermav) (Directeur de thèse)
Français, Cr. Sébastien Fort
Directeur de Recherches, (Cermav) (CoDirecteur de thèse)
Brésilienne, Pr. Nádya Pesce da Silveira
Professeur, Universidade Federal do Rio Grande do Sul (Rapporteur)
Brésilien, Pr. Valdir Soldi
Professeur,Universidade Federal de Santa Catarina (Directeur de thèse)
Brésilien, Pr. Cristiano Giacomelli
Professeur, Universidade Federal de Santa Maria (Examinateur)

THESIS

A cotutelle collaboration between

Federal University of Santa Catarina

Graduate Program in Chemistry

and

Joseph Fourier University - Grenoble

Doctoral School of Chemistry and Life Sciences

PREPARATION AND CHARACTERIZATION OF NEW AMPHIPHILES FUNCTIONALIZED WITH OLIGO- AND POLYSACCHARIDES

ALEXANDRE GONÇALVES DAL-BÓ

Jury

Pr. Jean-Jacque Robin (rapporteur)

Dr. Redouane Borsali (Directeur de thèse Cermav)

Cr. Sébastien Fort (CoDirecteur de thèse Cermav)

Pr. Nádya Pesce da Silveira (rapporteur)

Pr. Valdir Soldi (Directeur de thèse UFSC)

Pr. Cristiano Giacomelli (Examinateur)

Florianópolis,

2011

ALEXANDRE GONÇALVES DAL-BÓ

PREPARATION AND CHARACTERIZATION OF NEW AMPHIPHILES FUNCTIONALIZED WITH OLIGO- AND POLYSACCHARIDES

Thesis submitted to the Graduate Program in Chemistry of the Federal University of Santa Catarina and Joseph Fourier University - Grenoble Doctoral School of Chemistry and Life Sciences as a requirement for the obtainment of a Doctorate in Chemistry.
Focus Area: Physical Chemistry
Advisor: Dr. Valdir Soldi (UFSC)
Advisor: Dr. Redouane Borsali (Directeur de thèse Cermav)
Cr. Sébastien Fort (CoDirecteur de thèse Cermav)

Florianópolis
2011

ACKNOWLEDGEMENTS

My sincere thanks to:

My advisor Dr. Valdir Soldi for all of his dedication and knowledge transmitted, as well as for his friendship acquired during the course of my studies.

My advisors Dr. Sébastien Fort and Dr. Redouane Borsali who hosted me at CERMAV in Grenoble during part of my doctorate, to the researchers Isabelle Pignot-Paintrand, Cyrille Rochas, Jean Bruno and Sami Halila.

Dr. Fernando Giacomelli, Federal University of ABC (Greater São Paulo), for his support during the fitting of the X-ray scattering profiles obtained using SAXS.

The members of the examining board for their suggestions.

My family for all of the confidence they placed in me.

My wife Emanuela Valério Mendes.

My friends Ângelo Adolfo Ruzza, Arlindo Cristiano Felippe, Davi da Silva, Dino Zanette, Gilson Rodrigo de Miranda, Marly Da Silveira Soldi, Rogério Laus.

All of the lecturers who in one way or another contributed to my learning.
CAPES and CNPq for financial support.

The European Synchrotron Radiation Facility (ESRF) in Grenoble (France) and the National Synchrotron Light Laboratory (LNLS, Campinas, Brazil).

CONTENTS

Dal-Bó, Alexandre Gonçalves. **Preparation and characterization of New Amphiphiles with Oligo- and Polysaccharides**. Florianópolis, 2011. 97p. Doctorate Thesis in Chemistry – Graduate Program in Chemistry, Federal University of Santa Catarina and Joseph Fourier University – Grenoble, Doctoral School of Chemistry and Life Sciences.

ABSTRACT

This thesis reports the preparation and characterization of new rod-coil amphiphiles functionalized with oligo- and polysaccharides through Huisgen 1,3-dipolar cycloaddition reactions between species functionalized by an azide group on one side and an terminal alkyne on the other catalyzed by copper. The amphiphiles were synthesized and characterized based on different hydrophobic parts conjugated with the polymer poly(ethylene oxide) PEO with a hydrophilic spacer arm and the oligo- and polyssaccharides 2-propargyl-2-acetamido-2-deoxy-β-D-glucopyranose (GlcNAc) and propargyl β-D-galactopyranosyl-(1→4)-β-D-glucopyranose (Lac). The amphiphiles synthesized were characterized in terms of their chemical structure and composition through nuclear magnetic resonance (NMR), Fourier transform infrared (FTIR) spectroscopy, mass spectroscopy (MALDI-TOF-MS and ESI-MS) and high resolution mass spectroscopy (HRMS). After the dissolution in water, the amphiphiles self-associate in highly regular micelles with an average diameter of $2R_H \sim 10$ nm. Dynamic light scattering (DLS), transmission electron microscopy (TEM) and small angle x-ray scattering (SAXS) were used in order to investigate the structure and dynamics of these saccharide amphiphiles. The presence of carbohydrate epitopes on the surface of the micelles and their bioavailability for the segmentation of lectin were also demonstrated by DLS. Specific interactions of GlcNAc and Lac residues with lectins from wheat germ agglutinin (WGA) and peanut agglutinin (PNA), respectively, reveal the potential applications of such amphiphilic derivatives of carbohydrates as vectorizing systems, both simple and specific to a drug delivery site.

Résumé

Ce travail de thèse décrit la préparation et l'étude des propriétés d'auto-assemblage de nouveaux amphiphiles fonctionnalisés par des sucres. Des glycosides propargyliques du lactose et de la N-acétyl-glucosamine ont été conjugués par chimie click (cycloaddition de Huisgen catalysée par des sels de cuivre) à des dérivés de poly(ethyleneglycol) dont une des extrémités a au préalable été modifiée par une fonction azide et l'autre par un bloc hydrophobe de type polyphénylène ou bien aliphatique. Après une caractérisation par résonance magnétique nucléaire et spectrométrie de masse, les propriétés d'auto-assemblage de ces amphiphiles ont été étudiées par diffusion dynamique de la lumière (DLS), diffraction des rayons-X aux petits angles (SAXS) et microscopie électronique. Il a été montré qu'en phase aqueuse, les systèmes amphiphiles dérivés du PEG 900 s'auto-assemblent pour former de micelles de taille extrêmement régulière dont le diamètre moyen est de l'ordre de 10 nm. La présence et la biodisponibilité des sucres à la surface de ces nanoparticules ont également pu être démontrées par diffusion dynamique de la lumière avec les lectines PNA et WGA. Les interactions spécifiques observées entre les lectines et micelles associées aux propriétés d'encapsulation de ce type de nanoparticules permettent d'imaginer de futures applications pour la délivrance de médicaments ou encore l'imagerie médicale.

CHAPTER 1

INTRODUCTION AND BACKGROUND

The results reported in this thesis were obtained at the University of Santa Catarina (UFSC) and at the Center for Development of Plant Macromolecules (CERMAV), affiliated with the Joseph Fourier University in Grenoble - France.

In recent years, a considerable increase in studies on colloidal systems (soft matter) has been observed, due to a growing demand in several industrial sectors, particularly those associated with the development of nanomaterials or materials with morphological control on the nanometric scale.

The concept of nanoscience and nanotechnology has been drawing ever more attention from the public in general through electronic and printed media. More than US$ 30 million were made available by the National Science Foundation (NSF) in 2005, solely for the creation of programs to inform the public regarding nanotechnology issues, and to address socially related issues[1]

The recent surveys carried out by the European Union are sufficient to justify the high priority with which nanotechnology has been treated by developed countries and by those under rapid development, such as China and South Korea. Currently, the global investment is around US$ 4 billion per year only at the governmental level, this being distributed in an equal manner between the four entities: Japan, United States, European Union and all the other countries together. This investment, which has been growing, is fuelled by the expectation that in 10 years from now nanotechnology should be moving over US$ 1 trillion in the world economy.[2]

Finally, it is important to highlight that nanotechnology is an area with open prospects which offers innumerous opportunities to be seized and explored by countries such as Brazil. In this context, new technological opportunities need to be rapidly identified, consolidated and advanced in the construction of a solid field of knowledge.

In Brazil, the investments are still modest. However, important advances have already been made in the structuring of four national networks along with several thematic sub-networks, mobilizing more than 300 researchers and 600 graduate student nationwide with a National Nanotechnology Plan, in the modernization of the patent laws and policy of incentives, as well as the development of networks and partnerships in the business and research sectors aiming at national partnerships.

Currently, the major interest of the scientific community is to develop ever more nanoscience with the aim and promise of manipulating matter atom by atom, molecule by molecule, in order to create devices with higher performance and functionalities superior to those provided by the current technology.

The applications are very broad, ranging from the electronics industry, where nanometrically spaced aggregates are used to develop circuits and devices also on nanometric scale, to the medical-pharmaceutical industry, where the development and improvement of these systems allow the controlled release of medicines and nutrients as well as with the aim of obtaining rheological control in the cosmetic and paint industries.

Polymeric micelles prepared from rod-coil amphiphiles are of great importance since they enable the preparation of particles with different morphologies as spheres, cylinders, and vesicles, with controllable sizes, both on the micrometric (latex) and nanometric (micelles, vesicles, etc.) scales.

These structures are typically formed by a nucleus made of solvophobic blocks, and a crown of solvophilic chains. The micellar aggregates are stabilized in solution through the interaction of the soluble segments with the solvent.[3] Since most colloidal systems are normally structured in nanometric (less than 100 nm) or submicrometric (between 100 and 1000 nm) scales, their characterization can be carried out by means of transmission electron microscopy (TEM) techniques, static light scattering (SLS) and small angle x-ray scattering (SAXS). Similarly, dynamic processes can be accessed through dynamic light scattering (DLS) measurements.[4]

Nanoparticles based on hydrophobic synthetic polymers are frequently prepared in the presence of organic solvents. However, the environmental aspects and, as a consequence, the international standards, impose the elimination of these organic solvents and their replacement with water, aiming to apply them in areas such as medicine and cosmetology. Confronted with the application of these standards, the industry must consider urgently the replacement of certain traditional hydrophobic polymers, used in formulations, with natural hydrosoluble polymers such as oligo- and polysaccharides, aimed at obtaining an ideal and universal carrier system.

The development and preparation of nanoparticles based on natural molecules such as oligo- and polysaccharides currently represent a challenge in both the academic and industrial arenas.

There are still few systems which employ natural polymers in the development of nanoparticles. Examples include amphiphilic cyclodextrin nanoparticles, latex obtained by polymerization, the encapsulation of polysaccharides in capsules and the coating of dendrimers with oligosaccharides.

In this regard, the potential of these nanostructures originated from structures functionalized by oligo- and polysaccharides has been constantly explored, with the aim of developing different nanostructures which can reach and be adapted to the biological environment mimicking the significant side effects.

The functionalization of the particle surface with oligo- and polysaccharide units is one of the viable ways to transport drugs to the targets of interest and also to incorporate many different types of nutrients and essences.

In order to deepen the theme discussed above, this thesis deals mainly with the preparation and characterization of rod-coil amphiphiles with different hydrophobic parts and the use of the polymer poly(ethylene oxide) (PEO) as the hydrophilic spacer arm functionalized or not by carbohydrates, with the aim of obtaining organized structures in aqueous solvents and to evaluate the dynamic structure of these colloidal systems in the absence and presence of specific lectins.

CHAPTER 2

OBJECTIVES

2.1 General objectives

The objective of this study was to prepare and characterize new amphiphiles in order to obtain nanoparticles which will serve as a support for the binding of oligo- and polysaccharides through click chemistry reactions, of the type Huisgen 1,3 dipolar cycloaddition, between species functionalized through an azide group on one side and a terminal alkyne on the other.

2.2 Specific Objectives

- ✓ To synthesize new rod-coil amphiphiles with a hydrophobic part comprising four aromatic rings and as the hydrophilic spacer arm the polymer poly(ethylene oxide) PEO, functionalized at it extremity with the monosaccharide 2-propargyl-2-acetamido-2-deoxy-β-D-glucopyranose (GlcNAc) and the disaccharide propargyl β-D-galactopyranosyl-(1→4)-β-D-glucopyranose (Lac).
- ✓ To synthesis new rod-coil amphiphiles with the hydrophobic part containing different carboxylic acids and PEO as the hydrophilic spacer arm functionalized with the monosaccharide GlcNAc and the disaccharide Lac.
- ✓ To characterized the amphiphiles synthesized as synthetic intermediaries regarding the chemical structure and composition through nuclear magnetic resonance (NMR), Fourier transform infrared (FTIR) spectroscopy, mass spectroscopy (MALDI-TOF-MS and ESI-MS) and high resolution mass spectroscopy (HRMS).
- ✓ To determine the critical micellar concentration by fluorescence spectroscopy.
- ✓ To prepare and characterize nanoparticles (micelles) from the amphiphiles synthesized with the aim of obtaining a good size distribution.
- ✓ To analyze the morphology of the nanoparticles obtained, through the techniques of transmission electron microscopy (TEM) and small angle x-ray scattering (SAXS).
- ✓ To determine parameters such as the gyration radius and dynamic properties of self-aggregation, among others, through the techniques of static and dynamic light scattering.

- ✓ To evaluate the capacity of the different nanoparticle formulations which will serve as supports for the bonding of oligo- and polysaccharides by way of specific interactions with lectins.

CHAPTER 3

LITERATURE REVIEW

3.1 Nanotechnology and nanoscience

Nanotechnology and nanoscience are currently considered one of the most fascinating advances in the areas of knowledge and constitute one of the main focal points of research, development and innovation activities in all industrialized countries.[5]

Many consider the initial point of nanotechnology, the lecture given in 1959 by Richard Feynman - Nobel laureate in physics (1965) – in which he suggested that one day it would be possible to manipulate atoms individually, a revolutionary idea for the time.[6] The prediction of Feynman, however, would only become reality in the 1980s with the development of the so-called scanning probe microscopies. These microscopes map objects of nanometric dimensions by way of a very fine needle (probe), building an image with atomic scale resolution. This device made it possible to individually manipulate atoms, the smallest possible unit of a chemical element.

Nanotechnology already has applications in almost all industrial and service sectors. These can be on a large scale, such as polymeric nanocomposites produced from commodities such as thermoplastics and clays, together with products manufactured in reduced quantities but with high added value and created for information and telecommunications technologies. It has been estimated that from 2010 to 2015 the world market for materials, products and processes based on nanotechnology will be one trillion dollars.[7]

Nano is the prefix used in scientific notation to express a billionth (10^{-9}). One nanometer (nm), for example, is equivalent to 10^{-9} m, that is, a billionth of a meter. At this scale, a miniscule virus, invisible to the naked eye, appears as an incredible entity with around 200 nm. Despite this tiny dimension, it camouflages, in fact, a complex molecular machine equipped with all of the devices required to invade the cells of higher organisms and use them in their reproduction, resulting in a typical example of nanotechnology placed in practice by nature.[2]

3.2 A brief report on nanoparticles

From the technological point of view, nanoparticles can be chemically altered through the modification of their surfaces with specific molecules or polymers, which broadens considerably their applications. For instance, nanoparticles can be used in chemical or biological sensors, simply by modifying them with species which recognize other complementary groups, as in the case of the antigen-antibody interaction, which occurs in the immune system.[2]

The polymeric nanoparticles are carriers on a nanometric scale (with a diameter of less than 1µm) prepared from natural or synthetic polymers and have been the object of several studies for over 20 years, evolving during this period. This definition does not take into account the morphological and structural changes in the organization of the polymer.

The surface characteristics of nanoparticles have an important influence on the interaction with their biological environment. In the past decade, interest has intensified in the development of polymers and block copolymers with amphiphilic characteristics (in which sugars, peptides, folic acid, antibodies and medicines can be bound or associated in some form with the polymer) allowing the use of nanoparticles as carrier systems directed toward specific targets and as diagnostic tools.[8-10]

3.3 Functionalization of nanoparticle surface

The surface characteristics of nanoparticles have an important influence on the interaction with their biological environment. In the past decade, interest has intensified in the development of polymers and block copolymers with amphiphilic characteristics (in which sugars, peptides, folic acid, antibodies and medicines can be bound or associated in some form with the polymer) allowing the use of nanoparticles as carrier systems directed toward specific targets and as diagnostic tools.[11-13]

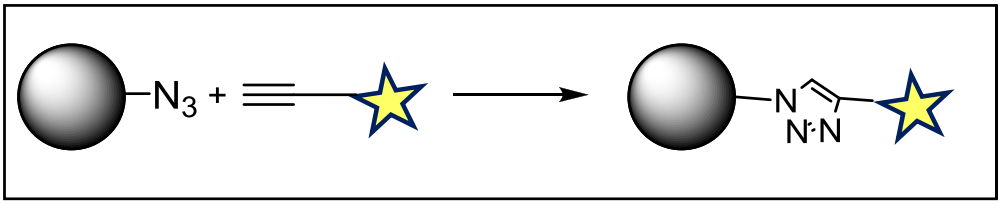

Figure 1. Functionalization of nanoparticles through covalent bonding

The functionalization of block copolymers and rod-coil amphiphiles is carried out through several types of interactions or reactions. The search for the intelligent functionalization of amphiphiles and copolymers to efficiently anchor probes able to mimic biological systems and provide cellular recognition sites, through covalent bonds, has been intensified.

The challenges related to intelligent functionalization have lead to the development of more selective "chemical bonding" in the covalent coupling of functional groups under mild aqueous conditions.[14] Few methods have as yet been applied to the chemical coupling of biomolecules in nanoparticles. Of these methods, amino-acid coupling is one of the most commonly applied worldwide, with an efficient reaction. For example, folic acid, which has a carboxylic acid group, has been conjugated with nanoparticles coated at their extremities with NH_2 groups.

Such nanoparticles have been prepared by polymerization *in situ* by functionalized comonomers with amines or for the synthesis of amphiphilic copolymers which serve as surfactants and surface modifiers in a nanoprecipitation technique.[15] The folic acid was then successfully conjugated on the nanoparticle surface using N,N'-dicyclohexylcarbodiimide (DCC).

Furthermore, the introduction of thiol groups to the nanoparticle surface creates endless possibilities for ligand conjugations, particularly in conjugation reactions between thiol maleimides (thiol-maleimide couplings), due to their selectivity and reactivity under mild conditions, and has received growing interest. The conjugation of antibodies or protein is generally carried out using crosslinking with m-maleimidobenzoyl-N-hydroxysuccinimide ester **(**MBS) which offers two binding sites: one primary amine group (present in antibodies, medicines and specific peptides) and a thiol function.[16] These coupling reactions have been reported to be quantitative under physiological conditions.[17-19]

The search for more efficient bonds and satisfactory quantitative yields in the anchoring of bioactive molecules gained a boost with the Huisgen 1,3-dipolar cycloaddition reactions between species functionalized by an azide group on one side and a terminal alkyne on the other catalyzed by copper. The basic reaction, which today is summarized under the name of "click chemistry" is a variant of the Huisgen 1,3-dipolar cycloaddition reaction between triple C-C and triple C-N bonds, and alkyl/aryl/azides (see Figure 2).

In the cycloaddition reaction, a cyclic compound is obtained from two unsaturated molecules. In the cyclo-formation reaction two new σ bonds are formed through two π bonds

(dipolar [4+2]). In this reaction a dipole, a 1,3-dipolar octet, reacts with a dipolarophile, a system with multiple bonds.

The azide/alkyne click chemistry reaction is a recently rediscovered reaction which fulfils many requirements for the affixation of ligands in the post-process modification of polymers, which frequently include quantitative yields, a high tolerance to functional groups, and an insensitivity of this reaction to solvents, regardless of their protic, aprotic, polar or non-polar nature. The reactions occur at several types of interfaces, such as solid/liquid, liquid/liquid, or even solid/solid. This review focuses on issues related to the reaction itself, as well as on the requests for a broadening of the sciences of polymers, materials and surfaces.

These reactions are included within a series of reactions known as click reactions, which are defined as involving a gain in thermodynamic enthalpy of at least 20 kcal/mol, leading to reactions characterized by high yields, simple reaction conditions, fast reaction times and high selectivity. Among the many reactions tested, the 1,3-dipolar cycloaddition process has appeared as a method of choice since it satisfies the requirements of the binding of two molecules in a fast and efficient process.

The wide application of click chemistry-type reactions occurred after the important discovery that the Huisgen process is purely thermal and can be considerably accelerated by the addition of various metal species (Ru, Ni, Pt, Pd), but mainly by Cu (I) species, within the reaction system.[20]

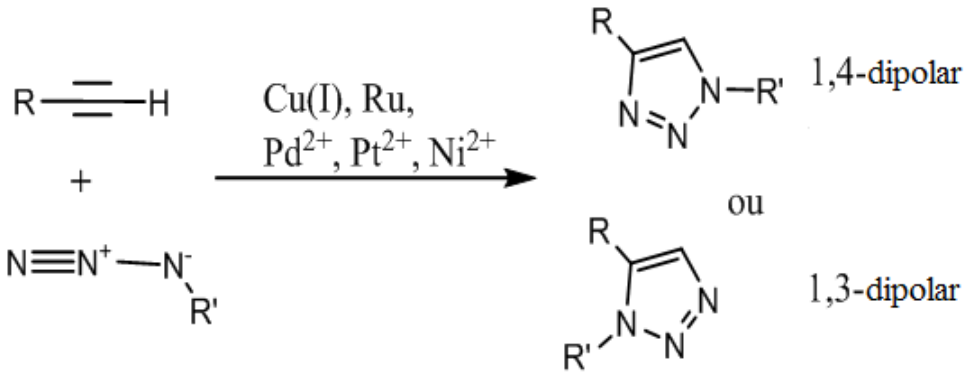

Figure 2. Illustration of the 1,4 and 1,3-dipolar cycloadditions catalyzed by different metal salts.

The selection of the appropriate technique for the modification of the surface of the nanoparticles and biomolecules is therefore crucial. It should be noted that the analysis of the biological recognition is, however, necessary in order to test the bioavailability of the molecules.

3.4 Functionalization of the macromolecule surface with specific probes.

The first group is composed of bioactive macromolecules (such as polysaccharides, oligopeptides), which do not specifically interact with the tissues. Of these, polysaccharides are of great interest particularly to obtain nanoparticles with bioadhesive and mucoadhesive properties. Thus, polysaccharide nanoparticles have been modified on the surface, such as chitosan, hyaluronic acid and dextran.[21, 22] Nanoparticles coated with dextran that presented a prolonged permanence time in the blood, which depends not only on their dimension but also on the coating properties, can be cited. Furthermore, this type of nanoparticle coated with dextran allows the segmentation of specific tissues, such as lymphatic ganglia or brain tumours.[9]

The coating of nanoparticles with chitosan is of great interest, particularly in the cumulative properties of mucoadhesion and increased permeability, without causing any irreversible damage to the membrane. Moreover, the nanoparticles coated with chitosan also interact with nucleic acids (DNA oligonucleotides).[22]

The combination of soluble polymeric nanoparticles functionalized with hyaluronic acid can allow the obtainment of an efficient carrier system for the preparation of a series of eye drops, prolonging the ocular residence time. [23, 24]

Finally, considering the great variety of polysaccharides in nature, there is the potential for the preparation of engineered nanoparticle surfaces presenting a specific surface adapted to the segmentation effect.

In order to increase the rapid capture of nanoparticles by the reticuloendothelial system (RES) and considerably increase the blood circulation, researchers opt to coat these nanoparticles with PEO, dextran or heparin.[11, 25-27]

The development of organized nanostructures based on carbohydrates in recent years has intensified with the interest in biomimetics or environmental preservation and the valuing of natural resources. The difficulties associated with the chemical modification of oligo- and polysaccharides in terms of solubility and selectivity have facilitated the generalized use of monosaccharides and disaccharides which only partially reflect the potential of polysaccharides. Consequently, there are many possibilities that amphiphilic oligosaccharides can generate organized structures on the nanometric scale.

One of the greatest challenges is to define the ideal vector of molecules and ligands for the specific delivery of nanoparticles to the target tissue. The strategy depends on the

segmentation capacity of the probes to bind specifically to the receptors of the cell surface and thus the nanoparticles will reach specifically the target cells. In order to overcome these difficulties associated with the modifications and solubility a variety of specific ligands, such as mono- or oligosaccharides, biotin, folic acid, and antibodies, are commonly used and anchored to block copolymers and amphiphiles through electrostatic interactions, hydrophobic interactions and covalent bonds. Figure 3 illustrates a variety of specific ligands which are generally used as bioactive probes for the functionalization of the surface of nanoparticles. Of these, mono- or oligosaccharides are of special interest. In fact, on the cell surface, carbohydrates, glycoproteins and glycolipids function as recognition sites between cells and microorganisms.[28, 29]

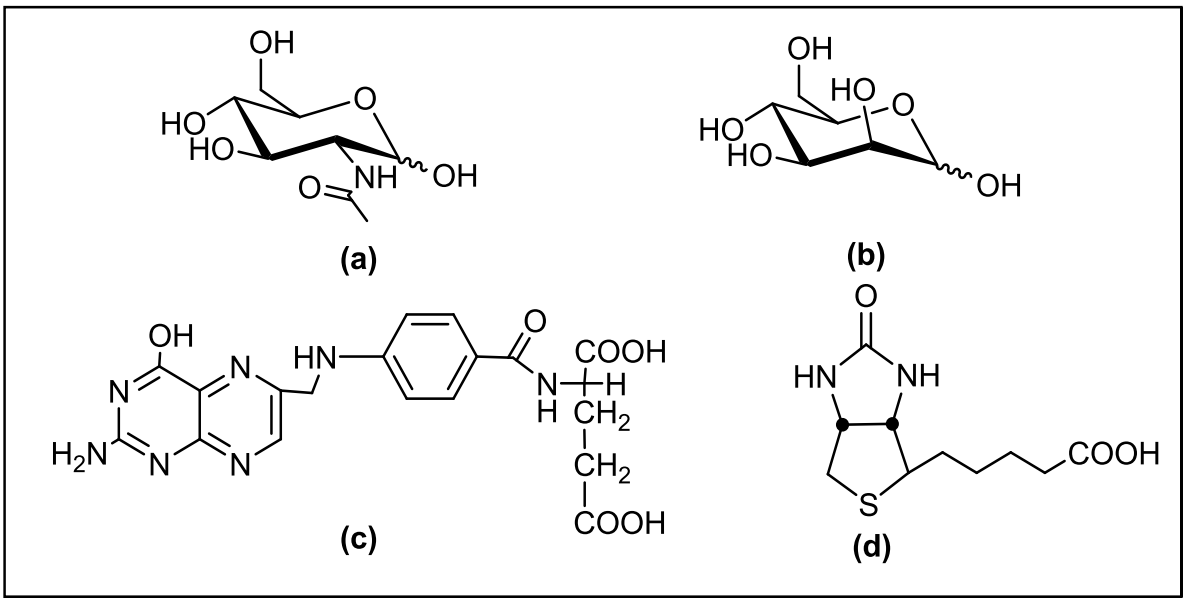

Figure 3. Illustration of some structures which can be used as biological probes (ligand type) for the functionalization of nanoparticles: **(a)** N-acetyl-D-glucosamine (GlcNAc), **(b)** mannose, **(c)** folic acid and **(d)** biotin.

3.5 Lectins

Lectins represent a structurally heterogeneous group of multivalent proteins which bind specifically and recognize sugar complexes bound to proteins, lipids and functionalized amphiphiles.[30-33] There are many different families of lectins with varied structures and specificities. Although originally isolated from plant sources, they have been found in different life forms such as animals, bacteria and viruses.[34] Their abundance and the relative

facility of purification have enabled lectins to be extensively characterized and widely used in different areas of biology, biochemistry and pharmaceutics.

Despite their abundance in many plants, the true function of plant lectins has not been clearly defined. Among those proposed are the storage and transport of carbohydrates in seeds, the inhibition of the growth of fungi and insecticidal activity.[35, 36]

Lectins are currently attracting great interest from researchers in several areas, such as biology and medicine, due to the fact that they bind specifically to carbohydrates and act as mediators of cellular recognition in a variety of systems.[37] Each molecule of lectin normally contains two or more recognition sites, that is, they are di- or polyvalent. Thus, when they react with cells, for example, erythrocytes, they not only combine with the sugars on their surfaces, but also carry out the crosslinking of cells with their subsequent precipitation, a phenomenon known as cell agglutination. An important attribute is hemagglutination, used routinely for their detection and the characterization of biological functions. Since then lectins have be found in an increasing number of applications, in the separation and characterization of glycoproteins and glycopeptides, in the monitoring of changes in the cell surface during physiological processes and pathologies, in the differentiation of cancer cells and in the labeling of blood cells and bacteria, among others. [38]

Currently, an important area of interest is in the obtainment of molecules which have self-association with different morphologies for the encapsulation of drugs in nano- and microparticle systems containing lectins for the treatment of infectious diseases which affect a large part of the world population, such as malignant neoplasm, tuberculosis and viruses.

3.6 Interaction of amphiphiles functionalized by oligo- and polysaccharides with lectins

In recent decades, the focus has shifted from self-associations and interactions between ionic surfactants and polymers to amphiphiles or block copolymers functionalized with oligo-and polysaccharides, oligopeptides or bioactive probes, in order to study these colloidal systems in the presence and absence of specific lectins.[39, 40]

The mechanisms of recognition are essentially based on specific interactions between carbohydrates and soluble or membrane proteins called lectins. The network of communication based on carbohydrate-protein interactions is crucial to a variety of important biological phenomena such as cell growth, inflammation, cancer and viral/bacterial infections.

Based on these specific lectin-carbohydrate interactions, several glycomimetics have been developed with diagnostic and therapeutic aims.[31-33, 41, 42]

In particular, drug delivery mediated by a carbohydrate allows cells which have glycoreceptors in their plasma membranes to be reached. This type of targeting of active principles is considered as one of the more promising pathways of specific cell targeting. In fact, the lectin membranes of some types of cells are able to internalize their ligands and, consequently, the glycoconjugates that are recognized by these lectins which can be used as efficient carriers of nutrients and active principles.[42, 43]

Although the properties of the surface of amphiphilic glycosides have been extensively studied, few reports discuss the use of the saccharide part for the segmentation of specific receptors. Lee *et al*. were able to demonstrate that the structures of amphiphiles functionalized with mannose self-associated in different morphologies and interact with the lectin ConA and with the type 1 pilus receptors of the bacteria *Escherichia coli*, also called mannose-sensitive because they adhere to the mannose receptors.[41, 44, 45]

The synthesis and characterization of carbohydrate glycoconjugates with the insertion of hydrophobic hydrocarbons was described by Thomas and coworkers who demonstrated the spontaneous self-association of these surfactants in vesicles which served as a model to investigate the protein-carbohydrate interactions and the aggregation of these surfactants was also induced by protein ConA.[46]

Rieger and coworkers reported the synthesis of a series of block copolymers of the type poly(ethylene oxide)-*b*-poly(-caprolactone) PEO-*b*-PCL which were functionalized with the carbohydrate mannose and the self-association, and the specific interaction of these nanoparticles with the lectin BclA produced by the bacteria *E. coli*. was studied by isothermal titration calorimetry (ITC) and cryo-TEM. [47, 48]

Nanoparticles based on metals have recently attracted great interest as new materials and lead to new applications in biological systems, mainly those functionalized by carbohydrates which can be recognized by specific proteins and can be easily detected, having an intense color in the visible region.[49, 50]

Lin *et al*. developed gold nanoparticles functionalized with the carbohydrate mannose and studied the selective binding of these nanoparticles with the type 1 pili of the enterobacteria *E. Coli.* through TEM and Biacore experiments.[51]

The architecture of rod-coil amphiphiles with bioactive functions is illustrated in Figure 4, where these structures can be associated with different morphologies, depending on

their hydrophobic fraction and the preparation method. Nanostructures functionalized with carbohydrates, peptides, folic acid and biotin can be used in diverse bioapplications from drug and nutrient release to the development of new vaccines.

In this regards, various oligosaccharide structures are studied as a function of the properties of nanoparticles. Mannoside, galactoside or rhamnoside structures have been used as a way to vectorize the particles in specific receptors in the lungs, liver or epidermal cells, and in the controlled release of drugs and nutrients. [41, 52-55]

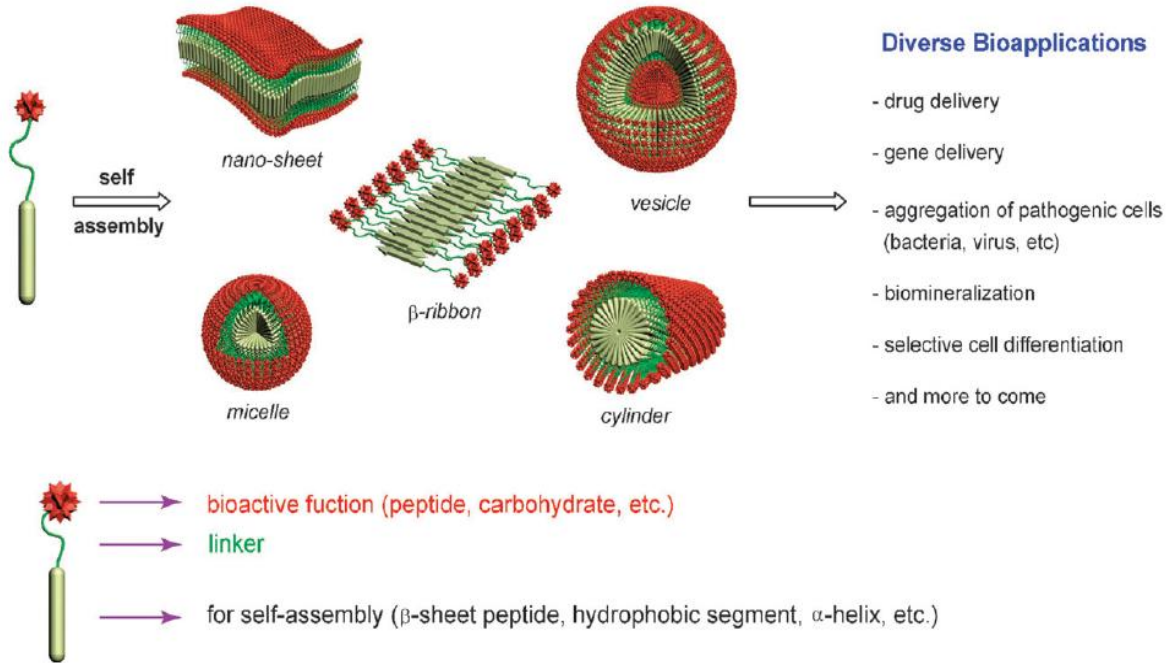

Figure 4. Illustration of self-association of bioactive nutrients.[56]

Figure 5 shows the formation of vesicular nanoparticles coated with units of the carbohydrate mannose and also an internal reservoir coated with units of the same carbohydrate, thus enabling the incorporation of hydrophilic medicines, proteins, vaccines and molecules for release at specific targets, such as the lymphatic system and brain, when these particles interact specifically with enterobacteria *E. Coli* type 1 pili.[45]

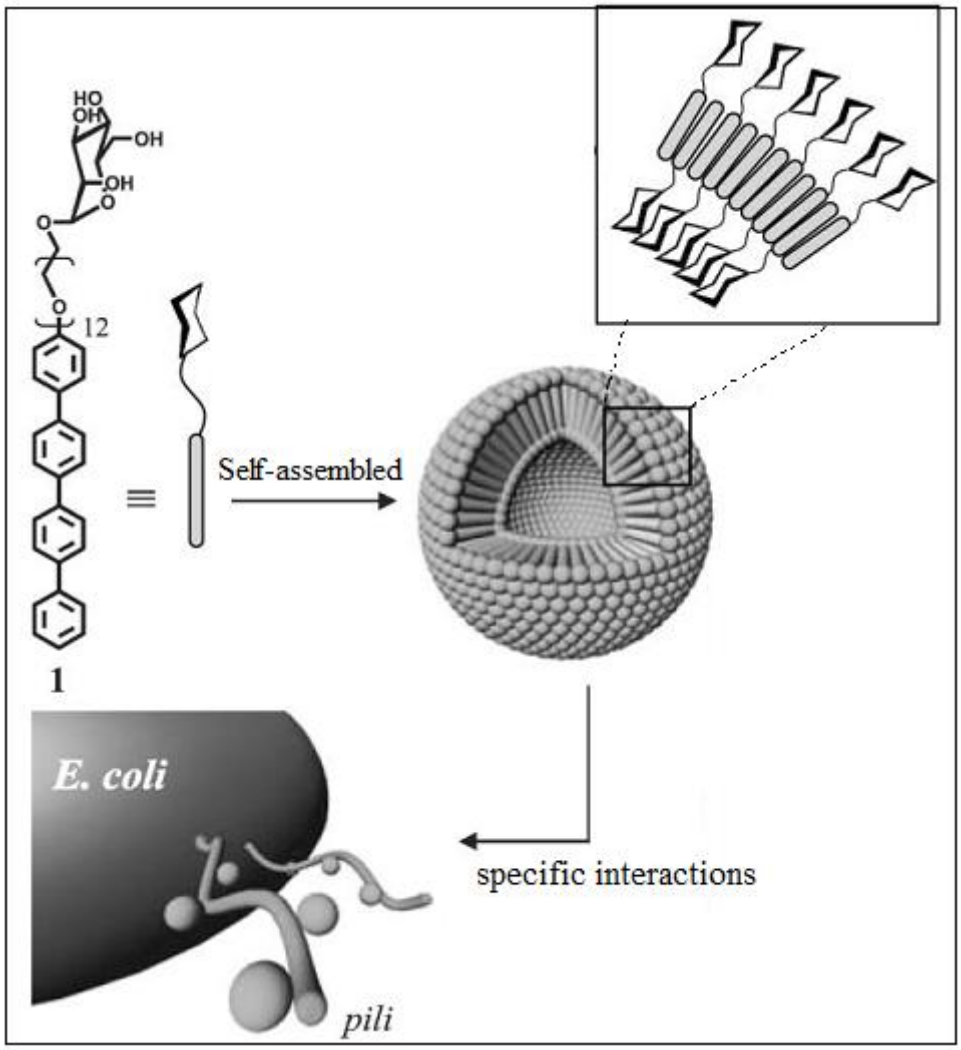

Figure 5. Schematic representation of interaction of nanoparticles coated with the monosaccharide mannose with type 1 pilus receptors found in the bacteria *Escherichia Coli*.[45]

REFERENCES

1. Lovinger, A.J., *Polymer research in an area of prefixes.* Polym. Rev, 2005. **45**(3): p. 195-199.
2. Toma, H.E. and K. Araki, Ciência Hoje, 2005. **37**(217): p. 24-31.
3. Hamley, I.W., John Wiley: New York, 2006.
4. Giacomelli, F.C. and N.P. da Silveira, Centro de Nanociência e Nanotecnologia (CNCTCNANO). *Tópicos em Nanociência e Nanotecnologia*. 1. Ed. Porto Alegre, 2008. **1**: p. 93-106.
5. Pires, T.C., *Parcerias Estratégias/Centro de Estudos Estratégicos*. 2004: Brasilia.
6. Feynman, R., *There's plenty of room at the bottom.* Annual Meeting of the Americam Physical Society, 20 dez 1959. California Institute of Technology (Caltech). Eng Sci. California: Caltech, fev 1960..
7. NSTC, *National Science and Tecnhology Council (NSTC).* Nanotechnology Research Directions; WGN Workshop Report, Washington, 1999.
8. Ruoslathi, E. and M.D. Piersbacher, *Science*, 1987. ***238***: p. 491-497.
9. Brigger, I., C. Dubernet, and P. Couvreur, Advanced Drug Delivery Reviews, 2002. **54**(5): p. 631-651.
10. Brannon-Peppas, L. and J.O. Blanchette, Advanced Drug Delivery Reviews, 2004. **56**(11): p. 1649-1659.
11. Gref, R., et al., Science, 1994. **263**(5153): p. 1600-1603.
12. Allen, T.M. and P.R. Cullis, Science, 2004. **303**(5665): p. 1818-1822.
13. Torchilin, V.P., Journal of Microencapsulation, 1998. **15**(1): p. 1-19.
14. Lemieux, G.A. and C.R. Bertozzi, Trends in Biotechnology, 1998. **16**(12): p. 506-513.
15. Stella, B., et al., Journal of Pharmaceutical Sciences, 2000. **89**(11): p. 1452-1464.
16. Jiang, F.N., et al., Journal of Immunological Methods, 1990. **134**(1): p. 139-149.
17. Gaucher, G., et al., Journal of Controlled Release, 2005. **109**(1-3): p. 169-188.
18. Langer, K., et al., European Journal of Pharmaceutics and Biopharmaceutics, 2000. **49**(3): p. 303-307.
19. Nobs, L., et al., International Journal of Pharmaceutics, 2003. **250**(2): p. 327-337.
20. Tornoe, C.W., C. Christensen, and M. Meldal, Journal of Organic Chemistry, 2002. **67**(9): p. 3057-3064.
21. Yamamoto, H., et al., Journal of controlled Release, 2005. **102**(2): p. 373-381.
22. Lemarchand, C., R. Gref, and P. Couvreur, European Journal of Pharmaceutics and Biopharmaceutics, 2004. **58**(2): p. 327-341.
23. Langer, K., et al., International Journal of Pharmaceutics, 1997. **158**(2): p. 219-231.

24. Langer, K., et al., *M* International Journal of Pharmaceutics, 1997. **158**(2): p. 211-217.
25. Mornet, S., et al., Journal of Materials Chemistry, 2004. **14**(14): p. 2161-2175.
26. Kabanov, A.V. and S.V. Vinogradov, Angewandte Chemie International Edition, 2009. **48**(30): p. 5418-5429.
27. Zalipsky, S., Bioconjugate Chemistry, 1995. **6**(2): p. 150-165.
28. Jones, M.N., Advanced Drug Delivery Reviews, 1994. **13**(3): p. 215-249.
29. Jelinek, R. and S. Kolusheva, Chemical Reviews, 2004. **104**(12): p. 5987-6015.
30. Sharon, N., Trends in Biochemical Sciences, 1993. **18**(6): p. 221-226.
31. Lis, H. and N. Sharon, Chemical Reviews, 1998. **98**(2): p. 637-674.
32. Vijayan, M. and N. Chandra, Current Opinion in Structural Biology, 1999. **9**(6): p. 707-714.
33. Loris, R., Biochimica Et Biophysica Acta-General Subjects, 2002. **1572**(2-3): p. 198-208.
34. Bies, C., C.M. Lehr, and J.F. Woodley, Advanced Drug Delivery Reviews, 2004. **56**(4): p. 425-435.
35. Trigueros, V., et al., Biochimica Et Biophysica Acta-General Subjects, 2003. **1621**(3): p. 292-298.
36. Sharon, N. and H. Lis, Science, 1989. **246**(4927): p. 227-234.
37. Tavares, G.A., et al., Acta Crystallographica Section D-Biological Crystallography, 1996. **52**: p. 1046-1047.
38. Sharon, N. and H. Lis, Faseb Journal, 1990. **4**(14): p. 3198-3208.
39. Neumann, D., et al., Advanced Drug Delivery Reviews, 2004. **56**(4): p. 437-457.
40. Neumann, D., et al., European Journal of Biochemistry, 2002. **269**(5): p. 1518-1524.
41. Kim, B.S., et al., Journal of the American Chemical Society, 2005. **127**(46): p. 16333-16337.
42. Smart, J.D., et al., European Journal of Pharmaceutical Sciences, 1999. **9**(1): p. 93-98.
43. Varki, A., *T.* Glycobiology, 1993. **3**(2): p. 97-130.
44. Lim, Y. and M. Lee, Organic & Biomolecular Chemistry, 2007. **5**(3): p. 401-405.
45. Kim, B.S., et al., Chemical Communications, 2005(15): p. 2035-2037.
46. Thomas, G.B., et al., Journal of the American Chemical Society, 2009. **131**(15): p. 5471-5477.
47. Rieger, J., et al., Biomacromolecules, 2009. **10**(3): p. 651-657.
48. Rieger, J., et al., Biomacromolecules, 2007. **8**(9): p. 2717-2725.

49. Niemeyer, C.M., Angewandte Chemie-International Edition, 2001. **40**(22): p. 4128-4158.
50. Niemeyer, C.M. and B. Ceyhan,. Angewandte Chemie-International Edition, 2001. **40**(19): p. 3685-+.
51. Lin, C.C., et al., Journal of the American Chemical Society, 2002. **124**(14): p. 3508-3509.
52. Gabizon, R., et al., Proceedings of the National Academy of Sciences of the United States of America, 1988. **85**(18): p. 6617-6621.
53. Ikehara, Y., et al.,. Cancer Research, 2006. **66**(17): p. 8740-8748.
54. Barragan-Montero, V., et al.,. European Journal of Medicinal Chemistry, 2005. **40**(10): p. 1022-1029.
55. Mauk, M.R., R.C. Gamble, and J.D. Baldeschwieler,. Proceedings of the National Academy of Sciences of the United States of America-Biological Sciences, 1980. **77**(8): p. 4430-4434.
56. Lim, Y.-b., K.-S. Moon, and M. Lee. Chem Soc Rev, 2009. **38**(4): p. 925-34.

CHAPTER 4

RESULTS AND DISCUSSION

Cite this: Soft Matter, 2011, 7, 3453-3461
Cite this: DOI: 10.1039/c0sm01411g

Self-assembled carbohydrate-based micelles for lectin targeting

Alexandre G. Dal Bó, [†,‡] *Valdir Soldi,*[‡] *Fernando C. Giacomelli,*[§] *Bruno Jean,* [†] *Isabelle Pignot-Paintrand,* [†] *Redouane Borsali,* [†] *and Sébastien Fort* [†,*]

[†]Centre de Recherches sur les Macromolécules Végétales (CERMAV-CNRS), BP 53, F-38041 Grenoble Cedex 9, France (affiliated with Université Joseph Fourier Grenoble 1 and member of the Institut de Chimie Moléculaire de Grenoble) ;

[‡]Departamento de Química, Universidade Federal de Santa Catarina, 88040-900 Florianópolis – SC, Brazil;

[§]Centro de Ciências Naturais e Humanas, Universidade Federal do ABC, 09210-170 Santo André – SP, Brazil;

*Corresponding author: Sebastien Fort

e-mail. sebastien.fort@cermav.cnrs.fr

Tel. +33 (0)4 76 03 76 64

Fax. +33 (0)4 76 54 72 03

Abstract

Biocompatible low-polydispersity micelles designed for lectin targeting have been prepared by spontaneous self-assembly in water of macromolecular glycosylated amphiphiles. Propargyl-β-lactoside and *N*-acetyl-β-D-glucosaminide were conjugated by copper-catalyzed Huisgen cycloaddition to azide-terminated PEG900 stearate. Upon dissolution in water, the resulting amphiphiles immediately self-assemble into highly regular micelles having a mean diameter of 10 nm. Dynamic Light Scattering (DLS), Transmission Electron Microscopy (TEM) and Small-Angle X-ray scattering (SAXS) were used to investigate the structure of the self-assembled saccharidic amphiphiles micelles. The presence of the carbohydrate epitopes on the surface of the micelles and their bioavailability for lectin targeting were also demonstrated by light scattering measurements. Specific interaction of the GlcNac and Lac residues with Wheat Germ Agglutinin (WGA) and Peanut Agglutinin (PNA) respectively, unveils potential applications of such carbohydrate-derived surfactants as simple and site-specific vectorization systems for drug delivery.

Introduction

Hierarchical self-assembly of synthetic molecules is a subject of great current interest and a challenging topic of interdisciplinary research in chemistry, biology, and materials science. Amphiphilic molecules, namely those that carry both hydrophilic and hydrophobic parts within one structure self-assemble into a variety of supramolecular objects including micellar structures, ellipsoids, disks, cylinders, vesicles, and lamellae.[1-6] This assembly usually depends strongly on the molecular architecture, concentration, solvent environment and is driven by non covalent interactions such as hydrogen bonding, π-π stacking or electrostatic interactions.[7] In particular, spherical micelles have attracted much attention for their use as drug carrier.[8] Encapsulation of hydrophobic drugs into self-assembled particles has been shown to enhance their water-solubility thus reducing their toxicity and to contribute to more sustained release profiles.[9-11] The latest developments in this field focus on the introduction of functional groups at the surface of the drug carrier such as peptides,[12] antibodies[13] or carbohydrates[14] aiming at the interaction with specific cell receptors for a site-directed delivery of the drugs.

Over the last decade, multivalent display of carbohydrates at the cell surface has been demonstrated to play a critical role in many biological events. Carbohydrate-protein

interactions are involved in standard as well as pathological processes including fertilization, viral and bacterial infection, inflammatory response, cell adhesion, and metastatic spreading.[15] Carbohydrate-based nanoparticles have thus recently received much attention as site-directed drug carriers. The preparation of particles from amphiphilic graft- or block-copolymers containing a polysaccharidic scaffold including dextran, chitosan, hyaluronic acid or water-soluble cellulose derivatives is abundantly documented.[16, 17] Although biomass-derived polysaccharides provide a valuable scaffold for the elaboration of nanoparticles, they barely interact with specific cell-surface carbohydrate receptors. The binding of lectins typically involves only the two or three terminal sugar residues of the mammalian glycans including galactose, mannose, *N*-acetyl-neuraminic acid, fucose or *N*-acetyl-glucosamine.[18] Recently, Kim et al. reported a series of carbohydrate amphiphiles prepared around PEG scaffolds and polyaromatic hydrophobic blocks.[19] Self-assembled nano-objects of different sizes and morphologies were obtained in water depending on the molecular architecture as well as the volume fraction of each constituent, and the bioavailability of the sugar units for *E. coli* receptors was confirmed. Although the biocompatibility and the immunogenicity of such drug carrier need to be investigated further into details, the perspectives offered by these glycosylated macromolecular amphiphiles are extremely broad.

Aiming at the development of new self-assembled nanoparticles whose surface is decorated by carbohydrates with potential applications for the site-directed vectorization of active molecules, we have designed a series of carbohydrate-containing amphiphilic macromolecules from a synthetic PEG ester. Poly(ethylene glycol) and its derivatives have several physicochemical properties that make them especially important in various biological, chemical and pharmaceutical settings where one can cite the wide range of solubility in both organic and aqueous media, the lack of toxicity and immunogenicity, nonbiodegradability and ease of excretion from living organisms.[20] PEG is often used as a covalent modifier of a variety of substrates producing conjugates that combine some of the properties of both the starting substrate and the polymer. Blood lifetime of PEGylated liposomes, nanoparticles, and proteins can be significantly extended and their uptake by reticuloendothelial system (RES) organs, liver and spleen diminished.[21-23] Fatty acid esters of PEGs, commonly known as macrogolglycerides are produced industrially and used in a variety of lipid-based formulations in cosmetic and pharmaceutical applications. Currently, these lipidic excipients are used as bioavailability enhancers in, for example, proxyphylline release from matrix hard gelatin capsules,[24] oral formulation of nicotine,[25] and dermal application of cyclosporin A.[26]

The present work reports the synthesis, self-assembly, and interaction study of new amphiphiles targeting lectins prepared by click-chemistry grafting of propargylated carbohydrates onto azido-PEG900-stearate. Stearic acid, one of the most common fatty acids, is widely used as a lubricant, in soaps, cosmetics, and food packaging. It is a component of Solutol HS15[27] and Gelucir 50/13[28] which have been proved to be effective stabilizers for the preparation of lipid particles. On the other hand, PEG having an average molecular weight of 900 was selected to act as a flexible hydrophilic spacer of appropriate size to provide amphiphiles with a hydrophobic volume fraction close to 20% that is required for the formation of spherical micelles.[10]

Experimental Section

Materials. All reagents were of commercial grade and they were used as received unless otherwise noticed. *Triticum vulgaris* (Wheat germ) lectin (WGA) and *Arachis hypogaea* (Peanut) lectin (PNA) were obtained from EY Laboratories, Inc. The solvents were dried and distilled according to literature procedures before use. The reactions were monitored by TLC using Silica Gel 60 F254 precoated plates (E.Merck, Darmstadt) and the detection was achieved by exposure to iodine vapors or by charring with sulfuric acid solution 3:45:45 H_2SO_4:MeOH:H_2O. For flash chromatography, E. Merck Silica Gel 60 was used.

Characterization of the amphiphiles. The NMR spectra were recorded on a Bruker AC 300 or Bruker Avance 400 spectrometer at 25 ^oC and they were calibrated against the residual signal of the solvent. Proton chemical shifts are reported in ppm relative to external $SiMe_4$ (0 ppm). Low-resolution mass spectra were recorded on a Bruker Daltonics Autoflex apparatus for MALDI and on a Waters Micromass ZQ spectrometer for ESI experiments. High-resolution mass spectrometry measurements were performed on a Micromass ZABSpec-Tof spectrometer at the Centre Regional de Mesures Physiques de l'Ouest CRMPO (Rennes, France). The infrared (IR) spectra were recorded using a Perkin-Elmer Spectrum RXI FTIR spectrometer.

Synthesis. Propargyl 2-acetamido-2-deoxy-β-D-glucopyranoside[29] and propargyl β-lactoside[30] were synthesized as previously reported in the literature.

Mono-tosyl-PEG 900 (1). To a chilled ($0^{\circ}C$) solution of PEG 900 (8.0 g, 8.9 mmol) in anhydrous methylene chloride (250 mL) was added silver oxide (3.1 g; 13.4 mmol) and

potassium iodide (0.6 g; 3.6 mmol). Recrystallized tosyl chloride TsCl (1.78g; 9.4 mmol) was then added in one portion. The reaction was monitored by TLC and after completion (~ 2 hours), the mixture was filtered over pad of Celite® and evaporated under reduced pressure to give a colorless oily product. Pure **1** (5.16 g; 55 %) was isolated after purification by silica gel flash chromatography using methylene chloride:methanol (9:1 v/v). ^{1}H NMR: (300 MHz, $CDCl_3$, ppm): δ = 7.78 (d, 2H, *J* = 8.5 Hz, Arom.), 7.31 (d, 2H, *J* = 8.5 Hz, Arom.), 4.12 (t, 2H, *J* = 4.4 Hz, C*H*$_2$OTs), 3.71−3.55 (m, ~78H, C*H*$_2$O), 2.42(s, 3H, CH_3).^{13}C NMR: (75 MHz, $CDCl_3$, ppm) : δ = 144.8, 133.0, 129.8, 128.0, 72.5, 70.7, 70.5, 70.3, 69.2, 68.6, 61.7, 21.6. MALDI-TOF MS Calcd for $C_{47}H_{88}O_{23}S$: *m/z* 1052; found: *m/z* 1075 $[M+Na]^+$

Mono-azide-PEG 900 (2). A solution containing **1** (2.5 g, 2.4 mmol) and NaN_3 (0.618, 9.5 mmol) dissolved in anhydrous DMF (25 mL) was heated at 60°C in an oil bath for 18 hours and then concentrated. The residue was purified by silica gel flash column chromatography using methylene chloride: methanol (9:1 v/v) as eluent to yield pure azide PEG **2** (1.86 g, 85 %). ^{1}H NMR: (300 MHz, $CDCl_3$, ppm) : δ = 3.71-3.58 (m, ~78H, C*H*$_2$O), 3.37 (m, 2H, C*H*$_2$$N_3$). ^{13}C NMR: (75 MHz, $CDCl_3$, ppm) : δ = 72.5, 70.6, 70.30, 70.0, 61.7, 50.7. FT-IR spectra (υ, cm^{-1}): azide absorbance peak 2100 cm^{-1}. MALDI-TOF MS Calcd for $C_{40}H_{81}N_3O_{20}$: *m/z* 923.61, found: *m/z* 946.56 $[M+Na]^+$

Azide-PEG 900-stearate (3). *N*,*N*'-dicyclohexylcarbodiimide (0.20 g, 1 mmol) and 4-dimethylaminopyridine (DMAP) (0.024 g, 0.2 mmol) were added into a stirred solution of stearic acid (0.85 g, 3.0 mmol) and mono-azide-PEG 900 **(2)** (0.92 g, 1 mmol) in anhydrous methylene chloride (30 mL). After 48 hours at room temperature under N_2 atmosphere, the mixture was filtered over pad of Celite® and evaporated under reduced pressure to give a colorless oily product. Pure stearate **3** (0.976, 82%) was isolated after purification by silica gel flash column chromatography using methylene chloride:methanol (9:1 v/v) as eluent. ^{1}H NMR: (400 MHz, MeOD, ppm) : δ = 4.21 (t, 2H, *J* = 4.8 Hz), 3.71-3.64 (m, ~82 H, C*H*$_2$O), 3.37 (t, 2H, *J* = 4.9 Hz), 2.36-2.26 (m, 2H), 1.62-1.60 (m, 2H), 1.29 (m, 28H), 0.90 (t, 3H, *J* = 6.6 Hz, CH_3). ^{13}C NMR: (100MHz, DMSO-d6, ppm) : δ =172.9, 69.9, 69.3, 68.4, 63.1, 50.1, 33.5, 31.4, 30.7, 29.1, 28.9, 28.8, 28.5, 24.5, 22.2, 14.0. FT-IR spectra: azide absorbance peak 2100 cm^{-1}. MALDI-TOF MS Calcd for $C_{58}H_{115}N_3O_{21}$: *m/z* 1189, found: *m/z* 1212 $[M+Na]^+$

***N*-acetyl-β-D-glucosaminyl-PEG 900-stearate conjugate (4).** Copper sulfate (53.4 mg, 0.34 mmol) and sodium ascorbate (73.0 mg, 0.37 mmol) were added into a stirred solution of propargyl-2-acetamido-2-deoxy-β-D-glucopyranoside (0.113 g, 0.44 mmol) and azide-PEG **3** (0.4 g, 0.34 mmol) in water/THF (1:1 v/v). The mixture was heated at 40°C and the reaction was monitored by TLC. After 24 hours, the solution was concentrated under vacuum. The residue was taken up in methylene chloride, filtered and concentrated. Pure $C_{18}PEG_{900}GlcNAc$ **4 (**0.35 g,72 %) was isolated after silica gel flash column chromatography using methylene chloride: methanol (8:2 v/v) as eluent. ^{1}H-NMR (400 MHz, DMSO-d6, ppm) : δ = 7.93 (s, 1H, triazolyl), 7.49 (d, 1H, *J* = 8.6 Hz, NH), 4.80-4.40 (m, 8H), 4.13 (t, 2H, *J* = 4.2 Hz), 3.82 (t, 2H, *J* = 4.8 Hz) 3.61-3.50 (m, 82H, C*H*$_2$O), 3.15 (2H, *J* = 4.8 Hz), 2.28 (t, 2H, *J* = 4 Hz), 2.08 (s, 11H), 1.78 (s, 3H), 1.5 (m, 2H), 1.24 (m, 18H), 0.86 (t, 3H, *J* = 6.6Hz, CH_3). ^{13}C NMR: (75 MHz, DMSO-d6, ppm) : δ = 172.8, 168.9, 143.5, 124.2, 100.2, 77.0, 74.2, 71.6, 70.7, 69.7, 69.6, 69.5, 68.7, 68.3, 67.9, 62.9, 61.2, 61.1, 55.3, 33.4, 31.2, 29.0, 28.8, 28.6, 28.4, 24.4, 23.0, 22.0, 13.9. ESI-HRMS Calcd. for $C_{69}H_{132}N_4O_{27}$: *m/z* 1471.89767 $[M+Na]^+$; found: 1471.8958

β-Lactosyl-PEG 900-stearate conjugate (5). Copper sulfate (61 mg, 0.39 mmol) and sodium ascorbate (79.2 mg, 0.40 mmol) were added to a stirred solution of propargyl-β-lactoside (0.190 g, 0.5 mmol) and azide-PEG900 **3** (0,456 g, 0.39 mmol) in water/THF (1:1 v/v). The mixture was heated at 40°C and the reaction was monitored by TLC. After 24 hours, the solution was concentrated under vacuum. The residue was taken up in methylene chloride, filtered and concentrated. Pure $C_{18}PEG_{900}Lac$ **5 (**0.403 g, 67 %) was isolated after silica gel flash column chromatography using methylene chloride:methanol (7:3 v/v) as eluent. ^{1}H NMR: (400 MHz, DMSO-d6, ppm) : δ = 8.03 (1H, triazolyl), 4.91-4.32 (m, 12H), 4.12 (t, 2H, *J* = 4.9 Hz), 3.82 (2H, *J* = 4.8 Hz, *CH*$_2$O) 3.58-3.50 (m, 78H, C*H*$_2$O), 3.33 (2H, *J* = 4.8 Hz), 2.29-2.27 (m, 2H), 1.5 (m, 2H), 1.24 (m, 28H), 0.86 (t, 3H, *J* = 6.6Hz, CH_3). ^{13}C NMR: (75 MHz, DMSO-d6, ppm) : δ = 172.68, 143.39,124.35, 103.72, 101.71, 80.62, 77.06, 75.41, 74.85, 73.18, 73.03, 71.53, 70.48, 69.68, 69.54, 69.46, 68.61, 68.23, 68.03 67.81, 62.89, 61.53, 60.51, 60.29, 49.25, 33.34, 31.18, 28.90, 28.75, 28.56, 28.29, 24.36, 21.96, 13.83. ESI-HRMS Calcd. for $C_{75}H_{143}N_3O_{33}$: *m/z* 1636.95016 $[M+Na]^+$; found: 1636.9507

Nanoparticles Preparation. The nanoparticles suspensions (aqueous micellar solutions - *C*p = 0.1 - 1.5 mg/mL) were prepared by direct dissolution of the amphiphiles **3**, **4** and **5** in Milli-

Q water or in phosphate buffered saline solution (PBS, 10mM, pH 7.2, 1 mM $CaCl_2$,1 mM $MnCl_2$) and stirred for 24 hours at 25°C. The solutions were then filtered using 0.45μm pore size nylon membrane filters in order to remove dust and large non-micellar aggregates.

Characterization of the Nanoparticles

Fluorescence Spectroscopy. The critical micelle concentration (CMC) of **3**, **4** and **5** was determined by fluorescence spectroscopy using pyrene (Py) as a probe.[31] Measurements of steady-state fluorescence of pyrene were performed in Milli-Q water at 25.0°C. Stock solution of pyrene (1mM) was prepared in dry ethanol. An aqueous solution of pyrene (10^{-6}M) was then prepared by adding 0.1mL of the pyrene stock solution into 100mL of Milli-Q water. The solutions were then prepared from the stock solution containing pyrene (10^{-6}M) and they were allowed to equilibrate for at least 12 h prior to the acquisition of emission spectra. This procedure minimizes errors in the emission intensity occurring in alternative methodologies.

The steady-state fluorescence spectra of pyrene were recorded on a Perkin-Elmer LS50B Spectrofluorimeter equipped with a thermostated cell holder set at 25.0°C. Both slits of excitation and emission monochromators were adjusted for 2.5 nm. The samples were excited at 335 nm and the emission intensity spectra were recorded at 372.8 nm (I_1) and 384.0 nm (I_3). Typically, the fluorescence spectrum was recorded after the addition of each microliter of amphiphilic solution. The relative intensities were corrected for each sample dilution prepared from the pyrene stock solution. The I_1/I_3 ratio was estimated by taking into account the ratio of the maximum peak intensity.

Dynamic Light Scattering (DLS). The size and polydispersity of the nanoparticles were accessed using DLS measurements. The experiments were performed using an ALV Laser Goniometer, which consists of a cylindrical 22 mW HeNe linear polarized laser with λ = 632.8 nm and an ALV-5000/ALV Multiple Tau Digital Correlator with a 125 ns initial sampling time.[32] The samples were kept at 25 °C. The accessible scattering angle of the equipment ranges from 20° to 150°. All samples were systematically studied at 90° and some of them were studied at different scattering angles varying from 40° to 140°. The solutions were put in ordinary 10 mm in diameter glass cells. The minimum sample volume required for an experiment was 1 mL. The data were acquired with the ALV-Correlator Control Software and the counting time for each sample was in average 300 s. The distributions of relaxation times - A(t) - were obtained by using the CONTIN analysis of the auto-correlation

function C(q,t).[33] The relaxation frequency, $\Gamma = 1/\tau$ is a function of the scattering angle.[34] The apparent diffusion coefficient (D_{app}) of the nanoparticles at a given copolymer concentration (C_p) is calculated from equation 1.

$$\frac{\Gamma}{q^2}|_{q\to 0} = D_{app} \qquad (1)$$

where q is the wave vector defined as

$$q = \frac{4\pi n}{\lambda}\sin\left(\frac{\theta}{2}\right) \qquad (2)$$

λ being the wavelength of the incident laser beam (632.8 nm), n the refractive index of the sample, and θ the scattering angle. The hydrodynamic radius (R_H) (or diameter, $2R_H$) was calculated from the Stokes-Einstein relation given in equation 3.

$$R_H = \frac{k_B T}{6\pi\eta\Gamma}q^2 = \frac{k_B T}{6\pi\eta D_{app}} \qquad (3)$$

where k_B is the Boltzmann constant, T is the temperature of the sample and η is the viscosity of the solvent (water in this case).[35]

Transmission Electron Microscopy (TEM). To prepare the TEM samples, 4µL of an aqueous micellar solution was dropped onto a glow-discharged carbon-coated copper grid. Then 4µL of 2% (w/v) uranyl acetate negative stain was added prior to complete drying. After few minutes, the liquid in excess was blotted with a filter paper and the grid was allowed to dry. The specimens were observed using a Philips CM200 microscope operated at 80kV. Images were recorded on Kodak SO163 films, and the negatives were digitized off-line using a Kodak Mega plus CCD camera.

Small-angle X-ray scattering (SAXS). The SAXS measurements were performed at the French CRG Beamline D2AM-BM02 of the European Synchrotron Radiation Facility (ESRF). The wavelength (λ) of the incoming beam and the sample-to-detector distance was chosen in such way that the q-range, *q being equal to* $(4\pi/\lambda)\sin(\theta/2)$ (θ is the scattering

angle) could be covered from 0.15 to 3.0 nm^{-1}. The samples were loaded into sealed borosilicate capillaries (~ 2 mm diameter). The collimated beam crossed the samples and was scattered to an indirect illumination CCD detector (Princeton Instruments). In all cases the 2D-images were found to be isotropic and they were corrected by taking into account the detector dark noise and normalized by the sample transmission**.** The *I*(*q*) vs. *q* curves resulting from the 360° azimutham integration of the 2D-patterns were further corrected by the subtraction of the scattering of the pure solvent (water). The *I(q) vs. q* scattering profile of the nanoparticles could be fitted by using the spherical copolymer micelle model developed by Pedersen and Gerstenberg.[36] The fitting procedures and other analyses were performed using the SASfit software, which makes use of the least-square fitting approach for minimizing the squared chi (χ^2) parameter. The SASfit software package was developed by J. Kohlbrecher and it is available on-line.[37]

Results and Discussion

Synthesis of the Amphiphiles.

The synthesis, as depicted in Scheme 1, is initiated with selective monotosylation of PEG 900 in presence of silver oxide (Ag_2O) and a catalytic amount of potassium iodide (KI) as reported by Bouzide et al..[38] This method, which proved to be an excellent protocol to mediate monotosylation of symmetrical diols and oligo (ethylene glycol)s (OEGs), provided the sulfonated PEG **1** in fairly good yield (55%). Substitution of the tosyl group in presence of sodium azide provided compound **2** in 85% yield. The absorption peak of the N_3 group at 2100 cm^{-1} observed by infrared spectroscopy and the ^{13}C signal of the methylene carbon adjacent to the azide group at 50.7 ppm seen by NMR confirmed the efficiency of the transformation. The stearic group was further introduced by an esterification reaction promoted by dicyclohexylcarbodiimide leading to 82% yield of the "ready-to-click" $C_{18}PEG_{900}N_3$ **3**. Propargyl β-glycosides of *N*-acetyl-glucosamine and lactose were introduced at the polar head of the surfactant by copper-catalyzed Huisgen cycloaddition.[39, 40] The reaction was carried out at 40°C with the copper/ascorbate catalytic system in a water/THF mixture to ensure a good solubility of the amphiphile. Glycosylated conjugates $C_{18}PEG_{900}$GlcNAc **4** and $C_{18}PEG_{900}$Lac **5** were respectively isolated in 72 and 67% yields after purification by silica gel chromatography.

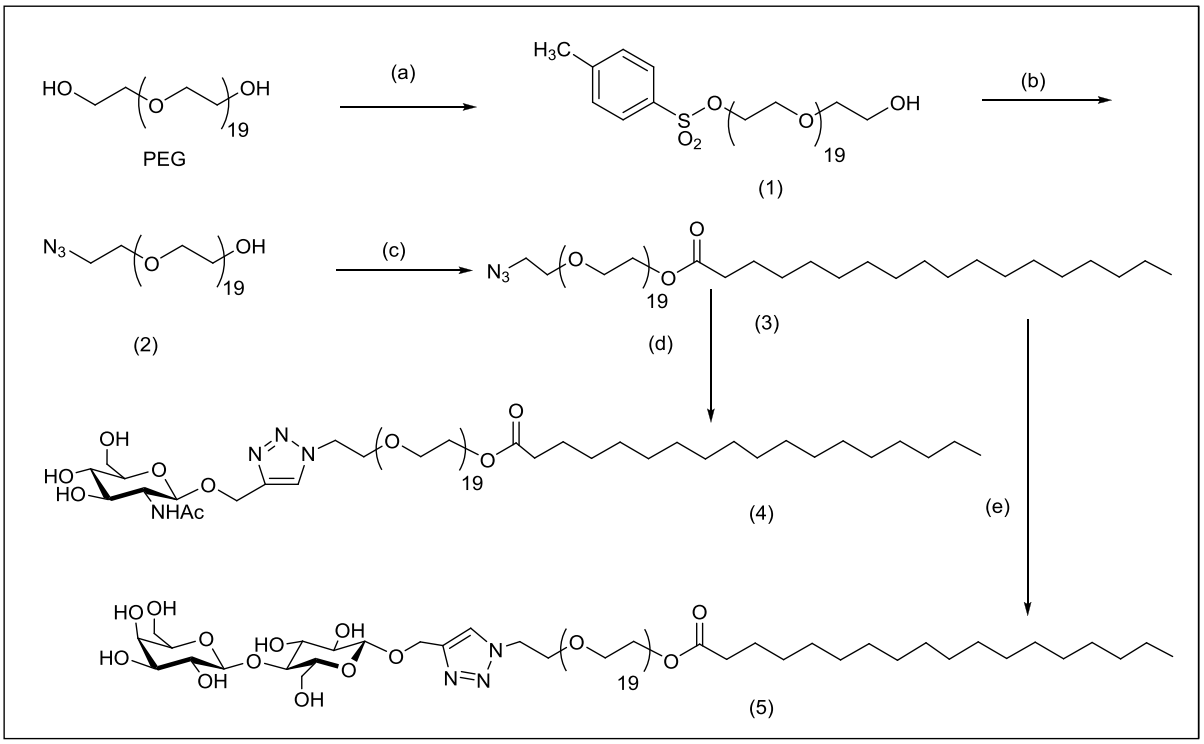

Scheme 1. Synthetic strategy used in the preparation of $C_{18}PEG_{900}GlcNAc$ **4** and $C_{18}PEG_{900}Lac$ **5**: **a)** TsCl , Ag_2O , KI , CH_2Cl_2 , 55% ; **b)** NaN_3, DMF, 85%; **c)** DCC, DMAP, stearic acid, CH_2Cl_2, 82% ; **d)** $CuSO_4$, sodium ascorbate, propargyl-2-*N*-acetamido-2-deoxy-β-D-glucopyranoside, H_2O/THF, 72%; **e)** $CuSO_4$, sodium ascorbate, propargyl β-lactoside, H_2O/THF, 67%.

Although the amphiphilic behavior of the molecules complicates their characterization, the structure of **4** and **5** could be unambiguously confirmed by mass spectrometry and NMR spectrometry in DMSO, a good solvent for each part of the molecule. Both ^{1}H and ^{13}C NMR spectra displayed characteristic signals of the aliphatic chains, the ethylenoxide parts and the carbohydrate units as well as the signals of the triazolyl ring. Figure 1 depicts as representative example the ^{13}C NMR spectra of $C_{18}PEG_{900}Lac$ **5** in (DMSO-d_6).

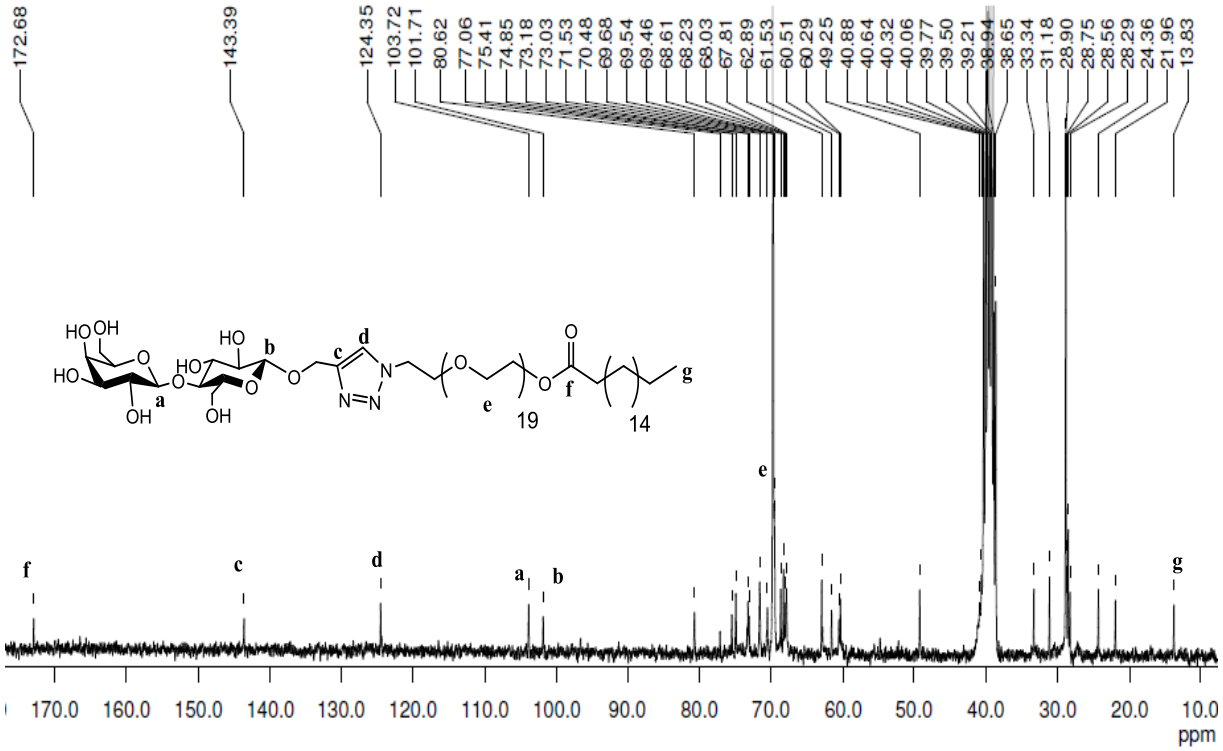

Figure 1. ^{13}C NMR spectra of $C_{18}PEG_{900}Lac$ **5** in (DMSO-d_6).

Self-Assembly of the Amphiphiles.

Fluorescence Spectroscopy. The CMC is the critical micelle concentration above which the amphiphile form micelles. Fluorescent probe techniques such as those using pyrene (Py) have been widely employed for monitoring the formation of amphiphilic aggregates and to determine the CMC of the surfactants. The I_1/I_3 ratio from Py fluorescence decreases for different systems as the total amphiphilic concentration increases, reflecting the incorporation of Py in hydrophobic domains due to aggregate formation. Figure 2 shows the I_1/I_3 intensity ratios derived from Py emission spectra recorded for solutions of $C_{18}PEG_{900}N_3$ **3** (filled circles) and $C_{18}PEG_{900}GlcNAc$ **4** (open circles). The *CMC* determined from the interception of the horizontal and the steep parts of the curves were 0.033 mg/mL for **3** and 0.055 mg/mL for $C_{18}PEG_{900}GlcNAc$ **4**. The same procedure was used to determine the CMC of the $C_{18}PEG_{900}Lac$ **5** (0.060 mg/mL - data not shown). As expected, no significant changes were observed between the unmodified and the glycosylated surfactants since the hydrophilic character of the different molecules is dictated by the PEG part.

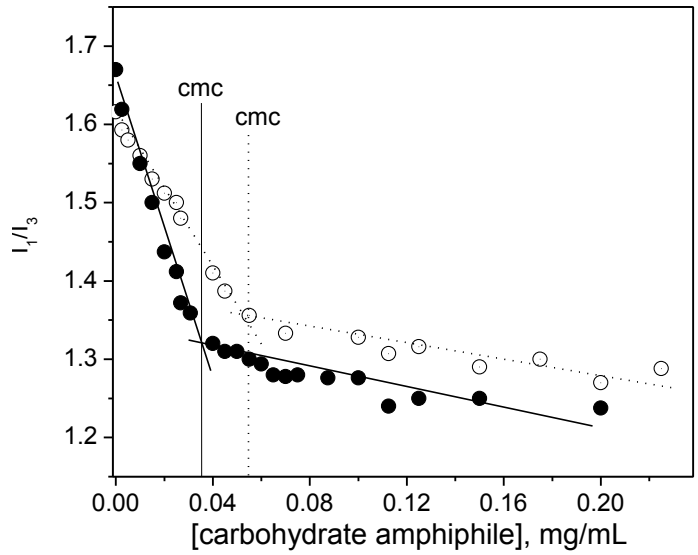

Figure 2. Pyrene fluorescence ratio I_1/I_3 as a function of the concentration measured in water at 25°C for $C_{18}PEG_{900}N_3$ **3** (●) and $C_{18}PEG_{900}$GlcNAc **4** (○).

Dynamic Light Scattering (DLS). Figure 3 shows the autocorrelation function C(q,t) measured at 90° and the respective distribution of the relaxation times A(t) as revealed by CONTIN analysis for 0.5 mg/mL solution of $C_{18}PEG_{900}N_3$ **3** in water. The non-glycosylated intermediate **3** self-assembles in aqueous solution into low-polydispersity nanoparticles (R_H = 10.4 nm). Besides the intensity contribution related to the presence of well-defined micelles, it can be noticed the presence of a light scattering contribution attributed to the formation of large aggregates with loose structure. However, the light scattering intensity is heavily weighted by the particle mass and size implying that DLS reports an intensity-average distribution. The inset in Figure 3 depicts the distribution of R_H by taking into account the contribution of the volume of particles instead of the light scattering contribution where it can be easily noticed that the presence of large aggregates can be neglected as clearly evidenced by the TEM images (hereafter). The same rationalization is also valid for the others protein-free explored systems.

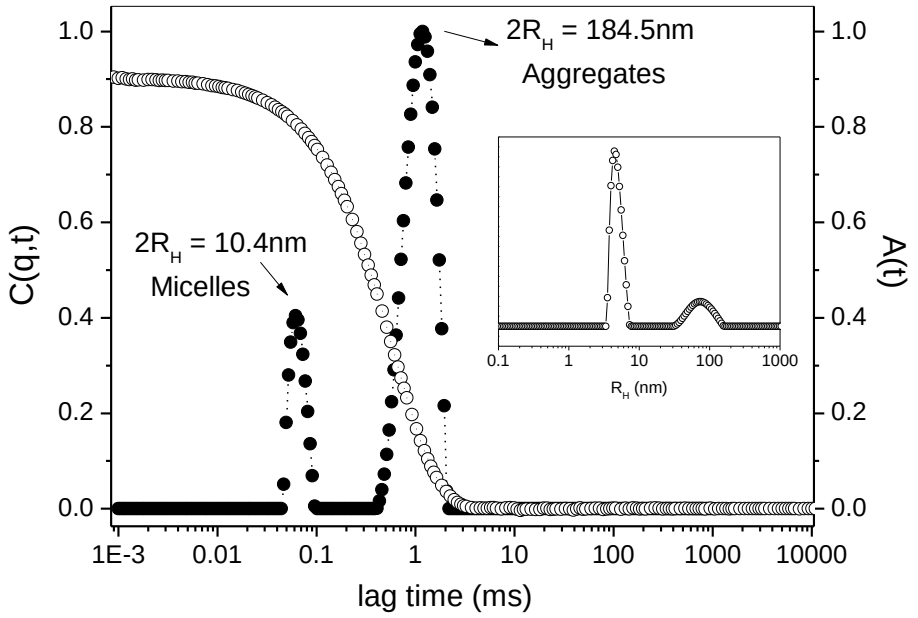

Figure 3. Typical autocorrelation function C(q,t) measured at θ = 90° and the respective distribution of relaxation times A(t) as revealed by CONTIN analysis for an aqueous 0.5 mg/mL solution of azido terminated $C_{18}PEG_{900}N_3$ **3** in water at 25°C. In the inset it is given the respective distribution of R_H by considering the contribution of the particles related to their total volume.

Figure 4 shows typical autocorrelation functions C(q,t) measured at different scattering angles and the respective distributions of the relaxation times A(t) at 90° as revealed by CONTIN analysis for 0.5mg/mL $C_{18}PEG_{900}$GlcNAc **4** and 0.5 mg/mL $C_{18}PEG_{900}$Lac **5** dissolved in water at 25 ^{o}C. The insets depict the typical angular variation of the frequency $\Gamma = 1/\tau$ measured as a function of q^2 indicating a diffusive behavior of the scattering particles.

The hydrodynamic radius of **4** and **5** were calculated by using the Stokes-Einstein relation and one can notice that the values are practically the same as compared to the value obtained before the click chemistry reaction (amphiphile **3**). The hydrodynamic sizes of the particles are equal to $2R_H$ = 10.5 nm and $2R_H$ = 10.2 nm for $C_{18}PEG_{900}$GlcNAc **4** and $C_{18}PEG_{900}$Lac **5** respectively.

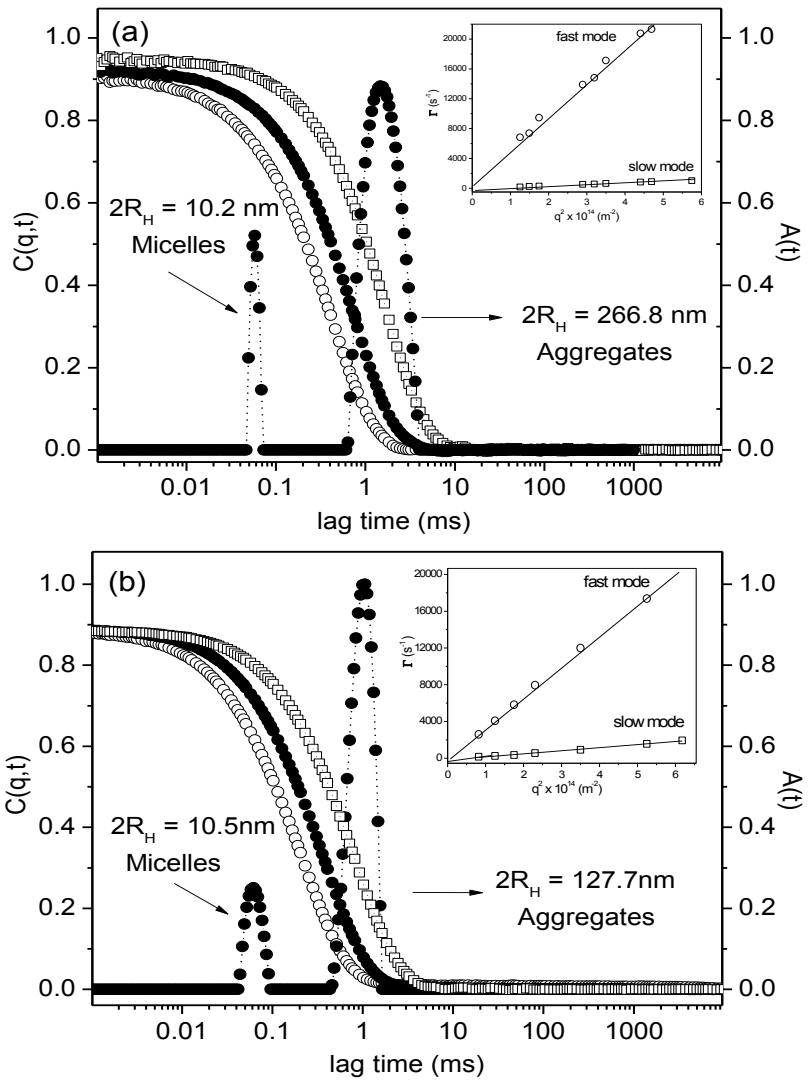

Figure 4. Autocorrelation functions C(q,t) measured at scattering angles 50 (○), 90 (●), and 130° (□), and distributions of the relaxation times A(t) at 90° as revealed by CONTIN analysis for **(a)** 0.5 mg/mL $C_{18}PEG_{900}Lac$ **5** and **(b)** 0.5 mg/L $C_{18}PEG_{900}GLcNAc$ **4** in water at 25°C.

Figure 5 summarizes the values obtained for $2R_H$ as a function of the concentration of $C_{18}PEG_{900}GLcNAc$ **4** and $C_{18}PEG_{900}Lac$ **5** demonstrating that the size of the micelles are concentration independent in both cases (for C>CMC).

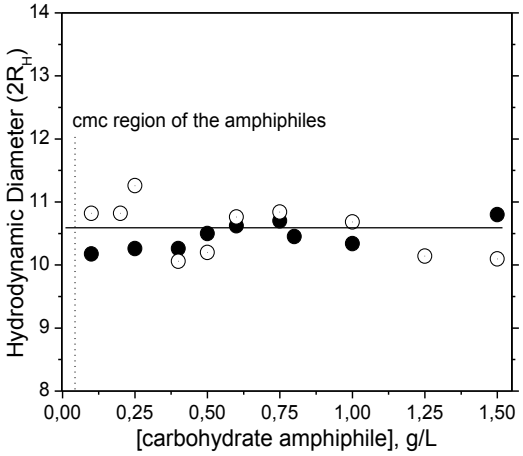

Figure 5. Hydrodynamic diameter ($2R_H$) as function of $C_{18}PEG_{900}GLcNAc$ **4** (○) and $C_{18}PEG_{900}Lac$ **5** (●) concentration measured in water at 25°C.

Transmission Electron Microscopy Study. The TEM images (Figure 6) revealed for all the amphiphiles the formation of nano-sized spherical structures in the range of 10 nm. Only a very small number of large aggregates can be observed in the micrographs suggesting that even though the dynamic light scattering technique is very sensitive to the presence of large aggregates, their real number in the current systems is negligible and as mentioned by several authors, the morphology, size and structure of nanoparticles is mainly dependent on the balance of forces of attraction and repulsion between the different blocks of the amphiphiles. The spherical micelles found here are compatible with the volumetric fraction of the hydrophobic region (φ) < 1/3.[4, 10, 41] Indeed, the calculated hydrophobic volumetric fraction of **3**, **4** and **5** based on the density of each constituent was equal to 0.28, 0.24 and 0.23 respectively, thus spherical micelles are expected.[4, 10, 35]

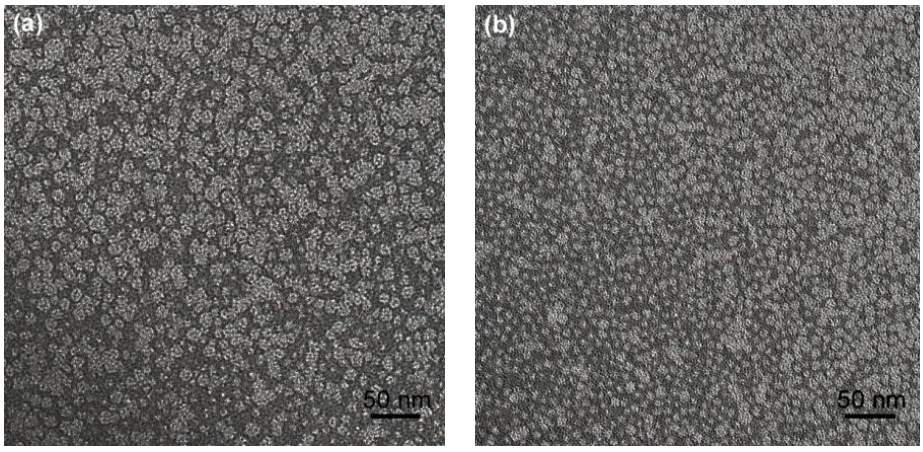

Figure 6. TEM observation of the self-assemblies: low-polydispersity spherical nanoparticles formed in water. Structures were visualized after negative staining **(a)** $C_{18}PEG_{900}GlcNAc$ **4** and **(b)** $C_{18}PEG_{900}Lac$ **5**. Scale bar corresponds to 50 nm.

Small-angle X-ray scattering (*SAXS*). In addition to TEM images, SAXS measurements were performed in order to probe the size, shape and internal structure of the scattering particles. The scattering intensity $I(q)$ of an isotropic solution of highly regular particles embedded in a matrix with a constant electron density, after normalization with the background scattering of the solvent, is given by:

$$I(q) = NP(q)S(q) \qquad (4)$$

Wherein N is the number of scattering particles per unit volume, $P(q)$ is the form factor of an individual particle, and $S(q)$ is the structure factor arising from long-range correlations between scattering centers. For widely separated (dilute) systems, $S(q) \sim 1$, and $I(q)$ is consequently proportional to the form factor $P(q)$ that reflects the size and shape of the scattering objects.

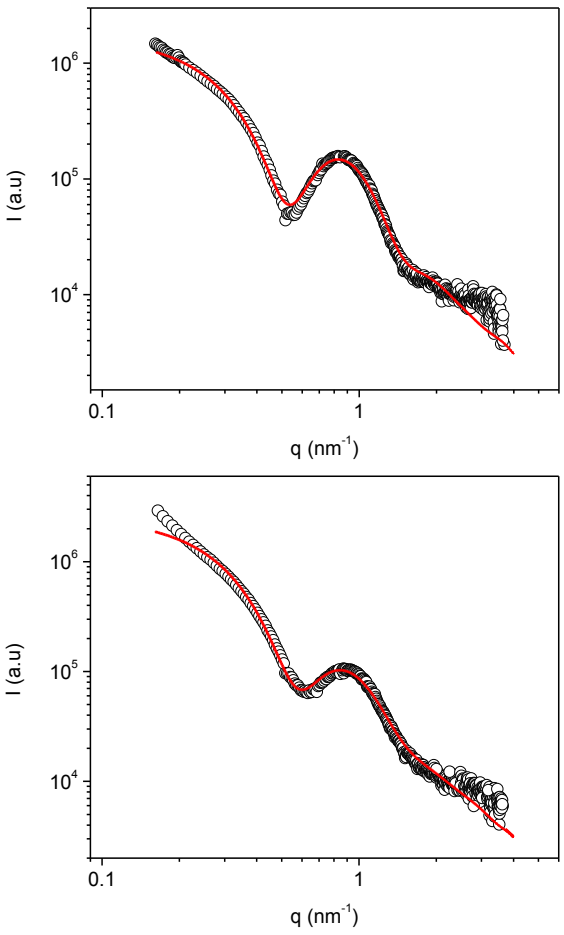

Figure 7. Small-angle X-ray scattering profiles for 40 mg/mL solutions of $C_{18}PEG_{900}$GlcNAc **4** (top) and $C_{18}PEG_{900}$Lac **5** (bottom) in water at 25°C.

Figure 7 shows the SAXS patterns for 40 mg/mL solution of $C_{18}PEG_{900}GlcNAc$ **4** (top) and $C_{18}PEG_{900}Lac$ **5** (bottom) in water at 25°C. Such copolymer concentration gives a reasonable signal-to-noise statistic and the presence of association colloids is suggested by the pronounced X-ray scattering intensity in the low-q region ($I(q)\rightarrow 0$). The high-q range ($I(q) >$ 1.5 nm^{-1}) profile for the self-assembled nanoparticles is dominated by the so-called "*blob*" scattering. This is due to the scattering contribution coming from the PEG chains dissolved in the micellar corona that dominates the X-ray scattering profile in the high-q region, which is ideally dictated by the Debye function and therefore by a nearly q^{-2} dependence depending on the conformation of the flexible PEG chains. SAXS spectra in Figure 7 clearly exhibit high amplitude form-factor oscillations that can only be observed in the case of well-defined particles with a narrow size distribution. The SAXS profiles could satisfactorily be fitted only by using the so-called spherical copolymer micelle model formerly developed by Pedersen and Gerstenberg.[36] Such a model describes the scattering of micelles consisting of a homogeneous spherical core with a radius (R_c) surrounded by corona chains that follow Gaussian statistics with dimension (R_G). The model has a large number of fitting parameters, namely: R_G, R_c, N_{agg} (aggregation number of the micelles), d (explained below) and the excess scattering length density of the core and corona forming blocks (β_{core} and β_{chain}). Therefore, it is usually not possible to get a single set of fitting parameters if some of the parameters are not preset. Hence, during the fitting procedures the parameters β_{chain} (7.30 x 10^{-12} cm) and d were held fixed. The parameter d was preset at $d = 1$, which mimics the nonpenetration of the corona chains into the core. Therefore, the starting point of the Gaussian chains is displaced to a value $R` \sim R_c + R_G$ away from the center of the particle.

The fitting parameters were therefore, N_{agg}, R_c, R_G and β_{core}. In Figure 7, the solid red lines correspond to the best fits achieved by using the spherical copolymer micelle model. The high quality of the fits can be straightforwardly noticed and is further attested by χ^2 values that remained below 2.5, thus corroborating that such a model can properly reproduce the whole experimental curves. Besides, we have observed that in some cases the very low-q region was not fitted to the same degree of accuracy, which is due to the presence of a small number of very large aggregates with loose structure as already evidenced by the DLS experiments.

Table 1. Parameters extracted from the fit of the SAXS curves in Figure 7 using the spherical copolymer micelle model. Ac was calculated from Equation 5.

Amphiphile	R_c (nm)	R_G (nm)	L^a (nm)	$R_{mic}{}^b$ (nm)	N_{agg}	β_{core} (10^{-12} cm)	A_c (nm^2)
$C_{18}PEG_{900}GLcNAc$	2.7	1.6	3.2	5.9	41	-1.8	2.2
$C_{18}PEG_{900}LAc$	2.3	2.0	4.0	6.3	34	-1.1	1.9

$^aL = 2R_G$ (thickness of the micellar corona); $^bR_{mic} = R_c + L$

Since R_c and N_{agg} were determined, the core surface area available per PEG chain in the micellar corona (A_c) can be quantitatively determined as:

$$A_c = \frac{4\pi R_c^2}{N_{agg}} \quad (5)$$

All the parameters extracted from the SAXS curve fittings are given in Table 1.

The conformation of the PEG chains should itself depend on such physical chemical variables. One can notice that a reduction in the micellar core radius is balanced by the increase in R_G. A larger R_G was determined for $C_{18}PEG_{900}Lac$ **5** whose micelles have a smaller R_c and A_c and thus forces the corona PEG chains to be slightly more stretched. The whole micellar dimension (R_{mic}) calculated as $R_c + 2R_G$ was found to be equal to 5.9 nm ($C_{18}PEG_{900}GLcNAc$ **4**) and 6.3 nm ($C_{18}PEG_{900}Lac$ **5**) which reasonably matches with the R_H values extracted from DLS.

Specific interactions of the nanoparticules with WGA and PNA lectins

Specific interactions with lectins were further evidenced by DLS confirming the bioavailability of the sugar residues on the surface of the micellar nanoparticles. Figure 8 shows the autocorrelation functions C(q,t) and the distributions of the relaxation times A(t) at a scattering angle of 90° as revealed by CONTIN analysis of 0.5 mg/mL solution of $C_{18}PEG_{900}Lac$ **5** before and after addition of non-binding or binding proteins.

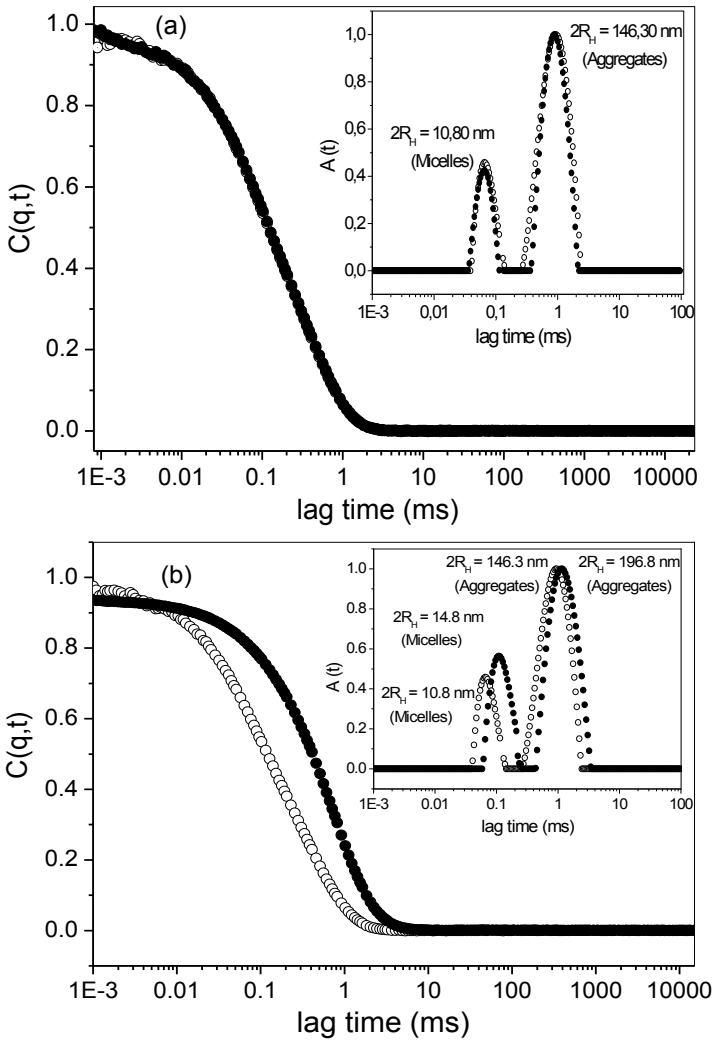

Figure 8. Typical autocorrelation functions C(q,t) and distributions of the relaxation times A(t) at scattering angle of 90° as revealed by CONTIN analysis functions of solutions of $C_{18}PEG_{900}Lac$ **5** (0.5 mg/mL) in 10mM PBS buffer, pH 7.2 containing 150mM NaCl, 0.1 mM $CaCl_2$ and 0.1mM $MnCl_2$ at 37°C, in absence (○) and in the presence of protein (•),**(a)** WGA (6µL, 1.0 mg/mL^{-1}), **(b)** PNA (4µL, 1.0 mg/mL).

The addition of WGA, which has no affinity for lactose, does not perturb the system at all. The autocorrelation curve as well as the distribution of relaxation times remained as before the addition of WGA. However, as shown in Figure 8b, the interaction of lactosyl-covered spherical micelles with PNA lectin significantly increases the micellar hydrodynamic radius R_H from 10.8 nm to 14.8 nm. It clearly evidences the specific interaction of the protein with lactose units that are on the surface of the nanoparticles.

Additionally, in Figure 9 are shown the autocorrelation functions and the distributions of relaxation times for 0.5 mg/mL $C_{18}PEG_{900}GlcNAc$ **4** at 10 mM phosphate buffer saline (pH 7.2) and 150 mM NaCl, 0.1mM $CaCl_2$ and 0.1mM $MnCl_2$ at 37°C in the absence (○) and in the presence of WGA lectin (**2**µL, 1.0 $g.L^{-1}$) (●).

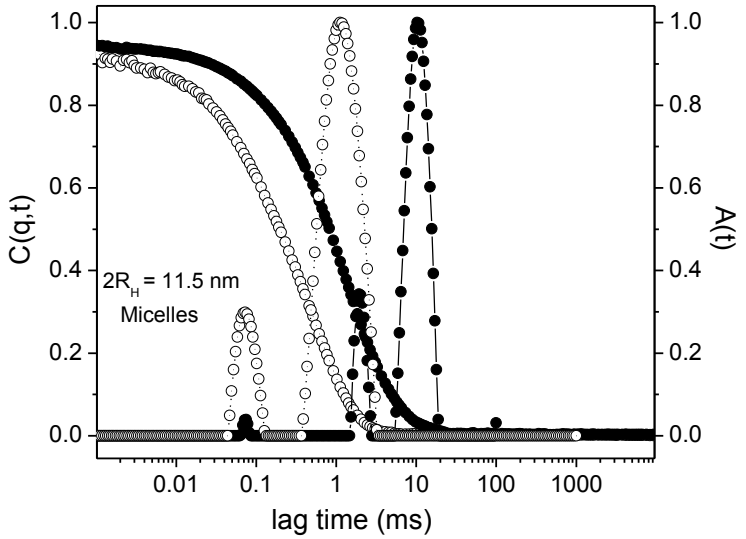

Figure 9. Typical autocorrelation functions C(q,t) and distributions of the relaxation times A(t) at scattering angle of 90° as revealed by CONTIN analysis functions of solutions of $C_{18}PEG_{900}GlcNAc$ **4** (0.5 mg/mL) in 10mM phosphate buffer (pH 7.2) and 150 mM NaCl, 0.1mM $CaCl_2$ and 0.1mM $MnCl_2$ at 37°C, in the absence (○) and after the addition of WGA (**2**µL, 1.0 mg/L)

The DLS measurements confirmed a pronounced change in the micellar hydrodynamic radius and a significant increase in the size of the micellar aggregates for **4** and **5**. These experiments clearly demonstrate that PNA and WGA lectins specifically interact with *N*-acetyl-glucosamine and lactose particles, respectively, thus supporting the assumption that the carbohydrates are exposed at the surface of the micelles.

Conclusions

The synthesis of carbohydrate-functionalized PEG900-stearate amphiphiles and their self-assembly in water is reported for the first time. *N*-acetyl-glycosamine and lactose have been efficiently introduced by azide-alkyne click chemistry at the polar extremity of PEG-stearate. Both glycoconjugates spontaneously self-assemble in water into spherical micelles having a mean diameter of 10 nm and a narrow polydispersity as evidenced by DLS, SAXS

and TEM experiments. The ability of the particles to interact with specific carbohydrate binding proteins has been further probed by dynamic light scattering thus confirming the possible application of such glycoconjugates as site-directed drug delivery systems. The negligible influence of the carbohydrate groups on the size and morphology of the micelles suggest that the present system could be easily applied to other saccharidic ligands targeting different receptors. Drug encapsulation and release are now being considered to definitely validate the potential of these nanoparticles as possible vectorization system.

Acknowledgments

We acknowledge the financial support from the CNRS and CAPES-COFECUB (project 620/08). The ESRF is acknowledged for supply of beam time (Proposal 02 01 784). The technical assistance of C. Rochas during the experiments at ESRF is greatly acknowledged. F.C.G. acknowledges FAPESP (Grant 2010/06348-0). Stephanie Boullanger is acknowledged for the mass spectrometry analyses.

References

1. Y.-b. Lim, K.-S. Moon and M. Lee, *Chem Soc Rev*, 2009, 38, 925-934.
2. G. Riess, *Progress In Polymer Science*, 2003, 28, 1107-1170.
3. S. Forster and T. Plantenberg, *Angewandte Chemie-International Edition*, 2002, 41, 689-714.
4. D. E. Discher and A. Eisenberg, *Science*, 2002, 297, 967-973.
5. F. S. Bates, *Science*, 1991, 251, 898-905.
6. C. Giacomelli, V. Schmidt, K. Aissou and R. Borsali, *Langmuir*, 2010, 26, 15734-15744.
7. L. Lindoy, *Self-assembly in supramolecular systems*, Royal Society of Chemistry, Cambridge, 2000.
8. T. M. Allen, *Science*, 2004, 303, 1818-1822.
9. A. J. Almeida and E. Souto, *Advanced Drug Delivery Reviews*, 2007, 59, 478.
10. Y. B. Lim, K. S. Moon and M. Lee, *Journal of Materials Chemistry*, 2008, 18, 2909-2918.
11. W. J. Li and F. C. Szoka, *Pharmaceutical Research*, 2007, 24, 438-449.

12. X. L. Wu, J. H. Kim, H. Koo, S. M. Bae, H. Shin, M. S. Kim, B.-H. Lee, R.-W. Park, I.-S. Kim, K. Choi, I. C. Kwon, K. Kim and D. S. Lee, *Bioconjugate Chemistry*, 2010, 21, 208-213.
13. Z. Pang, W. Lu, H. Gao, K. Hu, J. Chen, C. Zhang, X. Gao, X. Jiang and C. Zhu, *Journal of Controlled Release*, 2008, 128, 120-127.
14. Suo, Qian and Yao, *International Journal of Nanomedicine*, 2010, 1029-1029.
15. A. Varki, *Glycobiology*, 1993, 3, 97-130.
16. C. Lemarchand, R. Gref, S. Lesieur, H. Hommel, B. Vacher, A. Besheer, K. Maeder and P. Couvreur, *Journal of controlled Release*, 2005, 108, 97-111.
17. H. Yamamoto, Y. Kuno, S. Sugimoto, H. Takeuchi and Y. Kawashima, *Journal of controlled Release*, 2005, 102, 373-381.
18. N. Sharon, *Glycobiology*, 2004, 14, 53R-62R-53R-62R.
19. B. S. Kim, D. J. Hong, J. Bae and M. Lee, *Journal of the American Chemical Society*, 2005, 127, 16333-16337.
20. P. Bailon and C.-Y. Won, *Expert Opinion on Drug Delivery*, 2009, 6, 1-16.
21. G. S. Kwon and K. Kataoka, *Advanced Drug Delivery Reviews*, 1995, 16, 295-309.
22. K. Kataoka, A. Harada and Y. Nagasaki, *Advanced Drug Delivery Reviews*, 2001, 47, 113-131.
23. A. Rosler, G. W. M. Vandermeulen and H. A. Klok, *Advanced Drug Delivery Reviews*, 2001, 53, 95-108.
24. V. Ratsimbazafy, E. Bourret, R. Duclos and C. Brossard, *European Journal Of Pharmaceutics And Biopharmaceutics*, 1999, 48, 247-252.
25. J. T. Green, B. K. Evans, J. Rhodes, G. A. O. Thomas, C. Ranshaw, C. Feyerabend and M. A. H. Russell, *British Journal Of Clinical Pharmacology*, 1999, 48, 485-493.
26. H. S. Tran, D. Malli, F. A. Chrzanowski, P. M. Puc, M. S. Matthews and C. W. Hewitt, *Journal Of Surgical Research*, 1999, 83, 136-140.
27. K. Buszello, S. Harnisch, R. H. Muller and B. W. Muller, *European Journal of Pharmaceutics and Biopharmaceutics*, 2000, 49, 143-149.
28. A. Fini, J. R. Moyano, J. M. Gines, J. I. Perez-Martinez and A. M. Rabasco, *European Journal of Pharmaceutics and Biopharmaceutics*, 2005, 60, 99-111.
29. D. L. Ma, T. Y. T. Shum, F. Y. Zhang, C. M. Che and M. S. Yang, *Chemical Communications*, 2005, 4675-4677.
30. H. B. Mereyala and S. R. Gurrala, *Carbohydrate Research*, 1998, 307, 351-354.

31. K. Kalyanasundaram and J. K. Thomas, *Journal of the American Chemical Society*, 1977, 99, 2039-2044.
32. B. Berne and R. Pecora, *Dynamic light scattering : with applications to chemistry, biology, and physics*, Dover Publications, Mineola N.Y., 2000.
33. S. W. Provencher, *Makromolekulare Chemie-Macromolecular Chemistry and Physics*, 1979, 180, 201-209.
34. M. Tammer, L. Horsburgh, A. P. Monkman, W. Brown and H. D. Burrows, *Advanced Functional Materials*, 2002, 12, 447-454.
35. C. Giacomelli, V. Schmidt and R. Borsali, *Macromolecules*, 2007, 40, 2148-2157.
36. J. S. Pedersen and M. C. Gerstenberg, *Macromolecules*, 1996, 29, 1363-1365.
37. Espace.
38. A. Bouzide, N. LeBerre and G. Sauve, *Tetrahedron Letters*, 2001, 42, 8781-8783.
39. H. C. Kolb, M. G. Finn and K. B. Sharpless, *Angewandte Chemie International Edition*, 2001, 40, 2004-2021.
40. C. W. Tornøe, C. Christensen and M. Meldal, *The Journal of Organic Chemistry*, 2002, 67, 3057-3064.
41. L. F. Zhang and A. Eisenberg, *Macromolecules*, 1996, 29, 8805-8815.

Supporting Information for the Manuscript Entitled

Cite this: Soft Matter, 2011, 7, 3453-3461
Cite this: DOI: 10.1039/c0sm01411g

Self-assembled carbohydrate-based micelles for lectin targeting

Alexandre G. Dal Bó, [†,‡] *Valdir Soldi,* [‡] *Fernando C. Giacomelli,* [§] *Bruno Jean,* [†] *Isabelle Pignot-Paintrand,* [†] *Redouane Borsali,* [†] *and Sébastien Fort* [†,*]

[†]Centre de Recherches sur les Macromolécules Végétales (CERMAV-CNRS), BP 53, F-38041 Grenoble Cedex 9, France (affiliated with Université Joseph Fourier Grenoble 1 and member of the Institut de Chimie Moléculaire de Grenoble) ;

[§]Departamento de Química, Universidade Federal de Santa Catarina, 88040-900 Florianópolis – SC, Brazil;

[§]Centro de Ciências Naturais e Humanas, Universidade Federal do ABC, 09210-170 Santo André – SP, Brazil;

*Corresponding author: Sebastien Fort

e-mail. sebastien.fort@cermav.cnrs.fr

Tel. +33 (0)4 76 03 76 64

Fax. +33 (0)4 76 54 72 03

1. Summary of the Spherical Copolymer Micelle Model developed by Pedersen and Gerstenberg (*Macromolecules*, 1996, *13*, 1063).

The Spherical Copolymer Micelle Model describes the scattering for micelles as consisting of a homogeneous spherical core having corona chains that follow Gaussian statistics attached to the core surface as depicted in Figure S1.

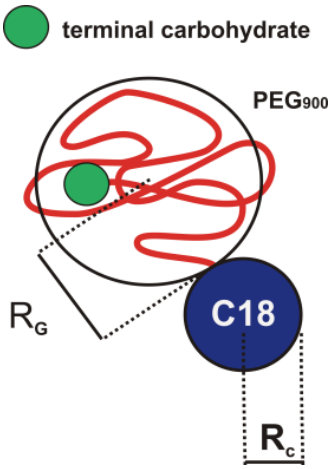

Figure S1. Schematic representation for the micellar form factor analysis according to the spherical copolymer micelle model. It considers a spherical core of radius R_c and Gaussian chains with radius of gyration R_G attached to the core.

The micellar form factor $P_{mic}(q)$ involves four terms: self-correlation of the core, self-correlation of the chains, cross term between core and chains and the cross term between different chains:

$$P_{mic}(q) = N_{agg}^2 \beta_{core}^2 F_{core}(q, R_c) + N_{agg} \beta_{chain}^2 F_{chain}(q, R_G) + N_{agg}(N_{agg} - 1)\beta_{chain}^2 S_{chain-chain}(q) + 2N_{agg}^2 \beta_{chain}\beta_{core} S_{core-chain}(q) \quad (1)$$

N_{agg} is the number of aggregation of the micelles and β_{core} and β_{chain} accounts for the excess scattering length density of the core-forming (C_{18}) and corona-forming block (PEG). $F_{core}(q,R_c)$ is the self-correlation of a spherical core with radius R_c and it is given by the form factor amplitude of a sphere with a smoothly decaying scattering density at the surface:

$$F_{core}(q,R_c) = [\Phi(q,R_c)]^2 = \left[3\frac{\sin(qR_c) - qR_c\cos(qR_c)}{(qR_c)^3}\right]^2 \quad (2)$$

The chains self-term is described by the Debye function:

$$F_{chain}(q,R_G) = \frac{2[\exp(-q^2R_G^2) - 1 + q^2R_G^2]}{(q^2R_G^2)^2} \quad (3)$$

wherein, R_G is the radius of gyration of the Gaussian chains anchored to the core. The core-chain term is given by:

$$S_{core-chain}(q) = \psi(q,R_G)\Phi(q,R_c)\frac{\sin[q(R_c + dR_G)]}{q(R_c + dR_G)} \quad (4)$$

the function $\psi(q,R_G)$ is:

$$\psi(q,R_G) = \frac{1 - \exp(-q^2R_G^2)}{q^2R_G^2} \quad (5)$$

and $d \sim 1$ should be used in order to mimic the nonpenetration of the corona chains into the core, which is physically impossible. If $d \sim 1$, the starting point of the Gaussian chains is displaced to a value $R` \sim R_c + R_G$ away from the center of the particle.

The chain-chain term is given by:

$$S_{chain-chain}(q) = \psi^2(q,R_G)\left[\frac{\sin[q(R_c + dR_G)]}{q(R_c + dR_G)}\right]^2 \quad (6)$$

The value of β_{chain} for PEG_{900} as calculated in the following way:

$$\beta_{chain} = NV_{PEG}(\sigma_{PEG} - \sigma_{solvent}) \quad (7)$$

where N is the degree of polymerization of the polymer segment ($N = 19$), V_{PEG} is the volume of one PEG monomer unit, σ_{PEG} is the scattering length density of the polymer segment and $\sigma_{solvent}$ is the scattering length density of the solvent (water). The volume occupied by a single monomer unit V_{PEG} was determined by taking into account the homopolymer density (d_{PEG}) as:

$$V_{PEG} = \frac{M_{PEG}}{d_{PEG}N_A} \quad (8)$$

and the values of the scattering length densities of the solvent and monomer unit was calculated using the average chemical composition of each component and its mass density (d_x) as:

$$\sigma_x = \frac{b_e d_x N_A}{M_x} \sum_i n_i z_i \tag{9}$$

where x accounts for H_2O or PEG, N_A is the Avogadro's number, and n_i accounts for the number of atoms i in each component and z_i is the atomic number of the atom i ($n_i z_i$ is the number of electrons in each unit). Finally, b_e is the Thomson scattering length (the scattering length of an electron - $b_e = 2.817 \times 10^{-13}$ cm). All the parameters thus calculated are given in Table S1

Table S1. Parameters used to determine β_{chain}

	d[a] (g/cm^3)	V (10^{-23} cm^3)	M (g/mol)	chemical composition	$\Sigma n_i z_i$	σ (10^{10} cm^{-2})
PEG	1.08	6.76	44.0	C_2H_4O	24	9.99
H_2O	1.00	2.99	18.0	H_2O	10	9.42

[a] values taken from reference 1.08 g/cm^3 (PEG) and g/cm^3 (H_20) from Kell Mortensen Polym. *Adv. Technol.* **2001**, 12, 2-22

2. NMR Data

NMR spectra of Azide-PEG 900-stearate (3)

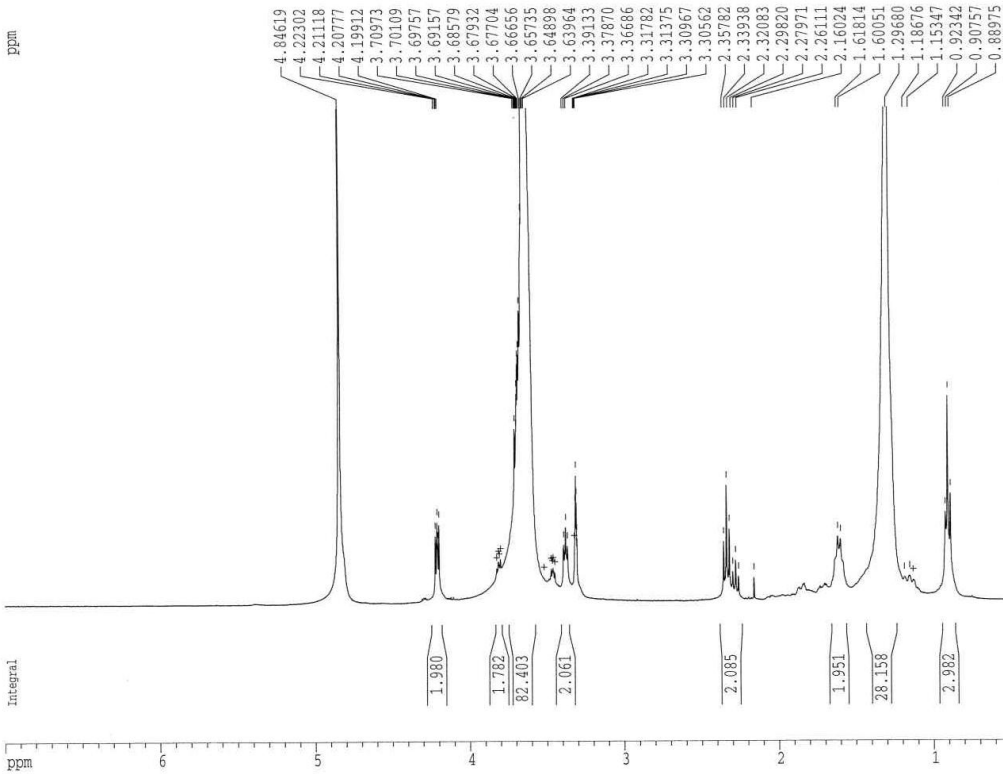

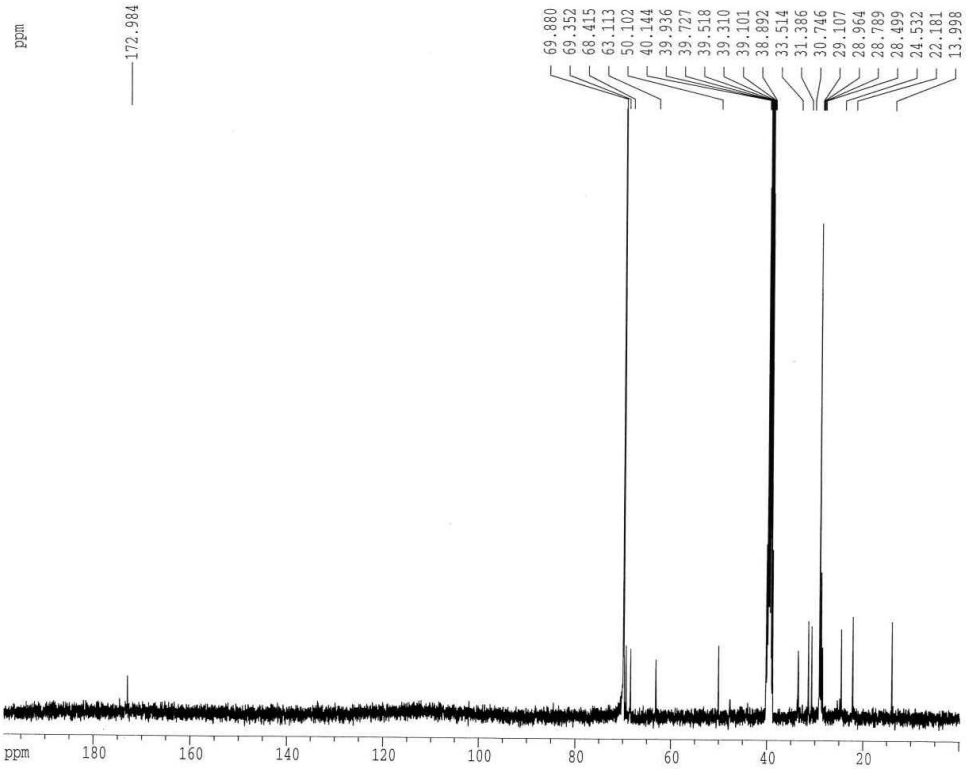

NMR spectra of *N*-acetyl-β-D-glucosaminyl-PEG 900-stearate conjugate (4)

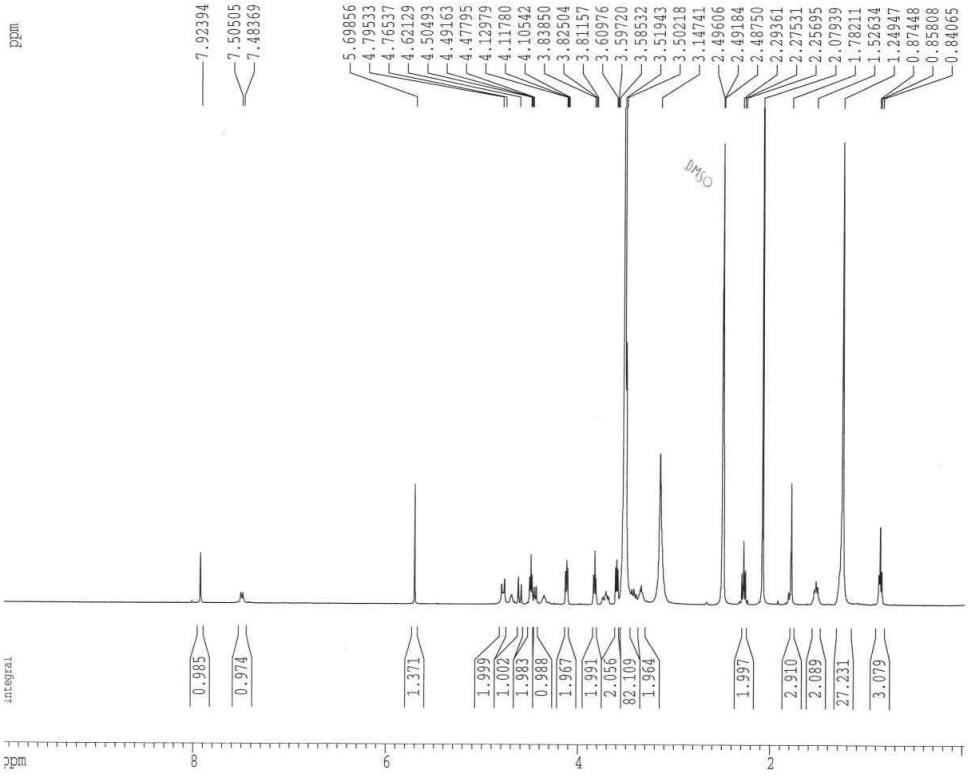

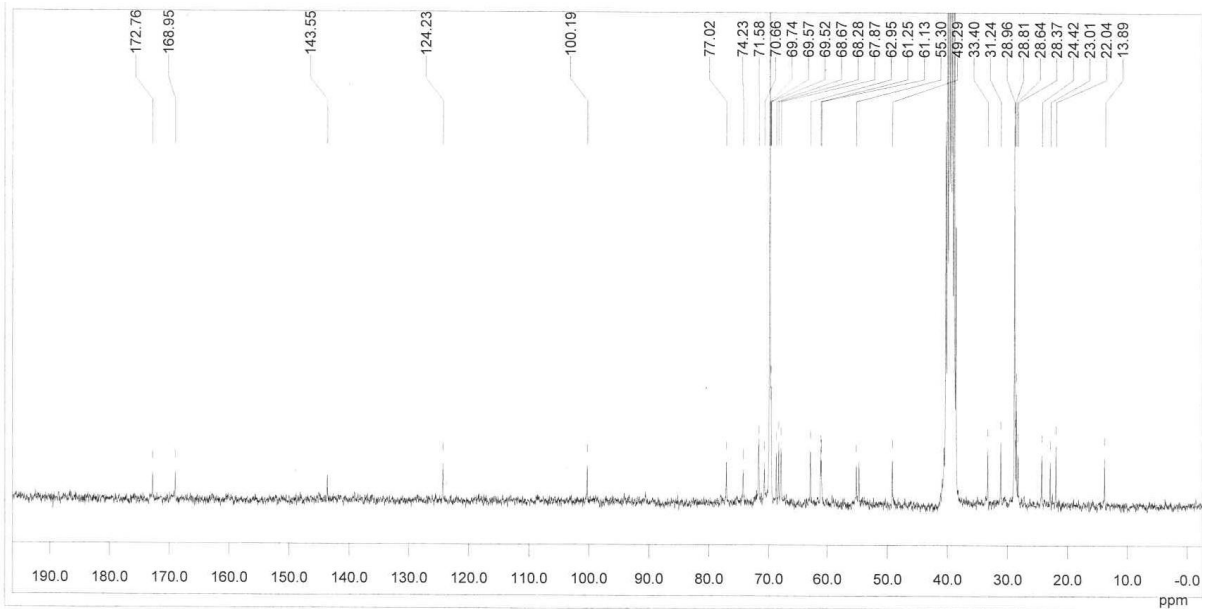

NMR spectra of β-Lactosyl-PEG 900-stearate conjugate (5)

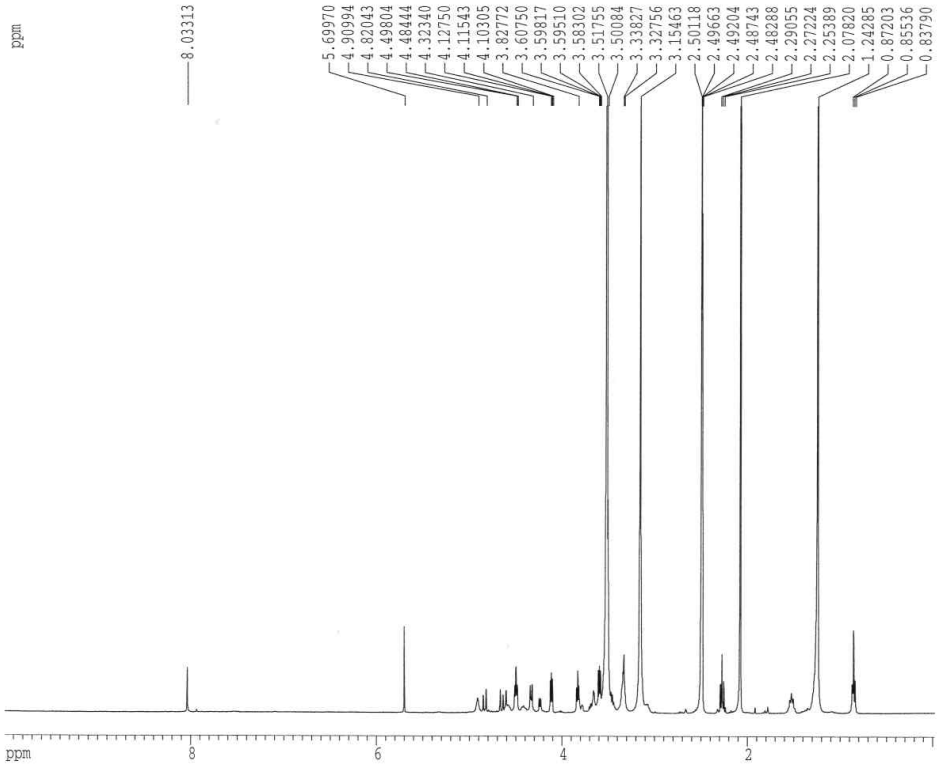

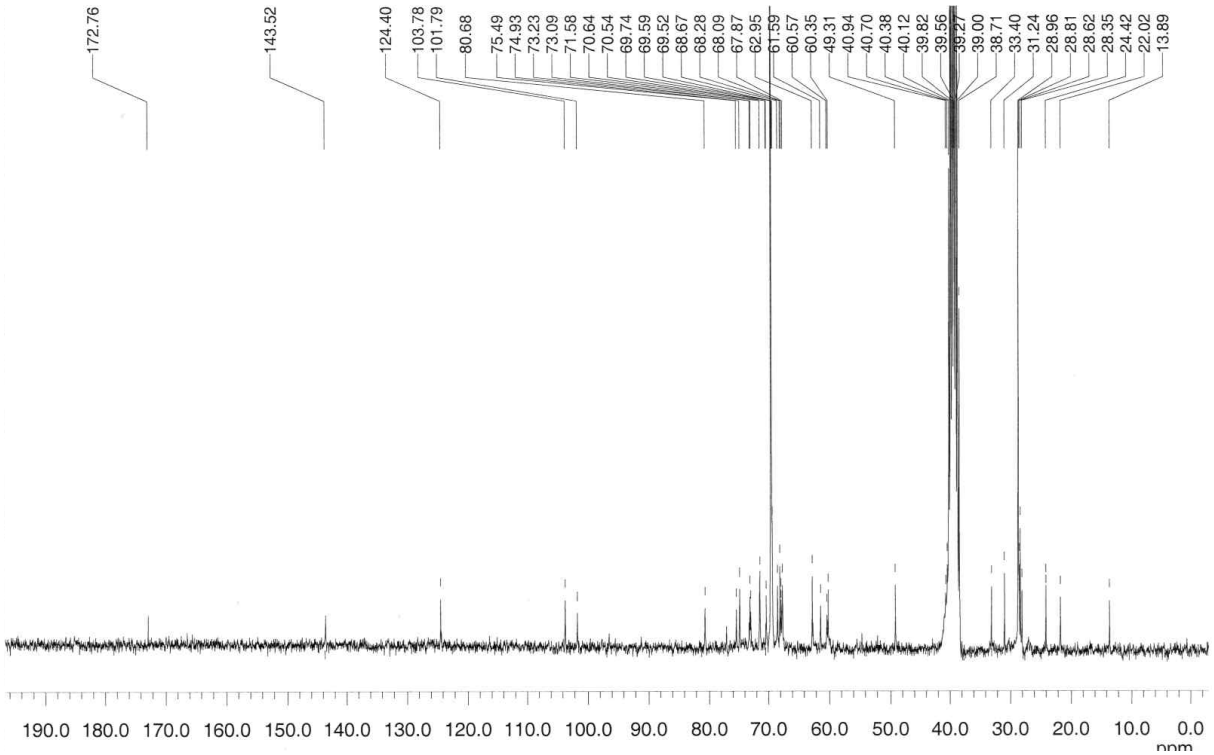

Paper to be submitted to the journal Langmuir

Synthesis and self-assembly of carbohydrate-clicked rod-coil amphiphiles

Alexandre G. Dal Bó, [†,‡] *Valdir Soldi,* [‡] *Fernando C. Giacomelli,* [§] *Bruno Jean,* [†] *Isabelle Pignot-Paintrand,* [†] *Redouane Borsali,* [†] *and Sébastien Fort* [†,*]

[†]Centre de Recherches sur les Macromolécules Végétales (CERMAV-CNRS), BP 53, F-38041 Grenoble Cedex 9, France (affiliated with Université Joseph Fourier Grenoble 1 and member of the Institut de Chimie Moléculaire de Grenoble) ;

[‡]Departamento de Química, Universidade Federal de Santa Catarina, 88040-900 Florianópolis – SC, Brazil;

[§]Centro de Ciências Naturais e Humanas, Universidade Federal do ABC, 09210-170 Santo André – SP, Brazil;

*Corresponding author: Sebastien Fort

e-mail. sebastien.fort@cermav.cnrs.fr

Tel. +33 (0)476 03 76 64

Fax. +33 (0)476 54 72 03

ABSTRACT:

This work describes the synthesis and self-assembly of carbohydrate-clicked rod-coil amphiphilic systems. Propargyl-β-lactoside and *N*-acetyl-β-D-glucosaminide were conjugated by copper-catalyzed Huisgen cycloaddition to azide-terminated-PEG_{900}-tetra(*p*-phenylene). Upon dissolution in water, these amphiphilic systems immediately self-assemble into highly regular micelles having a mean diameter of 10 nm. Dynamic Light Scattering (DLS), Transmission Electron Microscopy (TEM) and Small-Angle X-ray scattering (SAXS) were used to investigate the structure of the self-assembled micelles. The presence of the carbohydrate epitopes on the surface of the micelles and their lectin adhesion properties were also demonstrated using light scattering measurements. Specific interaction of the GlcNac and lactosyl residues with Wheat Germ Agglutinin (WGA) and Peanut Agglutinin (PNA) respectively, unveils attracting applications of such self-assembled sugar micelles as biosensor devices.

Introduction

Design of functional nanoparticles possessing optical, magnetic or bio-affinity properties is currently subject of intensive research with important outcomes in medicine for cancer diagnosis and therapy. [1, 2] Although it is well established that nanoparticles preferentially localize at the tumors as a result of the enhanced permeation and retention effect,[3, 4] much efforts are now devoted to the preparation of functionalized delivery systems allowing active targeting while sparing healthy cells.[5] Selective accumulation of drugs or probes for imaging in the tumor tissues can be achieved through receptor-ligand interactions with carbohydrates-decorated nanoparticles.[6] Indeed, interactions taking place at the cell surface between oligosaccharides and carbohydrate binding proteins known as lectins play a crucial role in

standard as well as pathological processes including fertilization, viral and bacterial infection, inflammatory response, cell adhesion, and metastatic spreading.[7] It has been shown that lectins affect tumor cell survival, adhesion to the endothelium, or extracellular matrix, as well as tumor vascularization and other processes that are crucial for metastatic spread and growth.[8, 9] Development of nanoparticles containing carbohydrate moieties that are directed to certain lectins or incorporating lectins that bind to cell surface carbohydrates (reverse lectin targeting) is considered as a promising way to detect cancer at early stage and to improve drug delivery.[10-13]

A practical and efficient way to prepare well-defined nanoparticles, among other, relies on self-assembly of amphiphilic molecules. In aqueous solution, the spontaneous auto-organization of amphiphiles driven by noncovalent interactions including hydrophobic, electrostatic, π-π stacking, and hydrogen bonding can induce well-defined nanostructures. [14] These organized nanostructures can be rationalized in terms of the hydrophobe volume fraction, molar mass, and flexibility of the amphiphile giving access to a wide range of different morphologies including spherical and cylindrical micelles, vesicles, nanofibers, toroids, and tubes, etc...[15-18] The preparation of particles from amphiphilic graft- or block-copolymers containing a polysaccharidic scaffold including dextran, chitosan, hyaluronic acid or water-soluble cellulose derivatives is abundantly documented.[19, 20] Although biomass-derived polysaccharides provide a valuable scaffold for the elaboration of nanoparticles, they barely interact with lectins. The binding of lectins typically involves only the two or three terminal sugar residues of the mammalian glycans including galactose, mannose, *N*-acetyl-neuraminic acid, fucose or *N*-acetyl-glucosamine.[21] Recently, Kim et al. reported a series of carbohydrate amphiphilic systems prepared from PEG scaffolds and polyaromatic hydrophobic blocks.[22, 23] Self-assembled nano-objects of different sizes and morphologies were obtained in water depending on the molecular architecture as well as on the volume

fraction of each constituent, and the bioavailability of the sugar units for *E. coli* receptors was confirmed.

With the aim to develop a practical and versatile way to prepare self-assembled nanoparticles whose surface is covered by carbohydrates, we have designed azido-terminated rod-coil amphiphiles consisting in a tetra(*p*-phenylene) and an oligo(ethylene oxide) segment. On one hand, PEGylation offers a unique approach to improve solubility of hydrophobic molecules in aqueous media and it is well known to reduce clearance rates of drug delivery systems and of proteins in vivo.[24-26] On the other hand, oligophenylene are linear hydrophobic stiff molecules with promising applications in biosensing devices due to photo- and electroluminescent properties[27] as well as conducting properties when doped with oxidizing or reducing reagents.[28] Although their processability is generally hampered by solubility issues, derivatization with oligoethylene groups improved their manipulation and can lead to self-assembled nanostructures. Block-copolymer exhibiting strong fluorescence in the blue region and consisting in alternated tetra(*p*-phenylene) and solubilizing poly(ethyleneglycol) spacers were reported by Hargadon et al. using a Suzuki coupling strategy.[29] Oligophenylene-based conjugates were also shown to adopt a wide range of self-assembled nanostructures including ribbons, nanotubes or micelles.[30-34]

In the present work, we report the synthesis, self-assembly, and interaction study of new amphiphilic systems targeting lectins prepared using click-chemistry grafting of propargylated carbohydrates onto azido-PEG-tetra(*p*-phenylene). Poly(ethyleneglycol) having an average molar mass of 900 was selected to act as a flexible hydrophilic spacer of appropriate size to provide amphiphiles with a hydrophobic volume fraction close to 20% that is required for the formation of spherical micelles.[14] Besides, an amphiphile incorporating a shorter PEG segment (MW 600) was also prepared in order to evaluate the influence of the hydrophilic balance onto the resulting self-assembled particles. Propargyl-β-lactoside and *N*-acetyl-β-D-

glucosaminide were conjugated by the popular and efficient copper-catalyzed Huisgen cycloaddition[35, 36] to the azide-terminated-PEG-tetra(*p*-phenylene). The self-assembled nanoparticles and their lectin adhesion properties were characterized by mean of light scattering and microcopy techniques.

Experimental Section

Materials. All reagents were of commercial grade and they were used as received unless otherwise noticed. *Triticum vulgaris* (Wheat germ) lectin (WGA) and *Arachis hypogaea* (Peanut) lectin (PNA) were obtained from EY Laboratories, Inc. The solvents were dried and distilled according to literature procedures before use. The reactions were monitored by TLC using Silica Gel 60 F254 precoated plates (E.Merck, Darmstadt) and the detection was achieved by exposure to iodine vapors or by charring with sulfuric acid solution 3:45:45 H_2SO_4:MeOH:H_2O. For flash chromatography, E. Merck Silica Gel 60 was used.

Characterization of the amphiphilic systems. NMR spectra were recorded on a Bruker AC 300 or Bruker Avance 400 spectrometer at 25 ^oC and they were calibrated against the residual signal of the solvent. Proton chemical shifts are reported in ppm relative to external $SiMe_4$ (0 ppm). Mass spectra were recorded on a Bruker Daltonics Autoflex apparatus for MALDI and on a Waters Micromass ZQ spectrometer for ESI experiments. Infrared (IR) spectra were recorded using a Perkin-Elmer Spectrum RXI FTIR spectrometer.

Synthesis. Propargyl 2-acetamido-2-deoxy-β-D-glucopyranoside[37] and propargyl β-lactoside[38] were synthesized as previously reported in the literature.

Monotosyl-PEG 900 (1a). To a chilled (0°C) solution of PEG 900 (8.0 g, 8.9 mmol) in anhydrous methylene chloride (250 mL) was added silver oxide (3.1 g; 13.4 mmol) and potassium iodide (0.6 g; 3.6 mmol). Recrystallized tosyl chloride TsCl (1.78g; 9.4 mmol) was then added in one portion. The reaction was monitored by TLC and after completion (~ 2 hours), the mixture was filtered over pad of Celite® and evaporated under reduced pressure to give a colorless oily product. Pure **1a** (5.16 g; 55 %) was isolated after purification by silica gel flash chromatography using methylene chloride:methanol (9:1 v/v). ^{1}H NMR: (300 MHz, $CDCl_3$, ppm): δ = 7.78 (d, 2H, *J* = 8.5 Hz, Arom.), 7.31 (d, 2H, *J* = 8.5 Hz, Arom.), 4.12 (t, 2H, *J* = 4.4 Hz, CH_2O), 3.71−3.55 (m, ~76H, CH_2O), 2.42(s, 3H, CH_3).^{13}C NMR: (75 MHz, $CDCl_3$, ppm) : δ = 144.8, 133.0, 129.8, 128.0, 72.5, 70.7, 70.5, 70.3, 69.2, 68.6, 61.7, 21.6. MALDI-TOF MS Calcd for $C_{47}H_{88}O_{23}S$: *m/z* 1052; found: *m/z* 1075 $[M+Na]^+$

Monotosyl-PEG 600 (1b) was isolated in 58% yield under the same reaction condition and purification by silica gel flash chromatography using methylene chloride:methanol (20:1 v/v).^{1}H-NMR: (300 MHz, $CDCl_3$, ppm) : δ = 7.77 (d, 2H, *J* = 8.4 Hz, Arom.), 7.31 (d, 2H, *J* = 8.4 Hz, Arom.), 4.14 (t, 2H, *J* = 4.5 Hz, CH_2O), 3.71−3.56 (m, ~50H, CH_2O), 2.42(s, 3H, CH_3). ^{13}C NMR: (75 MHz, $CDCl_3$, ppm) : δ = 144.7, 133.2, 129.8, 127.9, 72.5, 70.5, 70.3, 69.2, 68.7, 61.70, 21.6. MALDI-TOF MS Calcd for $C_{33}H_{60}O_{16}S$ *m/z;* 744.41, MALDI-TOF-MS *m/z* 767.09 $[M+Na]^+$

4'-Bromo-[1,1'-biphenyl]-4-*O*-PEG 900 (2a) A solution of **1** (5.0 g, 4.74 mmol), 4'-bromo-[1,1'-biphenyl]-4-ol (1.18g, 4.4 mmol) and K_2CO_3 (3.27g, 23.7 mmol) in anhydrous acetonitrile (125 mL) was heated at reflux and stirred for 32 h. The solution was poured into water and extracted with methylene chloride. The methylene chloride solution was washed with water, dried over anhydrous magnesium sulfate, and filtered. The solvent was evaporated

under reduced pressure to give a colorless oily product. Pure **2** (2.79g; 52 %) was isolated after purification by silica gel flash chromatography using methylene chloride:methanol (15:1 v/v). ^{1}H-NMR: (300 MHz, $CDCl_3$, ppm) : δ = 7.49-7.34 (m, 6H, Arom.), 6.93 (d, 2H, *J* = 8.8 Hz, Arom.), 4.12 (t, 2H, *J* = 4.7 Hz, CH_2O), 3.87 (t, 2H, *J* = 4.8 Hz, CH_2O) 3.54-3.68 (m, ~74H, CH_2O). ^{13}C NMR: (75 MHz, $CDCl_3$, ppm) : δ = 158.5, 139.6, 132.5, 131.7, 128.2, 127.8, 120.7, 115.1, 72.5, 70.8, 70.5, 70.2, 69.6, 67.4, 61.6. MALDI-TOF MS Calcd for $C_{52}H_{89}BrO_{21}$: *m/z* 1128.58; found: *m/z* 1153.50 $[M+Na]^+$; m/z 1169.44 $[M+K]^+$

4'-Bromo-[1,1'-biphenyl]-4-*O*-PEG 600 (2b) was isolated in 52 % yield after reaction under the conditions described for **1a** and purification by silica gel flash chromatography using methylene chloride:methanol (18:1 v/v).^{1}H-NMR: (300 MHz, $CDCl_3$, ppm) : δ =7.52-7.37 (m, 6H, Arom.), 6.96 (d, 2H, *J* = 8.3Hz, Arom.), 4.15 (t, 2H, *J* = 4.5 Hz, CH_2O), 3.87 (t, 2H, *J* = 4.5 Hz, CH_2O), 3.54-3.68 (m, ~48H -CH_2O). ^{13}C NMR: (75 MHz, $CDCl_3$, ppm) : δ = 158.6, 139.7, 132.6, 131.8, 128.3, 127.9, 120.8, 115.0, 72.5, 70.8, 70.5, 70.3, 69.7, 67.5, 61.7. MALDI-TOF MS Calcd for $C_{38}H_{61}BrO_{14}$: *m/z;* 820.37, found: *m/z* 843.3, $[M+Na]^+$; *m/z* 859.27, $[M+K]^+$; ESI *m/z* 843.3 et 845.4 $[M+Na]^+$

Tetra(*p*-phenylene)-*O*-PEG 900 (3a). A solution containing **2** (2.6 g, 2.3 mmol) and 4-biphenyl boronic acid (0.456 g, 2.3 mmol) were dissolved in degassed THF (80 ml). Degassed 2M aqueous Na_2CO_3 (55 mL) was added to the solution and then tetrakis(triphenylphosphine)palladium(0) (16.5 mg, 0.0135 mmol) was added. The mixture was heated at reflux for 60h with vigorous stirring under nitrogen. Cooled to room temperature, the layers were separated, and the aqueous layer was then washed twice with methylene chloride. The solvent was evaporated under reduced pressure to give a white solid product. Pure **3** (1.385 g; 50 %) was isolated after purification by silica gel flash

chromatography using methylene chloride:methanol(16:1 v/v). ^{1}H-NMR**:** (300 MHz, $CDCl_3$, ppm) : δ = 7.69-7.27 (m, 15H, Arom.), 7.0 (d, 2H, *J* = 8.8 Hz, Arom.), 4.17 (t, 2H, *J* = 4.6 Hz, CH_2O-Ar), 3.87 (t, 2H, *J* = 4.6 Hz, CH_2OH), 3.71-3.55 (m, ~74 H, CH_2O). ^{13}C NMR: (75 MHz, $CDCl_3$, ppm) : δ = 158.5, 140.7, 140.1, 139.8, 139.6, 138.9, 133.3, 131.8, 128.8, 128.3, 128.0, 127.9, 127.5, 127.3, 127.00, 115.0, 72.5, 70.8, 70.6, 70.3 69.7, 67.5, 61.7. MALDI-TOF MS Calcd for $C_{64}H_{98}O_{21}$: *m/z* 1202.73; found: *m/z* 1225.43 $[M+Na]^+$; m/z 1241.37 $[M+K]^+$.

Tetra(*p*-phenylene)-*O*-PEG 600 (3b) was isolated in 50 % yield after reaction under the conditions described for **2a** and purification by silica gel flash chromatography using methylene chloride:methanol (20:1 v/v). ^{1}H-NMR: (300 MHz, $CDCl_3$, ppm): δ = 7.69-7.37 (m, 15H, Arom.), 6.96 (d, 2H, *J* = 8.8 Hz, Arom.), 4.14 (t, 2H, *J* = 4.6 Hz, CH_2O), 3.85 (t, 2H, *J* = 4.6 Hz, CH_2OH), 3.71-3.56 (m, ~48H, -CH_2O). ^{13}C NMR: (75 MHz, $CDCl_3$, ppm) : δ = 158.5, 140.7, 140.1, 139.8, 139.6, 138.9, 133.3, 131.8, 128.8, 128.3, 128.0, 127.9, 127.5, 127.3, 127.0, 115.0, 72.6, 70.8, 70.6, 70.3, 69.7, 67.5, 61.7. MALDI-TOF MS Calcd for $C_{50}H_{70}O_{14}$: *m/z* 894.52, found: *m/z* 917.47, $[M+Na]^+$; *m/z* 933.53, $[M+K]^+$

Tetra(*p*-phenylene)-*O*-PEG 900-tosyl (4a). Tosyl chloride (1.9 g; 10 mmol) was added to a stirred solution of **3** (1.3 g, 1.08 mmol) and triethylamine (1.38 g, 10 mmol) in anhydrous methylene chloride (10 mL). The reaction mixture was stirred overnight at room temperature, diluted with 25 ml of dichloromethane and successively washed with dilute HCl, saturated $NaHCO_3$, and water. The organic phase was dried over anhydrous magnesium sulfate and filtered. The solvent was evaporated under reduced pressure to give a colorless oily product. Pure **4** (1.276 g; 87 %) was isolated after purification by silica gel flash chromatography using methylene chloride:methanol(15:1 v/v).^{1}H-NMR: (300 MHz, $CDCl_3$, ppm) : δ = 7.91 (d, 2H,

J = 8.3 Hz, Arom.), 7.79-7.3 (m, 17H, Arom.), 6.98 (d, 2H, *J* = 8.8 Hz, Arom.), 4.17 (t, 2H , CH_2O, *J* = 4.8 Hz), 3.87 (t, 2H, *J* = 4.8 Hz, CH_2O), 3.72−3.39 (m, ~74 H, CH_2O), 2.42(s, 3H, CH_3). ^{13}C NMR: (75 MHz, $CDCl_3$, ppm) : δ = 158.5, 140.7, 140.1, 139.8, 139.7, 138.9, 133.3, 131.8, 130.2, 129.8, 128.8, 128.3, 128.0, 127.5, 127.3, 127.1, 115.0, 70.9, 70.7, 70.6, 69.2, 68.7, 67.6, 21.6. MALDI-TOF MS Calcd for $C_{71}H_{104}O_{23}S$: *m/z* 1356.74, found: *m/z* 1379.67 $[M+Na]^+$; *m/z* 1395.60 $[M+K]^+$

Tetra(*p*-phenylene)-*O*-PEG 600-tosyl (4b) was isolated in 75 % yield after reaction under the conditions described for **4a** and purification by silica gel flash chromatography using methylene chloride:methanol (15:1 v/v).^{1}H-NMR: (300 MHz, $CDCl_3$, ppm) : δ = 7.91 (d, 2H, *J* = 8.3 Hz, , Arom.), 7.78-7.25 (m, 17H, Arom.), 6.96 (d, 2H, *J* = 8.8 Hz, Arom.), 4.13 (t, 2H, *J* = 4.5 Hz, CH_2O), 3.85 (t, 2H, *J* = 4.5 Hz, CH_2O), 3.71−3.55 (m, ~ 48 H, CH_2O), 2.42(s, 3H, CH_3). ^{13}C NMR: (75 MHz, $CDCl_3$, ppm) : δ = 158.5, 146.7, 141.8, 140.7, 140.1, 139.8, 139.7, 133.3 131.8, 130.2, 129.8, 128.8, 128.3, 128.0, 127.5, 127.3, 127.1, 115.0, 70.9, 70.6, 69.7, 69.2, 68.7, 67.6, 21.8. MALDI-TOF MS Calcd for $C_{57}H_{76}O_{16}S$: *m/z* 1048.53, found: *m/z* 1071.58 $[M+Na]^+$: *m/z* 1087.47, $[M+K]^+$

Tetra(*p*-phenylene)-*O*-PEG 900-azide (5a). A solution of **4** (1.27 g, 0.936 mmol) and NaN_3, (0.183g, 2.81mmol) in anhydrous DMF (25 mL) was heated at 60°C for 18 hours and then concentrated. Pure **5** (0.977g, 85 %) was isolated after purification by silica gel flash column chromatography using methylene chloride: methanol (9:1 v/v). ^{1}H-NMR: (300 MHz, $CDCl_3$, ppm): δ = 7.68-7.36(m, 15H, Arom.), 6.99 (t, 2H, *J* = 9.3 Hz, Arom.), 4.16 (t, 2H, *J* = 4.9 Hz, CH_2O), 3.86 (t, 2H, *J* = 4.9 Hz, CH_2O), 3.62-3.55 (m, ~72H, CH_2O), 3.36 (t, 2H, *J* = 5.4 Hz, CH_2N_3). ^{13}C NMR: (75 MHz, $CDCl_3$, ppm) : δ = 158.5, 140.7, 140.1, 139.8, 139.6, 138.9, 133.3, 131.7, 128.8, 128.4, 128.3, 128.0, 127.5, 127.3, 127.03, 115.0, 72.4, 70.8, 70.6,

70.0, 69.7, 68.7, 67.5, 50.7. FT-IR spectra (υ, cm^{-1}): azide absorbance peak 2100 cm^{-1}. MALDI-TOF MS Calcd for $C_{64}H_{97}N_3O_{20}$: *m/z* 1227, found: *m/z* 1250.51, $[M+Na]^+$; *m/z* 1266.48, $[M+K]^+$

Tetra(*p*-phenylene)-*O*-PEG 600-azide (5b) was isolated in 80 % yield after reaction under the conditions described for **5a** and purification by silica gel flash chromatography using methylene chloride:methanol (9:1 v/v) as eluent.^{1}H-NMR: (300 MHz, $CDCl_3$, ppm) : δ = 7.67-7.35(m, 15H, Arom.), 6.98 (d, 2H, *J* = 9.3 Hz, Arom.), 4.14 (t, 2H, *J* = 4.8Hz, *CH*2O), 3.84 (t, 2H, *CH*2O, *J* = 4.8 Hz) 3.61-3.54 (m, ~46H, CH_2O), 3.36 (t, 2H, *J* = 5.2 Hz, , CH_2N_3). ^{13}C NMR: (75 MHz, $CDCl_3$, ppm) : δ = 158.2, 140.5, 139.9, 139.6, 139.5, 138.7, 133.0, 132.36, 128.8, 128.2, 127.9, 127.8, 127.5, 127.3, 127.0, 120.0, 115.0, 70.8, 70.6, 70.0, 69.7, 67.6, 50.7. FT-IR spectra (υ, cm^{-1}): azide absorbance peak 2100cm-1. MALDI-TOF MS Calcd for $C_{50}H_{69}N_3O_{13}$: *m/z* 919.52, found: *m/z* 958.34, $[M+K]^+$

***N*-acetyl-β-D-glucosaminyl-PEG 900-tetra(*p*-phenylene) (6a).** Copper sulfate (51.7mg, 0.325 mmol) and sodium ascorbate (70.7mg, 0.357 mmol) were added into a stirred solution of propargyl-2-acetamido-2-deoxy-β-D-glucopyranoside (0.109 g, 0.42 mmol) and **5** (0.4 g, 0.34 mmol) in water/THF (1:1 v/v). The mixture was heated at 40°C and the reaction was monitored by TLC. After 24 hours, the solution was concentrated under vacuum. The residue was taken up in methylene chloride, filtered and concentrated. Pure **6 (**0.290g, 60 %) was isolated after silica gel flash column chromatography using methylene chloride: methanol (8:2 v/v) as eluent.^{1}H NMR: (400 MHz, DMSO-d6, ppm) δ = 7.97 (s, 1H, triazolyl), 7.83-7.47 (m, 16H, Arom. and NH), 7.06 (d, 2H, *J* = 8.8 Hz, Arom.), 5.00-4.48 (m, 8H), 4.14 (t, 2H, *J* = 4.18 Hz, CH_2O), 3.80 (t, 2H, *J* = 4.8 Hz, CH_2O), 3.61-3.42 (m, ~74H, CH_2O), 3.09 (m, 2H), 1.77 (3H, CH_3). ^{13}C NMR: (100MHz DMSO-d6, ppm) δ = 169.05, 158.26, 143.61, 139.60,

139.10, 138.88, 138.62, 137.77, 131.93, 131.70, 129.0, 128.22, 127.64, 127.22, 126.97, 126.66, 126.55, 124.38, 114.98, 100.22, 77.26, 77.09, 74.27, 70.68, 69.95, 69.77, 69.61, 69.54, 68.95, 68.72, 67.23, 61.26, 61.14, 55.30, 49.32, 23.05. MALDI-TOF MS Calcd for $C_{75}H_{114}N_4O_{26}$: *m/z* 1486.84, found: *m/z* 1509.66 $[M+Na]^+$

***N*-acetyl-β-D-glucosaminyl-PEG 600-tetra(*p*-phenylene) (6b)** was isolated in 53 % yield after reaction under the conditions described for **6a** and purification by silica gel flash chromatography using methylene chloride:methanol (9:1 v/v).^{1}H NMR: (400 MHz, DMSO-d6, ppm) δ = 7.96 (s, 1H, triazolyl), 7.80-7.37 16H (m, 16H, Arom. NH), 7.05 (d, 2H, *J* = 8.8 Hz, Arom.), 5.0-4.48 (m, 8H), 4.12 (m, 2H, CH_2O), 3.78-3.48 (m, ~48H, CH_2O), 3.41 (t, 2H, *J* = 4.8 Hz, CH_2N), 1.78(s, 3H, CH3). ^{13}C NMR: ^{13}C NMR: (100 MHz, DMSO, ppm) δ = 168.9, 158.1, 143.5, 139.4, 138.7, 138.4, 131.9, 131.4, 128.7, 127.9, 127.4, 127.3, 127.2, 126. 9, 126.7, 126.4, 126.3, 123.8, 114.9, 100.1, 76.8, 74.1, 70.7, 67.8, 69.6, 69.4, 68.7, 68.7, 68.5, 67.2, 61.2, 61.1, 55.3, 49.1, 22.7. MALDI-TOF MS Calcd for $C_{61}H_{86}N_4O_{19}$: *m/z* 1178.52, found: *m/z* 1201.70 $[M+Na]^+$ *m/z* 1217.61 $[M+Na]^+$

β-Lactosyl-PEG 900-tetra(*p*-phenylene) (7). Copper sulfate (53.1mg, 0.334 mmol) and sodium ascorbate (72.7mg, 0.367 mmol) were added to a stirred solution of propargyl-β-lactoside (0.167 g, 0.44 mmol) and **5** (0.410g, 0.334 mmol) in water/THF (1:1 v/v). The mixture was heated at 40°C and the reaction was monitored by TLC. After 24 hours, the solution was concentrated under vacuum. The residue was taken up in methylene chloride, filtered and concentrated. Pure **7 (**0.295g 55 %) was isolated after silica gel flash column chromatography using methylene chloride:methanol (7:3 v/v) as eluent.^{13}C NMR (75 MHz, DMSO-d6, ppm) δ = 158.35, 143.45, 138.91 131.61, 131.12, 128.92, 128.14, 127.61, 127.56,

127.12, 126.88, 126.56, 126.47, 125.42, 124.43, 119.94, 114.94, 103.78, 101.77, 80.68, 75.47, 74.91, 73.21, 73.06, 71.58, 70.52, 69.98, 69.91, 69.72, 69.57, 69.50, 68.89, 68.67, 68.09, 67.87, 67.22, 61.59, 60.55, 60.35, 60.18, 49.31. MALDI-TOF MS Calcd for $C_{79}H_{121}N_3O_{31}$: *m/z* 1607.87 found: *m/z* 1630.76 $[M+Na]^+$

Nanoparticles Preparation. The suspension of nanoparticles (aqueous micellar solutions - *C*p = 0.2 - 1.0 mg/mL) were prepared by direct dissolution of the amphiphilic systems in Milli-Q water or in phosphate buffered saline solution (PBS, 10mM, pH 7.2, 1 mM $CaCl_2$,1 mM $MnCl_2$) and stirred for 24 hours at 25°C. The solutions were then filtered using 0.45μm pore size nylon membrane filters in order to remove dust and large aggregates.

Characterization of the Nanoparticles

Dynamic Light Scattering (DLS). The size and polydispersity of the nanoparticles were accessed using DLS measurements. The experiments were performed using an ALV Laser Goniometer, which consists of a cylindrical 22 mW HeNe linear polarized laser with λ = 632.8 nm and an ALV-5000/ALV Multiple Tau Digital Correlator with a 125 ns initial sampling time.[39] The samples were kept at 25 °C. The accessible scattering angle of the equipment ranges from 20° to 150°. All samples were systematically studied at 90° and some of them were studied at different scattering angles varying from 40° to 140°. The solutions were put in 10 mm diameter glass cells. The minimum sample volume required for an experiment was 1 mL. The data were acquired with the ALV-Correlator Control Software and the counting time for each sample was in average 300 s. The distributions of relaxation times - A(t) - were obtained using the CONTIN analysis of the auto-correlation function C(q,t).[40] where the relaxation frequency, Γ is equal to $1/\tau$.[41] The apparent diffusion coefficient (D_{app}) of the nanoparticles at a given copolymer concentration (C_p) is calculated from relation 1.

$$\frac{\Gamma}{q^2}|_{q\to 0} = D_{app} \qquad (1)$$

where q is the wave vector defined as

$$q = \frac{4\pi n}{\lambda}\sin\left(\frac{\theta}{2}\right) \qquad (2)$$

λ being the wavelength of the incident laser beam (632.8 nm), n the refractive index of the sample, and θ the scattering angle. The hydrodynamic radius (R_H) (or diameter, $2R_H$) was calculated from the Stokes-Einstein relation given in relation 3.

$$R_H = \frac{k_B T}{6\pi\eta\Gamma}q^2 = \frac{k_B T}{6\pi\eta D_{app}} \qquad (3)$$

where k_B is the Boltzmann constant, T is the temperature of the sample and η is the viscosity of the solvent (water in this case).[42] As for the radius of gyration (R_g), it was calculated from the elastic part I(q) of the scattered intensity using the Guinier approximation as follows:

$$\ln I = lnI_0 - \frac{1}{3}q^2R_g^2 \qquad (4)$$

Where I is the scattering intensity and I_0 is the scattering intensity at q = 0.

Transmission Electron Microscopy (TEM). The sample preparation was done as follows: 4µL of an aqueous micellar solution was dropped onto a glow-discharged carbon-coated copper grid. Then 4µL of 2% (w/v) uranyl acetate negative stain was added prior to complete drying. After few minutes, the liquid in excess was blotted with a filter paper and the grid was allowed to dry. The specimens were observed using a Philips CM200 microscope operated at

80kV. Images were recorded on Kodak SO163 films, and the negatives were digitized off-line using a Kodak Mega plus CCD camera.

Small-angle X-ray scattering (SAXS). The system was investigated through SAXS at the French CRG Beamline D2AM-BM02 of the European Synchrotron Radiation Facility (ESRF) and at the Brazilian Synchrotron Light Laboratory (LNLS). The results reported herein were obtained at the ESRF. The wavelength (λ) of the incoming beam and the sample-to-detector distance was chosen in such way that the *q*-range, *q* being equal to $(4\pi/\lambda)\sin(\theta/2)$ (θ is the scattering angle) could be covered from 0.15 to 3.0 nm^{-1}. The samples were loaded into sealed borosilicate capillaries (~ 2 mm diameter). The collimated beam crossed the samples and was scattered to an indirect illumination CCD detector (Princeton Instruments). In all cases the 2D-images were found to be isotropic and they were corrected by taking into account the detector dark noise and normalized by the sample transmission**.** The *I*(*q*) vs. *q* curves resulting from the 360° azimuthal integration of the 2D-patterns were further corrected by the subtraction of the scattering of the pure solvent (water). The *I(q) vs. q* scattering profile of the nanoparticles could be fitted by using the spherical copolymer micelle model developed by Pedersen and Gerstenberg.[43] The fitting procedures and other analyses were performed using the SASfit software, which makes use of the least-square fitting approach for minimizing the squared chi (χ^2) parameter. The SASfit software package was developed by J. Kohlbrecher and it is available on-line.[44]

Results and Discussion

Synthesis of the Amphiphiles.

The synthesis of glycosylated rod-coil amphiphiles consisting of tetra(*p*-phenylene) and poly(ethylene oxide) segments is depicted in Scheme 1. Selective monotosylation of PEG (MW 900 and 600) was carried out in presence of silver oxide (Ag_2O) and a catalytic amount of potassium iodide (KI) as reported by Bouzide et al..[45] The tetra-(*p*-phenylene) hydrophobic block was then installed in a two step sequence consisting in the nucleophilic substitution of the tosyl group by 4'-bromo-(1,1'biphenyl)-4-ol followed by a palladium-catalyzed Suzuki coupling with 4'-biphenyl boronic acid as described earlier by Kim et al.[23]. Azidation of the second extremity of the PEG block was further carried out through a tosylated intermediate affording the clickable amphiphiles **5a** and **5b**. The absorption peak of the N_3 group at 2100 cm^{-1} observed by infrared spectroscopy and the ^{13}C signal of the methylene carbon adjacent to the azide group at 50.7 ppm seen by NMR confirmed the efficiency of this transformation. Propargyl β-glycosides of *N*-acetyl-glucosamine and lactose were introduced at the polar head of the amphiphile by copper-catalyzed Huisgen cycloaddition. The reaction was carried out at 40°C with the copper/ascorbate catalytic system in a water/THF mixture to ensure a good solubility of the reactants. Glycosylated conjugates $\phi_4PEG_{900}GLcNAc$ **6a**, $\phi_4PEG_{600}GLcNAc$ **6b** and $\phi_4PEG_{900}Lac$ **7** were respectively isolated in 60%, 53% and 55% yields after purification by silica gel chromatography. The IR spectra confirmed the coupling efficiency with the disappearance of the signal due to the azide group. Finally, the structures of the three glycosylated amphiphiles were unambiguously confirmed by NMR spectrometry in DMSO, a good solvent for each part of the molecule and by MALDI-TOF-MS. **(Figure 1)**.

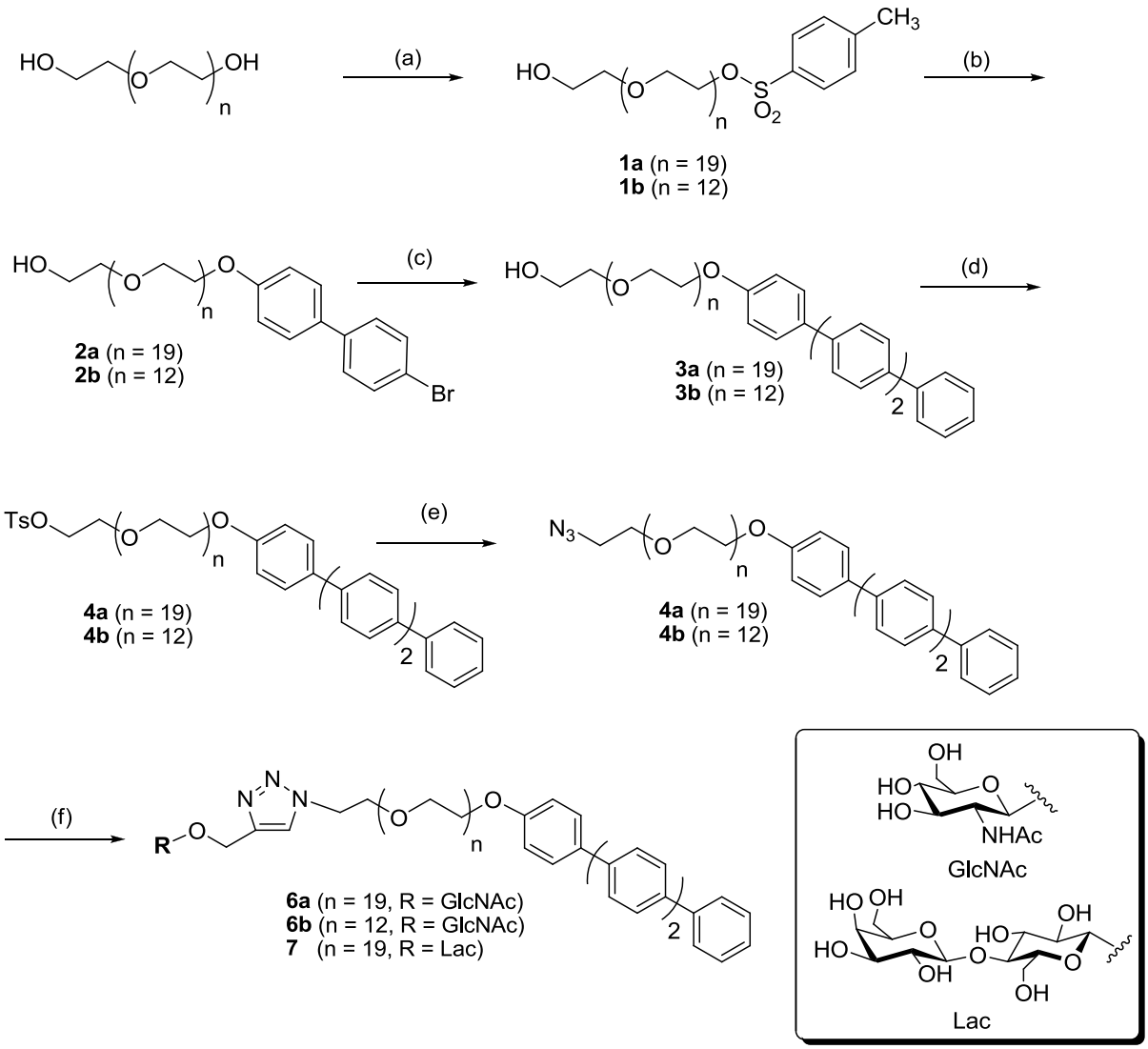

Scheme 1. Synthetic strategy used in the preparation of $\phi_4PEG_{900}GLcNAc$ **6a,** $\phi_4PEG_{600}GLcNAc$ **6b** and $\phi_4PEG_{900}Lac$ **7: a)** TsCl , Ag_2O , KI , CH_2Cl_2 (**1a:** 55%, **1b:** 58%); **b)** 4-(4-Bromophenyl)phenol, K_2CO_3, CH_3CN (**2a:** 52%, **2b:** 52%); **c)** 4-Biphenyl boronic acid, $(PPh_3)_4Pd$, Na_2CO_3 , THF (**3a:** 50%, **3b:** 50%); **d)** TsCl , $C_6H_{15}N$, CH_2Cl_2 (**4a:** 87%, **4b:** 75%), e) NaN_3, DMF (**5a:** 85%, **5b:** 80%); **f)** $CuSO_4$ sodium ascorbate, propargyl-2-*N*-acetamido-2-deoxy-β-D-glucopyranoside or propargyl β-lactoside, H_2O/THF (**6a:** 60%, **6b:** 53%, **7:** 55%)

Both ^{1}H and ^{13}C NMR spectra displayed characteristic signals of the aromatic groups, the ethylenoxide parts and the carbohydrate units as well as the signals of the triazolyl ring. Figure 1 depicts as representative example the ^{13}C NMR spectra of $\phi_4PEG_{900}GlcNAc$ **6a** in (DMSO-d_6).

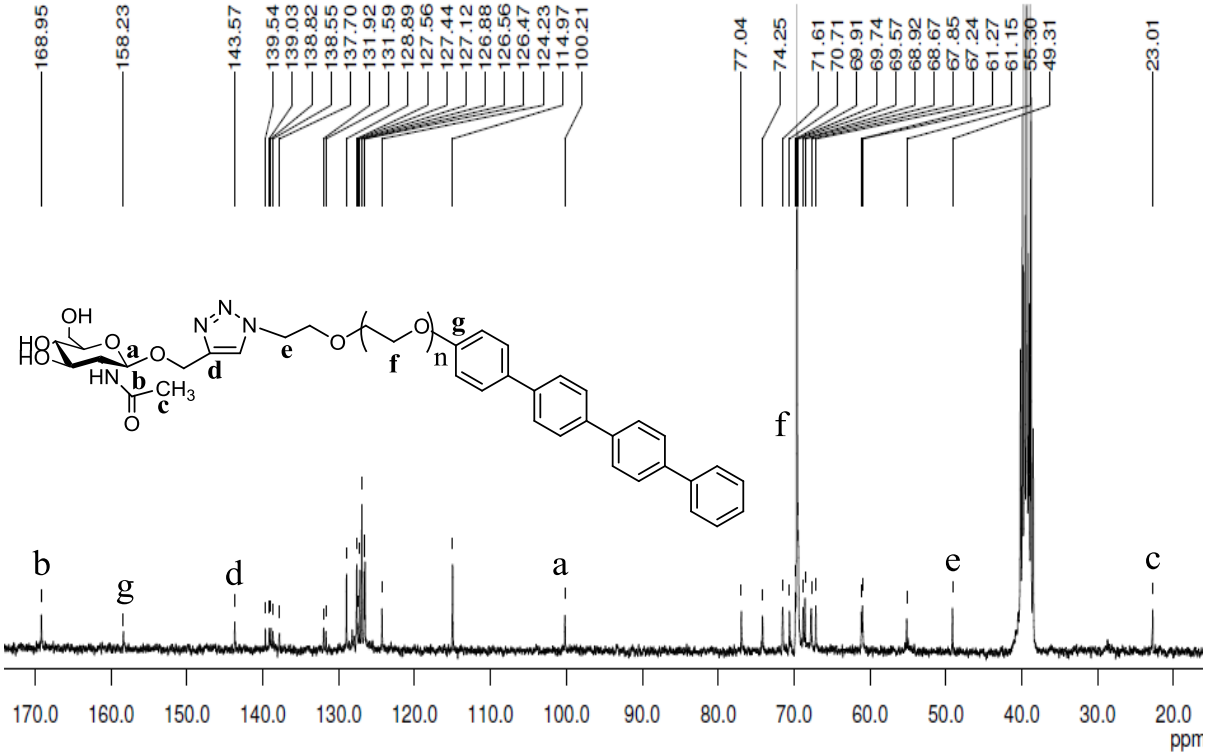

Figure 1. ^{13}C spectra of $\phi_4PEG_{900}GlcNAc$ **6a** in DMSO-d_6.

Self-Assembly of the PEG_{900}-Based Amphiphiles

Dynamic Light Scattering (DLS). Figure 2 shows typical autocorrelation functions C(q,t) measured at scattering angle of 90° and the respective distributions of the relaxation times A(t) as revealed by CONTIN analysis for 0.5 mg/mL $\phi_4PEG_{900}N_3$ **5a** solution in water. One can clearly notice the formation of monodisperse nanoparticles ($2R_H$ = 10.3 nm). Besides the intensity contribution related to the presence of well-defined micelles, it can be observed the

presence of a light scattering contribution attributed to the formation of large aggregates as recently observed by our research group in the study of the self-assembly of different carbohydrate-based nanoparticles.[46] However, as discussed in this previous paper, the light scattering intensity is sensitive to the concentration of aggregates multiplied by their molar mass ($I \sim K_1 c M_w$). Consequently, estimating for compact solid particles, the light scattering is proportional to R^3, being R the radius of the scattering object ($I \sim K_2 c R^3$). If one considers the distribution of R_H by taking into account the contribution of the total volume of particles, the amount of large aggregates is substantially small, almost negligible as it can be noticed in the inset of Figure 2a which depicts the distribution of R_H (determined from the distribution of τ using the Stokes-Einstein equation) when taking into account the contribution of the volume of particles instead of the light scattering contribution. The same rationalization is also valid for the others protein-free explored systems.

The negligible presence of large aggregates in the system can be also evidenced in the TEM image (Figure 2b) where one can clearly see the self-assembly of small spherical micelles. Such results are a very similar to those obtained by Lee *et al* when investigating similar systems.[22]

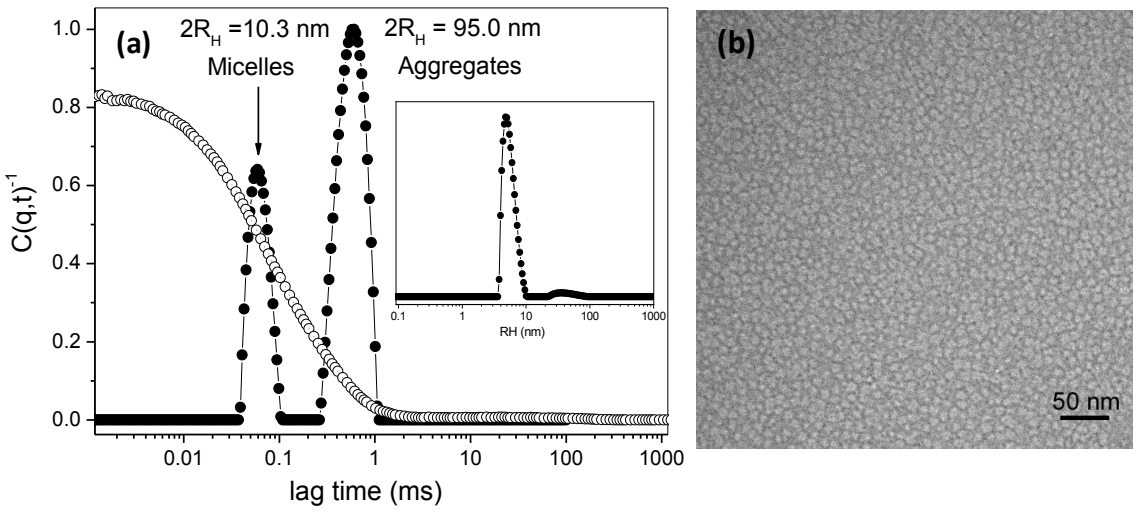

Figura 2. (a) Typical autocorrelation function C(q,t) measured at $\theta = 90°$ and the respective distribution of relaxation times A(t) as revealed by CONTIN analysis of an aqueous 0.5 mg/mL solution of $\phi_4PEG_{900}N_3$ **5a** in water at 25°C. In the inset it is given the respective distribution of R_H by considering the contribution of the particles related to their total volume. **(b)** TEM image of self-assembled $\phi_4PEG_{900}N_3$ spherical monodisperse nanoparticles in water. Scale bar is 50nm

Figure 3 (a and b) shows typical autocorrelation functions C(q,t) measured at scattering angles 50° (□), 90° (●), and 130° (○) and the distributions of the relaxation times A(t) at 90° as revealed by CONTIN analysis for **(a)** 0.5 mg/mL ϕ_4PEG_{900}GLcNAc **6a** and **(b)** 0.5 mg/L ϕ_4PEG_{900}Lac **7** in water at 25°C. The insets depict the typical angular variation of the frequency $\Gamma = 1/\tau$ measured as a function of q^2 indicating a diffusive behavior of the scattering particles. The hydrodynamic radius of **6a** and **7** were calculated using the Stokes-Einstein relation and they are practically the same as compared to the value obtained before the click chemistry reaction (amphiphile **5a**). The hydrodynamic size of both sorts of nanoparticles was determined as being equal to $2R_H = 10.0$ nm.

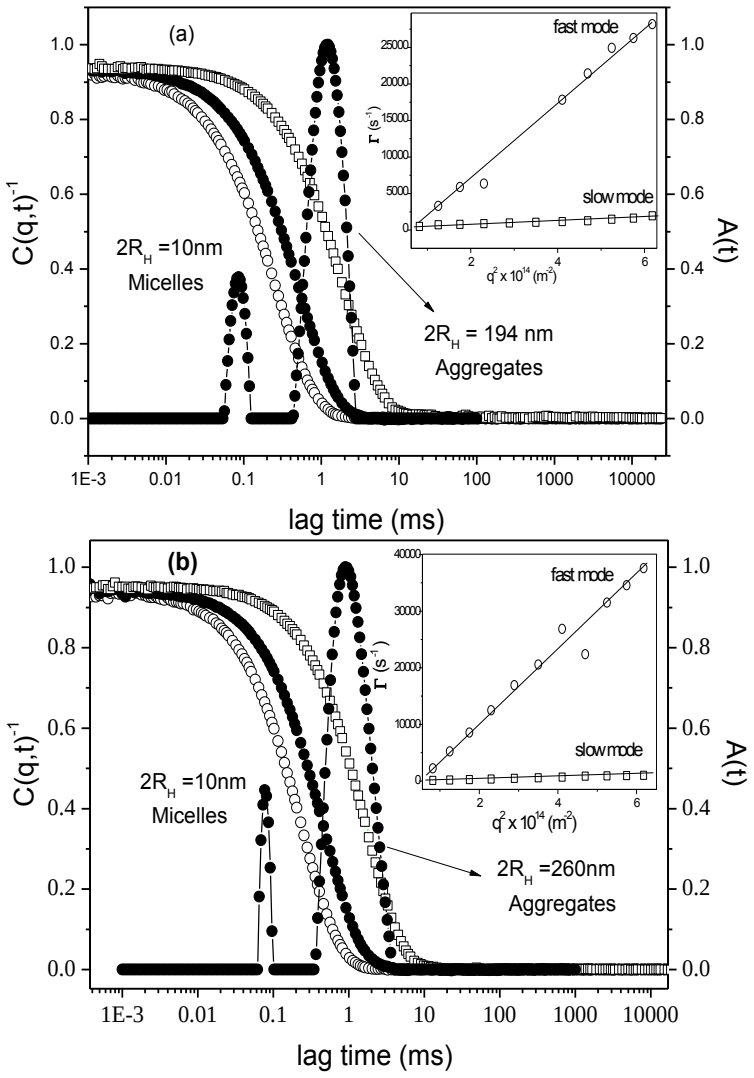

Figure 3. Autocorrelation functions C(q,t) measured at scattering angles 50 (□), 90 (●), and 130° (o), and the distributions of the relaxation times A(t) at 90° as revealed by CONTIN analysis for **(a)** 0.5 mg/mL ϕ_4PEG$_{900}$GLcNAc **6a** and **(b)** 0.5 mg/L ϕ_4PEG$_{900}$Lac **7** in water at 25°C. The insets show the dependence of the relaxation frequency (Γ) on the square of the wave vector (q^2).

Transmission Electron Microscopy (TEM). Figure 4 illustrates the TEM images of the nanoparticles resulting from the self-assembly of ϕ_4PEG$_{900}$GLcNAc **6a** or 4ϕPEG$_{900}$Lac **7** in water. The formation of mainly nano-sized spherical structures (D_H ~ 10nm) is clearly seen

suggesting that even though the dynamic light scattering technique is very sensitive to the presence of large aggregates, their real number in the current systems is negligible as mentioned before.

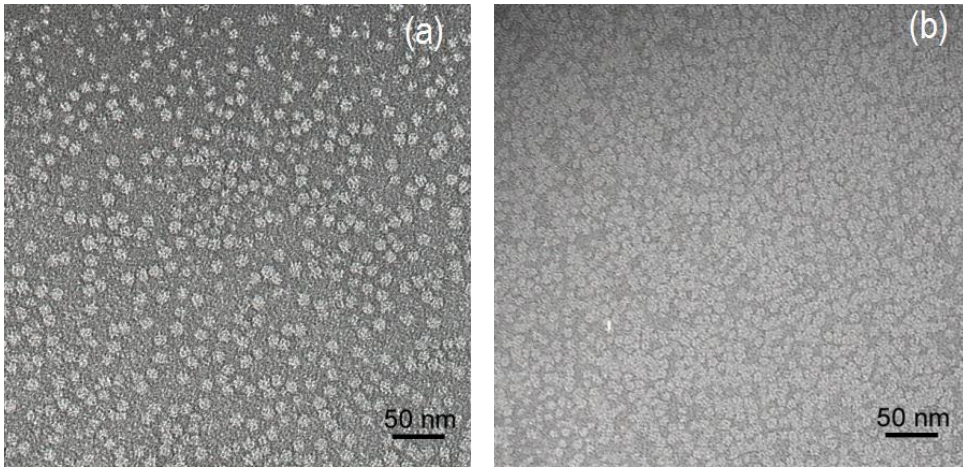

Figure 4. TEM observation of the self-assemblies: monodisperse spherical nanoparticles formed in water. The structures were visualized after negative staining **(a)** $\phi_4PEG_{900}GLcNAc$ **6a** and **(b)** $\phi_4PEG_{900}Lac$ **7**. Scale bar is 50 nm.

The morphology, size and structure of nanoparticles are mainly dependent on the balance of forces of attraction and repulsion between the different blocks of the amphiphiles. The spherical micelles found here are compatible with the volumetric fraction of the hydrophobic region (φ) < 1/3.[14, 16, 47] Indeed, the calculated hydrophobic volume fraction of **5a**, **6a** and **7** based on the density of each constituent was equal to 0.29, 0.24 and 0.23 respectively. Therefore, spherical micelles are expected.[14, 16, 42]

Small-angle X-ray scattering (*SAXS*). In addition to TEM images, SAXS measurements were performed in order to probe the size, shape and internal structure of the scattering particles. The scattering intensity $I(q)$ of an isotropic solution of highly regular particles embedded in a

matrix with a constant electron density, after normalization with the background scattering of the solvent is given by:

$$I(q) = n\,P(q)\,S(q) \qquad (5)$$

Where in n is the number of scattering particles per unit volume, $P(q)$ is the form factor of an individual particle, and $S(q)$ is the structure factor arising from long-range correlations between scattering centers. For widely separated systems as is the case of solutions with low copolymer content, $S(q) \sim 1$, and $I(q)$ consequently represents the form factor $P(q)$ that reflects size and shape of the scattering objects.

Figure 5 shows the SAXS patterns of ϕ_4PEG$_{900}$GLcNAc **6a** (top) and ϕ_4PEG$_{900}$Lac **7** (bottom) in water at 25°C and at c = 40 mg/mL. Such copolymer concentration gives a reasonable signal-to-noise statistics without affecting the micellar structure and still with no interference of $S(q)$. The presence of association colloids is suggested by the pronounced X-ray scattering intensity at the low-q range.

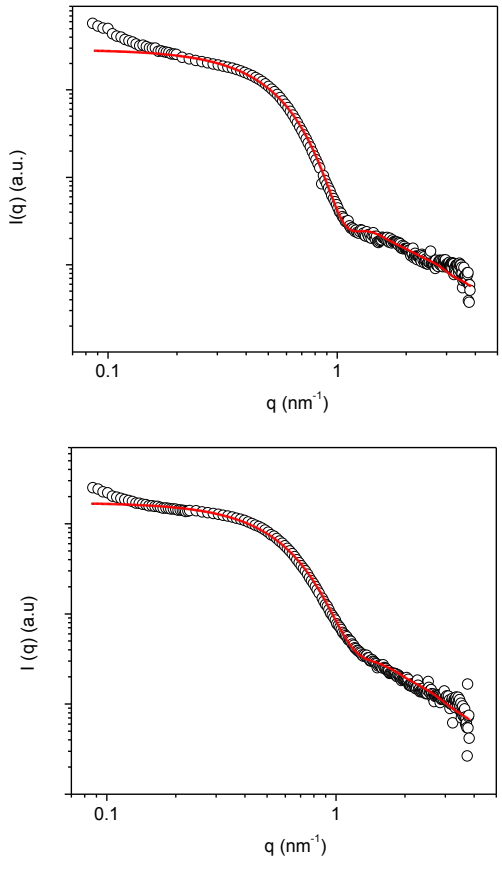

Figure 5. Experimental SAXS data (symbols) and respective curve fittings using the spherical copolymer micelle model (lines) for solutions containing ϕ_4PEG$_{900}$GLcNAc **6a** (top) and ϕ_4PEG$_{900}$Lac **7** (bottom) dissolved in water at c = 40 mg/mL and 25°C.

The high-q range profile for the self-assembled nanoparticles is dominated by the so-called "*blob*" scattering. This is due to the fact that the scattering contribution coming from the PEG chains dissolved in the micellar corona dominates the X-ray scattering profile at the high-q region which is dictated ideally by the Debye function and therefore by a nearly q^{-2} dependence depending on the conformation of the flexible polymer chains. Indeed, the SAXS profiles could be satisfactorily fitted by using the so-called spherical copolymer micelle model formerly developed by Pedersen and Gerstenberg.[43] Such a model describes the scattering for micelles consisting of a homogeneous spherical core having corona chains that follow Gaussian statistics attached to the surface of the core, as depicted in Figure 6.

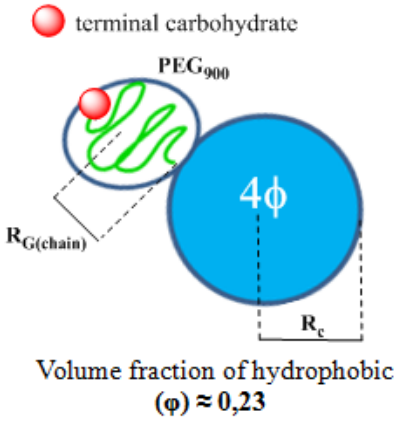

Figure 6. Schematic representation for the micellar form factor analysis according to the spherical copolymer micelle model. It considers a dense spherical core of radius R_c and Gaussian chains with radius of gyration $R_{G(chain)}$ attached to the core.

This model has a large number of fitting parameters, namely: $R_{G(chain)}$, d, R_c, N_{agg} and the excess scattering length density of the core and corona forming blocks (β_{core} and β_{chain}). Therefore, it is usually not possible to get a single set of fitting parameters if some of the parameters are not preset and generally the fittings provide ambiguous results. Hence, during the fitting procedures the parameters β_{chain} (7.30 x 10^{-12} cm) and d were kept fixed. The parameter d was preset as d = 1 which mimics the nonpenetration of the corona chains into the core. The value of β_{chain} was calculated in the following way:

$$\beta_{chain} = NV_{PEG}(\sigma_{PEG} - \sigma_{solvent}) \quad (6)$$

where N is the degree of polymerization of the polymer segment, V_{PEG} is the volume of one PEG monomer unit, σ_{PEG} is the scattering length density of the polymer segment and σ_{solv} is the scattering length density of the solvent. The volume occupied by a single monomer unit V_{PEG} was determined by taking into account the homopolymer density (d_{PEG} = 1.08 g/mL) and the values of the scattering length densities of the solvent (σ_{water} = 9.42 x 10^{10} cm^{-2}) and monomer unit (σ_{PEG} = 9.99 x 10^{10} cm^{-2}) were calculated using the average chemical composition of each component and its mass density (d_x):

$$\sigma_x = \frac{b_e d_x N_A}{M_x} \sum_i n_i z_i \quad (7)$$

where x accounts for H_2O or PEG, N_A is the Avogadro's number, and $n_i z_i$ is the number of electrons in each unit. Finally, b_e is the Thomson scattering length (the scattering length of an electron, $b_e = 2.817 \times 10^{-13}$ cm).

The fitting parameters were therefore N_{agg}, R_c, $R_{G(chain)}$ and β_{core}. In Figure 5, the solid red lines correspond to the best fittings achieved using the spherical copolymer micelle model. The high quality of the fittings can be straightforwardly noticed and indeed attested by χ^2-values which remained below 1.7. The fittings have been performed without taking into

account the polydispersity of the micelles attesting that such parameter is reasonable low as demonstrated by previous TEM and DLS results. Besides, we have observed that in some cases the very low-*q* region was not fitted to the same degree of accuracy, which is due to the presence of a small number of very large aggregates with loose structure as already evidenced by the DLS experiments. The parameters extracted from the SAXS curve fittings are listed in **Table 1**.

Table 1. Physical-chemical properties of scattering nano-objects determined using SAXS measurements.

Copolymer	R_c (nm)	R_G (nm)	L^a (nm)	$R_{mic}{}^b$ (nm)	N_{agg}	β_{core} (10^{-12} cm)	A_c (nm^2)	a
$\phi_4PEG_{900}GlcNAc$	2.5	0.9	1.8	4.3	41	2.6	1.9	-1.7
$\phi_4PEG_{900}Lac$	2.1	1.0	2.0	4.1	30	2.6	1.8	-2.0

[a] $L = 2R_G$ (thickness of the micellar corona) ; [b] $R_{mic} = R_c + L$

The core radius (R_c) was found to be ~ 2.0-2.5 nm and the R_G of the PEG corona chains is ~ 0.9-1.0 nm. The reduction in the micelar core radius is balanced by the slight increase in $R_{G(chain)}$. Since R_c and N_{agg} were determined, the core surface area available per PEG chain in the micellar corona (A_c) can be calculated following relation (9):

$$A_c = \frac{4\pi R_c^2}{N_{agg}} \qquad (9)$$

The values are also listed in **Table 1**. The conformation of the PEG chains should depend itself on such physical chemical variable: as A_c decreases a larger R_G might be expected and thus, the smaller the area available on the core surface, the more stretched configuration the PEG chains is assumed. In such cases, the q^{-a} slope in the high-q range reveals important information about the chains statistics[48] namely a = -2 for Gaussian chains (polymers in a theta solvent), a ~ -1.67 for chains with excluded volume (polymer in a good solvent), and a = -1 for rigid rodlike chains. The values of a (**Table 1**) suggest that the PEG chains at the ϕ_4PEG$_{900}$GlcNAc amphiphile are slightly more stretched compared to ϕ_4PEG$_{900}$LAc.

The micellar dimension (R_{mic}) calculated as $R_c + 2R_G$ was found to be in the range 4.1-4.3 nm. One should have in mind that for spherical shape (micellar core-shell) objects the structure sensitive parameter ρ ($\rho = R_G/R_H$) is theoretically equal to 0.774.[49] Therefore, the whole micellar size (R_{mic}) monitored through SAXS should be slightly smaller than R_H monitored by DLS (R_H ~ 5 nm).

Self-Assembly of the PEG$_{600}$-Based Amphiphiles

Besides the PEG$_{900}$ glycoconjugates, it was synthesized and investigated the self-assembly of PEG$_{600}$-based amphiphiles. The motivation was due to the fact that the self-assembly morphologies are strongly dependent on the hydrophilic and hydrophobic balance of the material and an order-to-order transition might be achieved by manipulating such property. In the current case, the hydrophobic polyaromatic segment of the amphiphile was kept constant while the PEG hydrophilic region was reduced to PEG$_{600}$.

Figure 7 shows the autocorrelation functions C(q,t) measured at scattering angles 50° (□), 90° (●), and 130° (O), and the distributions of the relaxation times A(t) at 90° as revealed by CONTIN analysis for (a) 0.4 mg/mL ϕ_4PEG$_{600}$N$_3$ **5b** and (b) 0.5 mg/mL ϕ_4PEG$_{600}$GLcNAc

6b in water at 25°C. The insets in Figure 5 show the variation of the relaxation frequencies (Γ) as a function of the square of the wave vector (q^2).

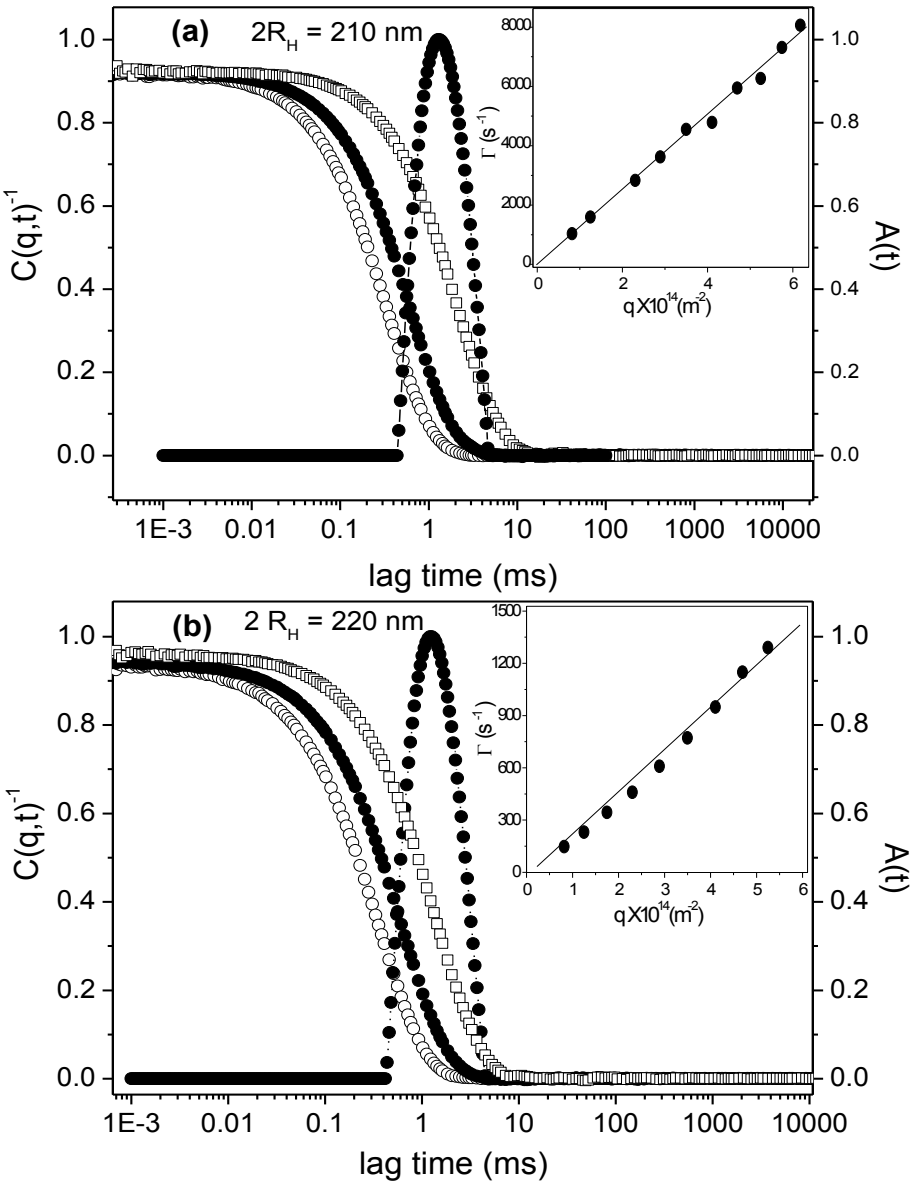

Figure 7.Autocorrelation functions C(q,t) measured at scattering angles 50° (□), 90° (●), and 130° (○), and distributions of the relaxation times A(t) at 90° as revealed by CONTIN analysis for **(a)** 0.4mg/mL $\phi_4PEG_{600}N_3$ **5b** and **(b)** 0.5mg/mL $\phi_4PEG_{600}GLcNAc$ **6b** in water at 25°C. The insets show the variation of the relaxation frequencies (Γ) as a function of the square of the wave vector (q^2).

The DLS experiments show that the reduction in the hydrophilic volume fraction of the amphiphilic systems led to completely different self-assembly morphologies. The PEG_{600}-based amphiphiles self-assembled in water into nanoparticles with $2R_H \sim 215$ nm. They were also investigated using static light scattering (SLS) measurements varying the scattering angle (θ) from 30° to 150° with a 15° stepwise increase since for large particles ($R_g > \lambda/20$) the angular dependence of the scattered light is related to the particle form factor $P(q)$ and ultimately for $qR_g < 1$ the form factor is given by:

$$P(q) = \frac{I(q)}{I(0)} \sim 1 - \frac{q^2 R_g^2}{3}$$

Therefore, one can use the Guinier approximation (eq. 4) in order to extract the radius of gyration of the scattering objects.

Figure 8 shows the representative Guinier plot from the elastic light scattering intensity of Figure 7a **(**$\phi_4PEG_{600}N_3$ **5b** in water at 25°C). The profile shows basically a straight line suggesting the absence of large aggregates and the main contribution of light scattering intensity coming from one single distribution of particles. The R_g value determined from the slope was equal to 103 nm.

The static and hydrodynamic dimensions of the scattering particles are dependent on the macromolecular structure and a combination of both may provide qualitative information about its architecture. This can be done from the values of the structure-sensitive parameter (ρ) which is defined by the ratio between R_g and R_H.[49] The predicted value of $\rho = R_g / R_H$ for a vesicular particle is ~ 1.0. Once the hydrodynamic radius (R_H) for 0.4 mg/mL $\phi_4PEG_{600}N_3$ was found equal to 105 nm, the experimental value obtained for amphiphile **5b** was $\rho = 0.98$ showing reasonable agreement with the theoretical value for vesicular morphologies.

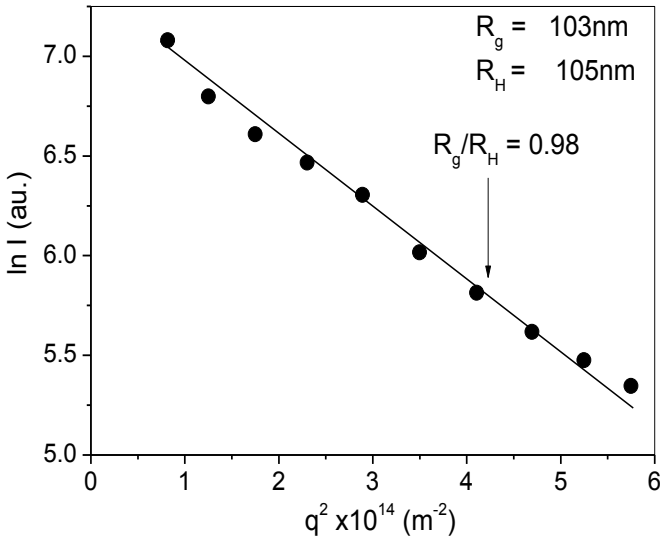

Figure 8. Guinier plot calculated from the elastic light scattering intensity of Figure 5 **(a)** $\phi_4PEG_{600}N_3$ **5b** in water at 25°C.

The vesicular morphology was further confirmed using TEM as illustrated in Figure 9.

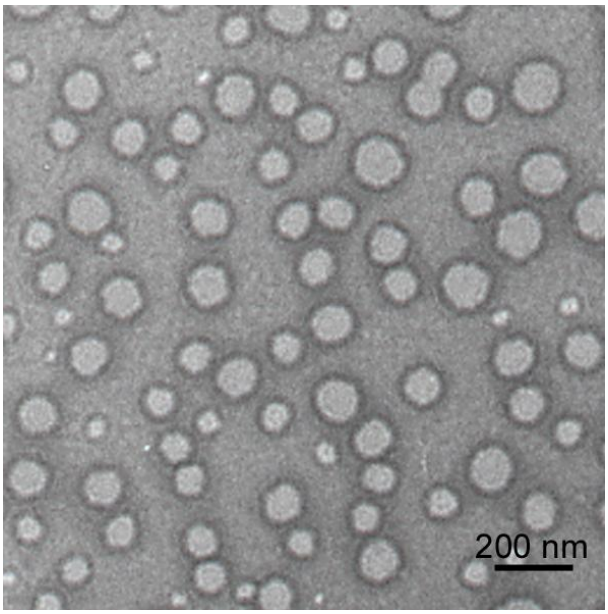

Figure 9. TEM image visualized after negative staining of self-assembled $\phi_4PEG_{600}N_3$ **5b** vesicles in water. Scale bar is 200 nm

Figure 9 shows the TEM image before the coupling reaction. The result is consistent with DLS and SLS measurements. It evidences that by changing the hydrophilic section of the amphiphiles from PEG_{900} to PEG_{600} it was successfully possible to change the architecture from spherical micelles to vesicles. As mentioned before, the spherical micelles are compatible with the volume fraction of the hydrophobic region (φ) < 1/3.[14, 16, 47] The calculated hydrophobic volume fraction of $\phi_4PEG_{900}N_3$ **5a**, ϕ_4PEG_{900}GLcNAc **6a,** and ϕ_4PEG_{900}Lac **7** were equal to **0.29**, **0.24** and **0.23** respectively, thus spherical micelles are expected. On the other hand, the calculated hydrophobic volume fraction of $\phi_4PEG_{600}N_3$ **5b** and ϕ_4PEG_{600}GLcNAc **6b** were equal to 0.38 and 0.31[14, 16, 42] matching with the theoretical values to the formation of vesicular morphologies.

Specific interactions of the nanoparticles with WGA and PNA lectins

Specific interactions with lectins were further evidenced by DLS confirming the bioavailability of the sugar residues on the surface of the micellar nanoparticles. Figure 10 shows the autocorrelation functions C(q,t) and the distributions of the relaxation times A(t) at a scattering angle of 90° as revealed by CONTIN analysis of 0.5 mg/mL solution of ϕ_4PEG_{900}Lac **7** before and after addition of non-binding or binding proteins.

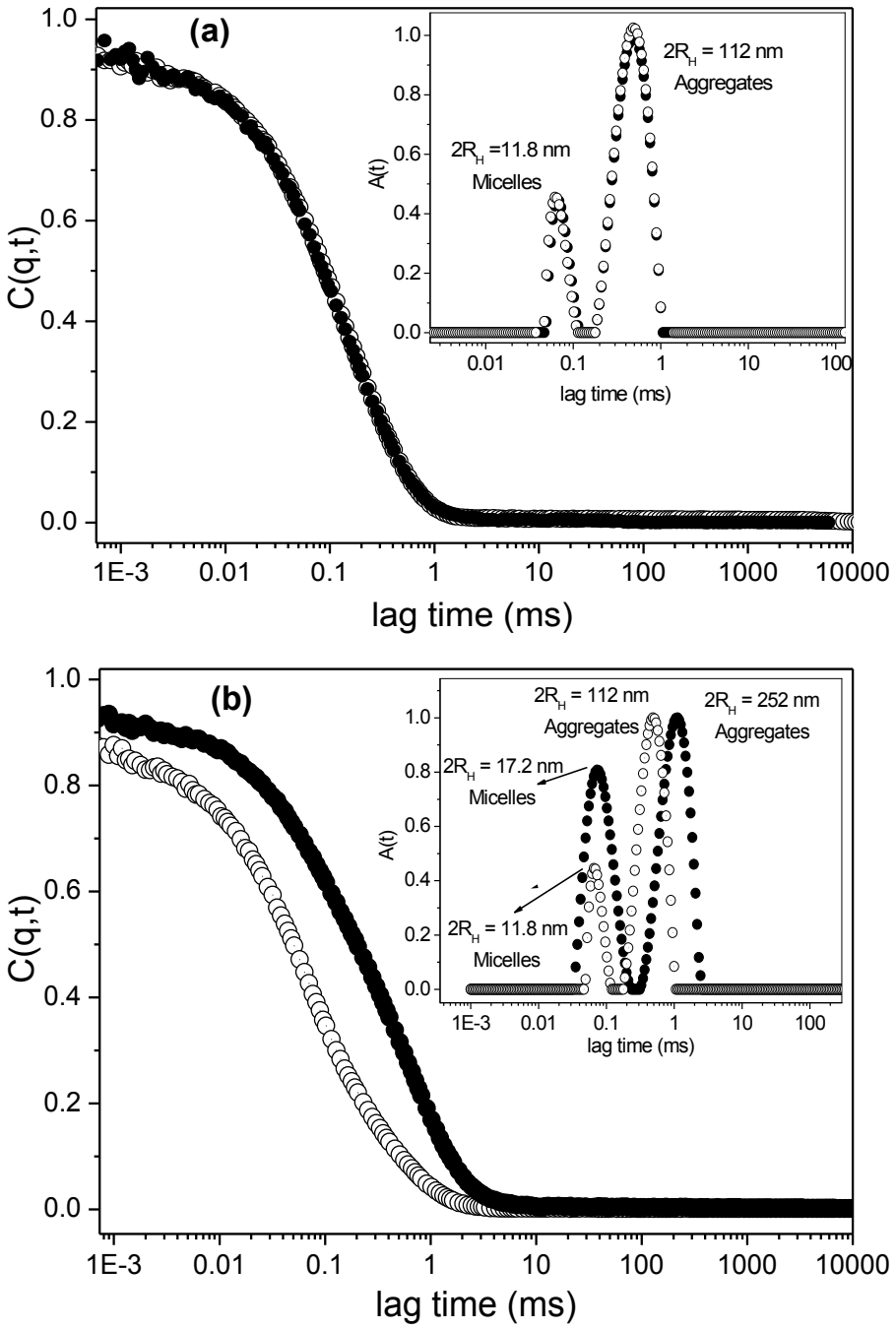

Figure 10. Typical autocorrelation functions C(q,t) and distributions of the relaxation times A(t) at scattering angle of 90° as revealed by CONTIN analysis functions of solutions of 0.5mg/mL $\phi_4PEG_{900}Lac$ in 10mM PBS buffer, pH 7.2 containing 150mM NaCl, 0.1 mM $CaCl_2$ and 0.1mM $MnCl_2$ at 25°C, in absence (○) and in the presence of protein (•),**(a)** WGA (4μL, 1.0 mg/mL) , **(b)** PNA (4μL, 1.0 mg/mL^{-1}).

The addition of WGA, that has no affinity for lactose, does not perturb the system at all. The autocorrelation curve as well as the distribution of relaxation times remained as before the addition of WGA. On the other hand, as shown in Figure 10b, the interaction of *N* lactosyl-covered spherical micelles with PNA lectin significantly increases the micellar hydrodynamic radius R_H from 11.8 nm to 17.2 nm. It clearly evidences the specific interaction of the protein with lactose units available on the shell of the nanoparticles.

Additionally, in Figure 11 it is depicted the distributions of relaxation times, A(t) from the DLS correlation functions at 1.0 mg/mL ϕ_4PEG_{900}GlcNac **6a** and 10 mM phosphate buffer saline (pH 7.2) and 150 mM NaCl, 0.1mM $CaCl_2$ and 0.1mM $MnCl_2$ at 25°C in the absence (○) and in the presence of protein (•),**(a)** PNA (4µL, 1.0 mg/mL) , **(b)** WGA (2µL, 1.0 mg/mL^{-1}) and **(c)** only lectin WGA (14µL, 1.0 mg/mL^{-1}). Figure 11 is divided into three parts: the first part **(a)** shows that the spherical nanoparticles coated with the GlcNAc units are not perturbed by the addition of the lectin PNA, keeping the same distribution of relaxation times. This observation is in good agreement with the fact that PNA is a galactosyl binding protein and having no affinity to GlcNAc residues. In contrast, in the second part of the Figure 11 **(b)**, variations in the distribution of relaxation times are observed due to the addition of WGA lectin (2µL, 1.0 mg/mL^{-1}), highlighting interactions of the spherical micelles with the protein. These modifications can unambiguously be attributed to specific binding of the nanoparticules with the lectin and not only to the sole presence of the protein in the solution as shown by the totally different distribution profile (Figure 11 (**c**)) of the WGA lectin alone at higher concentration WGA (18µL, 1.0 mg/mL^{-1}). This result attests the presence the GlcNAc residues on the surface of the self-assembled particles and their ability to specifically interact with the specific carbohydrate lectin.

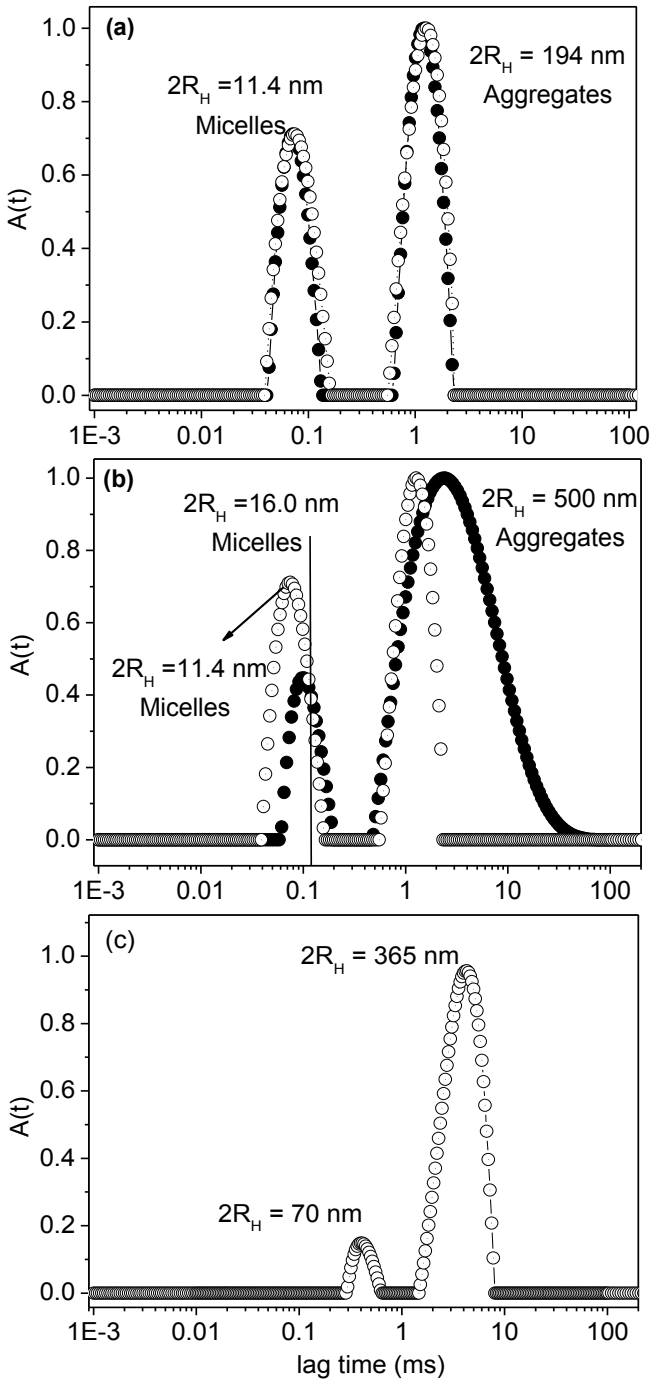

Figure 11. Respective distribution of the relaxation times, A(t) from the DLS correlation functions for 1.0 mg/mL $\phi_4PEG_{900}GlcNac$ **6a** at 10 mM phosphate buffer saline (pH 7.2) and 150 mM NaCl, 0.1mM $CaCl_2$ and 0.1mM $MnCl_2$ at 25°C in the absence (○) and in the presence of protein (•),**(a)** PNA (4µL, 1.0 mg/mL) , **(b)** WGA (2µL, 1.0 mg/mL^{-1}) and **(c)**

(c) WGA (18µL, 1.0 mg/mL^{-1})lectin solution obtained in 10mM phosphate buffer, pH 7.2 containing 150mM NaCl, 0.1mM $CaCl_2$ and 0.1mM $MnCl_2$ at 25°C.

Similar DLS measurements confirmed a pronounced change in the micellar hydrodynamic radius and a significant increase in the size of the micellar aggregates for ϕ_4PEG_{900}Lac **7** in presence of PNA lectin while the addition of the WGA did not modify the system at all (data not shown). These experiments clearly demonstrate that PNA and WGA lectins specifically interact with N-acetyl-glucosamine and lactose particles, respectively, thus supporting the assumption that the carbohydrates are exposed at the surface of the micelles and could provide specific labeling nanoparticulate systems.

Conclusions

In conclusion, new glycosylated rod-coil amphiphilic systems have been prepared by click coupling of sugar residues onto azido-terminated PEG-tetra(*p*-phenylene) precursors. These block copolymer systems have been shown to self-assemble in water into well-defined nanoparticles whose size and morphology were intimately related to the hydrophobic volume fraction of the amphiphile. Vesicles were obtained with a PEG_{600} corona while highly regular spherical micelles with a mean diameter of 10 nm were observed for the PEG_{900} glycoconjugates as indicated by DLS, TEM and SAXS characterization. The ability of the self-assembled nanoparticles to interact with specific carbohydrate lectin was also demonstrated by DLS confirming the potentiality of such micelles in medical applications such as diagnosis or drug delivery systems.

Acknowledgments

We acknowledge the financial support from CNRS and CAPES-COFECUB (project 620/08). The ESRF and LNLS are acknowledged for supply the beam time (Proposals 02 01 784 and 9967 respectivley). The technical assistance of C. Rochas during the experiments at ESRF is greatly acknowledged. F.C.G. acknowledges FAPESP (Grant 2010/06348-0). Stephanie Boullanger is acknowledged for the mass spectrometry analyses.

References

1. Sinha, R., Nanotechnology in cancer therapeutics: bioconjugated nanoparticles for drug delivery. *Molecular Cancer Therapeutics* **2006,** 5, (8), 1909-1917.
2. Hillaireau, H.; Couvreur, P., Nanocarriers' entry into the cell: relevance to drug delivery. *Cellular and Molecular Life Sciences* **2009,** 66, (17), 2873-2896.
3. Yuan, F.; Leunig, M.; Huang, S. K.; Berk, D. A.; Papahadjopoulos, D.; Jain, R. K., Microvascular permeability and interstitial penetration of sterically stabilized (stealth) liposomes in a human tumor xenograft. *Cancer Research* **1994,** 54, (13), 3352-3356.
4. Allen, T. M.; Hansen, C.; Martin, F.; Redemann, C.; Yau-Young, A., Liposomes containing synthetic lipid derivatives of poly(ethylene glycol) show prolonged circulation half-lives in vivo. *Biochimica et Biophysica Acta (BBA) - Biomembranes* **1991,** 1066, (1), 29-36.
5. Basu, S.; Harfouche, R.; Soni, S.; Chimote, G.; Mashelkar, R. A.; Sengupta, S., Nanoparticle-mediated targeting of MAPK signaling predisposes tumor to chemotherapy. *Proceedings of the National Academy of Sciences* **2009,** 106, (19), 7957-7961.
6. Niikura, K.; Nagakawa, K.; Ohtake, N.; Suzuki, T.; Matsuo, Y.; Sawa, H.; Ijiro, K., Gold Nanoparticle Arrangement on Viral Particles through Carbohydrate Recognition: A Non-Cross-Linking Approach to Optical Virus Detection. *Bioconjugate Chemistry* **2009,** 20, (10), 1848-1852.
7. Varki, A., Biological roles of oligosaccharides: all of the theories are correct 10.1093/glycob/3.2.97. *Glycobiology* **1993,** 3, (2), 97-130.

8. Raz, A.; Meromsky, L.; Lotan, R., Differential expression of endogenous lectins on the surface of nontumorigenic, tumorigenic, and metastatic cells. *Cancer Research* **1986,** 46, (7), 3667-3672.
9. Gorelik, E.; Galili, U.; Raz, A., On the role of cell surface carbohydrates and their binding proteins (lectins) in tumor metastasis. *Cancer Metastasis Reviews* **2001,** 20, (3-4), 245-277.
10. Smart, J., Lectin-mediated drug delivery in the oral cavity. *Advanced Drug Delivery Reviews* **2004,** 56, (4), 481-489.
11. Abu-Dahab, R., Lectin-functionalized liposomes for pulmonary drug delivery: effect of nebulization on stability and bioadhesion. *European Journal of Pharmaceutical Sciences* **2001,** 14, (1), 37-46.
12. Zhu, J. M.; Yan, F.; Guo, Z. W.; Marchant, R. E., Surface modification of liposomes by saccharides: Vesicle size and stability of lactosyl liposomes studied by photon correlation spectroscopy. *Journal of Colloid and Interface Science* **2005,** 289, (2), 542-550.
13. Yamazaki, N., Endogenous lectins as targets for drug delivery. *Advanced Drug Delivery Reviews* **2000,** 43, (2-3), 225-244.
14. Lim, Y. B.; Moon, K. S.; Lee, M., Rod-coil block molecules: their aqueous self-assembly and biomaterials applications. *Journal of Materials Chemistry* **2008,** 18, (25), 2909-2918.
15. Riess, G., Micellization of block copolymers. *Progress In Polymer Science* **2003,** 28, (7), 1107-1170.
16. Discher, D. E.; Eisenberg, A., Polymer vesicles. *Science* **2002,** 297, (5583), 967-973.
17. Giacomelli, C.; Schmidt, V.; Aissou, K.; Borsali, R., Block Copolymer Systems: From Single Chain to Self-Assembled Nanostructures. *Langmuir* **2010,** 26, (20), 15734-15744.
18. Bates, F. S., Polymer-Polymer Phase-Behavior. *Science* **1991,** 251, (4996), 898-905.
19. Lemarchand, C.; Gref, R.; Lesieur, S.; Hommel, H.; Vacher, B.; Besheer, A.; Maeder, K.; Couvreur, P., Physico-chemical characterization of polysaccharide-coated nanoparticles. *Journal of controlled Release* **2005,** 108, (1), 97-111.
20. Yamamoto, H.; Kuno, Y.; Sugimoto, S.; Takeuchi, H.; Kawashima, Y., Surface-modified PLGA nanosphere with chitosan improved pulmonary delivery of calcitonin by mucoadhesion and opening of the intercellular tight junctions. *Journal of controlled Release* **2005,** 102, (2), 373-381.

21. Sharon, N., History of lectins: from hemagglutinins to biological recognition molecules. *Glycobiology* **2004,** 14, (11), 53R-62R-53R-62R.

22. Kim, B. S.; Hong, D. J.; Bae, J.; Lee, M., Controlled self-assembly of carbohydrate conjugate rod-coil amphiphiles for supramolecular multivalent ligands. *Journal of the American Chemical Society* **2005,** 127, (46), 16333-16337.

23. Kim, B. S.; Yang, W. Y.; Ryu, J. H.; Yoo, Y. S.; Lee, M., Carbohydrate-coated nanocapsules from amphiphilic rod-coil molecule: binding to bacterial type 1 pili. *Chemical Communications* **2005**, (15), 2035-2037.

24. Kataoka, K.; Harada, A.; Nagasaki, Y., Block copolymer micelles for drug delivery: design, characterization and biological significance. *Advanced Drug Delivery Reviews* **2001,** 47, 113-131.

25. Kwon, G. S.; Kataoka, K., Block-Copolymer Micelles As Long-Circulating Drug Vehicles. *Advanced Drug Delivery Reviews* **1995,** 16, (2-3), 295-309.

26. Rosler, A.; Vandermeulen, G. W. M.; Klok, H. A., Advanced drug delivery devices via self-assembly of amphiphilic block copolymers. *Advanced Drug Delivery Reviews* **2001,** 53, (1), 95-108.

27. Chang, D. W.; Dai, L., Luminescent amphiphilic dendrimers with oligo(p-phenylene vinylene) core branches and oligo(ethylene oxide) terminal chains: syntheses and stimuli-responsive properties. *Journal of Materials Chemistry* **2007,** 17, (4), 364-364.

28. Ivory, D. M.; Miller, G. G.; Sowa, J. M.; Shacklette, L. W.; Chance, R. R.; Baughman, R. H., Highly conducting charge-transfer complexes of poly(p-phenylene). *The Journal of Chemical Physics* **1979,** 71, (3), 1506-1506.

29. Hargadon, M. T.; Davey, E. A.; McIntyre, T. B.; Gnanamgari, D.; Wynne, C. M.; Swift, R. C.; Zimbalist, J. R.; Fredericks, B. L.; Nicastro, A. J.; Goodson, F. E., Alternating Block Copolymers Consisting of Oligo(phenylene) and Oligo(ethylene glycol) Units of Defined Length: Synthesis, Thermal Characterization, and Light-Emitting Properties. *Macromolecules* **2008,** 41, (3), 741-750.

30. Sidorov, V.; Dzekunov, S. M.; Abdallah, D.; Ghebremariam, B.; Roepe, P. D.; Matile, S., Self-assembled single-chain oligo(p-phenylene) amphiphiles: reversed micelles, vesicles and gels. *Chemical Communications* **1999**, (15), 1429-1430.

31. Hong, D. J.; Lee, E.; Lee, J. K.; Zin, W. C.; Han, M.; Sim, E.; Lee, M., Stepped Strips from Self-Organization of Oligo(p-phenylene) Rods with Lateral Dendritic Chains. *Journal of the American Chemical Society* **2008,** 130, (44), 14448-+.

32. Garcia, F.; Fernandez, G.; Sanchez, L., Modulated Morphology in the Self-Organization of a Rectangular Amphiphile. *Chemistry-a European Journal* **2009,** 15, (27), 6740-6747.

33. Bae, J.; Choi, J. H.; Yoo, Y. S.; Oh, N. K.; Kim, B. S.; Lee, M., Helical nanofibers from aqueous self-assembly of an oligo(p-phenylene)-based molecular dumbbell. *Journal of the American Chemical Society* **2005,** 127, (27), 9668-9669.

34. Li, Y.; Li, G.; Wang, X.; Li, W.; Su, Z.; Zhang, Y.; Ju, Y., Unique Twisted Ribbons Generated by Self-Assembly of Oligo(p -phenylene ethylene) Bearing Dimeric Bile Acid Pendant Groups. *Chemistry - A European Journal* **2009,** 15, (26), 6399-6407.

35. Kolb, H. C.; Finn, M. G.; Sharpless, K. B., Click Chemistry: Diverse Chemical Function from a Few Good Reactions. *Angewandte Chemie International Edition* **2001,** 40, (11), 2004-2021.

36. Tornøe, C. W.; Christensen, C.; Meldal, M., Peptidotriazoles on Solid Phase: [1,2,3]-Triazoles by Regiospecific Copper(I)-Catalyzed 1,3-Dipolar Cycloadditions of Terminal Alkynes to Azides. *The Journal of Organic Chemistry* **2002,** 67, (9), 3057-3064.

37. Ma, D. L.; Shum, T. Y. T.; Zhang, F. Y.; Che, C. M.; Yang, M. S., Water soluble luminescent platinum terpyridine complexes with glycosylated acetylide and arylacetylide ligands: photoluminescent properties and cytotoxicities. *Chemical Communications* **2005**, (37), 4675-4677.

38. Mereyala, H. B.; Gurrala, S. R., A highly diastereoselective, practical synthesis of allyl, propargyl 2,3,4,6-tetra-O-acetyl-beta-D-gluco, beta-D-galactopyranosides and allyl, propargyl heptaacetyl-beta-D-lactosides. *Carbohydrate Research* **1998,** 307, (3-4), 351-354.

39. Berne, B.; Pecora, R., *Dynamic light scattering : with applications to chemistry, biology, and physics*. Dover Publications: Mineola N.Y., 2000.

40. Provencher, S. W., Inverse problems in polymer characterization - direct analysis of polydispersity with photon correlation spectroscopy *Makromolekulare Chemie-Macromolecular Chemistry and Physics* **1979,** 180, (1), 201-209.

41. Tammer, M.; Horsburgh, L.; Monkman, A. P.; Brown, W.; Burrows, H. D., Effect of chain rigidity and effective conjugation length on the structural and photophysical properties of pyridine-based luminescent polymers. *Advanced Functional Materials* **2002,** 12, (6-7), 447-454.

42. Giacomelli, C.; Schmidt, V.; Borsali, R., Nanocontainers formed by self-assembly of poly(ethylene oxide)-b-poly(glycerol monomethacrylate) - Drug conjugates. *Macromolecules* **2007,** 40, (6), 2148-2157.
43. Pedersen, J. S.; Gerstenberg, M. C., Scattering form factor of block copolymer micelles. *Macromolecules* **1996,** 29, (4), 1363-1365.
44. Choi, J. M.; Kim, Y.; Lee, M., Air side heat transfer coefficients of discrete plate finned-tube heat exchangers with large fin pitch. *Applied Thermal Engineering* **2010,** 30, (2-3), 174-180.
45. Bouzide, A.; LeBerre, N.; Sauve, G., Silver(I) oxide-mediated facile and practical sulfonylation of alcohols. *Tetrahedron Letters* **2001,** 42, (50), 8781-8783.
46. Dal Bó, A. G.; Soldi, V.; Giacomelli, F. C.; Jean, B.; Pignot-Paintrand, I.; Borsali, R.; Fort, S., Self-assembled carbohydrate-based micelles for lectin targeting. *Soft Matter* **2011**, 7, 3453-3461.
47. Zhang, L. F.; Eisenberg, A., Morphogenic effect of added ions on crew-cut aggregates of polystyrene-b-poly(acrylic acid) block copolymers in solutions. *Macromolecules* **1996,** 29, (27), 8805-8815.
48. Higgins, J. S.; Benoit, H. C., *Polymers and Neutron Scattering*. Clarendon Press: Oxford: 1994.
49. Burchard, W., Solubility and Solution Structure of Cellulose Derivatives. *Cellulose* **2003,** 10, (3), 213-225.

CHAPTER 5

CONCLUSION

In conclusion, new glycosylated amphiphilic systems have been prepared by click coupling of sugar residues onto azido-terminated PEG-tetra(*p*-phenylene) and azido-terminated PEG-aliphatic esters. DLS, TEM and SAXS techniques have been used to probe the self-assembling properties of the amphiphiles. These new block copolymer systems have been shown to self-assemble in water into well-defined nanoparticles whose size and morphology were intimately related to the hydrophobic volume fraction of the amphiphile. In particular, highly regular spherical micelles with a mean diameter of 10 nm were observed for the PEG_{900} glycoconjugates. The ability of the self-assembled nanoparticles to interact with specific carbohydrate lectin was also demonstrated by DLS confirming the potentiality of such micelles in medical applications such as diagnosis or drug delivery systems.

The results presented in the thesis are promising and further investigations will focus on the encapsulation properties of these amphiphilic systems as well as their biocompatibility and their ability to interact with cells.

List of Publications

Articles Published

1. Dal-Bó, A. G.; Soldi, V.; Giacomelli, F. C.; Bruno, J.; Pignot-Paintrand, I.; Borsali, R.; Fort, S. Self-assembled carbohydrate-based micelles for lectin targeting. Soft Matter, **2011**, 7, 3453-3461.

2. Dal-Bó, A. G.; Laus, R; Felippe, A. C.; Zanette, D.; Minatti, E. Association of anionic surfactant mixed micelles with hydrophobically modified ethyl(hydroxyethyl)cellulose. Colloids and Surfaces. A, Physicochemical and Engineering Aspects. accepted 2011, doi:10.1016/j.colsurfa.2011.02.028.

3. Dal-Bó, A. G.; Laus, R.; Minatti, E. Self-Association of Sodium Dodecanoate (SDoD) And Sodium Decanoate (SDeC) with the Hydrophobically Modified Polymer Ethyl(hydroxyethyl)Cellulose (EHEC). Química Nova (Impresso) accepted, 2011.

4. Modolon, S. M.; Dal-Bó, A. G.; Felippe, A. C.; Minatti, E.; Zanette, D. Self-association of sodium dodecyl sulfate (SDS) with the hydrophobically modified polymer ethyl (hydroxyethyl) cellulose (EHEC). Química Nova (Impresso), v. 32, p. 2046-2050, 2009.

5. Eising, R.; Dal-Bó, A. G.; Felippe, A. C.; Bellettini, I.; MoréS, S.; Zanette, D. Mixed micelles formation between bile salt sodium cholate and the anionic surfactant sodium dodecanoate. Química Nova (Impresso), v. 31, p. 2065-2070, 2008.

6. Felippe, A. C; Dal-Bó, A. G.; Schweitzer, B.; Zanette, D.; Minatti, E. . Self-Association of Sodium Cholate with Poly(ethylene oxide) Cooperatively Induced by Sodium Dodecyl Sulfate. Colloids and Surfaces. A, Physicochemical and Engineering Aspects, v. 294, p. 247-253, 2007.

7. Felipe, A. C.; Dal-Bó, A. G A. Lopes ; Schweitzer, B.; Zanette, D.The Absence of Cooperative Binding of Sodium Cholate to Poly(ethylene oxide) Evaluated by Surface Tension, Electrical Conductivity and Fluorescence Measurements (aceito para publicação)..

Colloids and Surfaces. A, Physicochemical and Engineering Aspects (Print), v. 279, p. 87-95, 2006.

8. Schweitzer, B.; Felippe, A. C.; Dal-Bó, A. G; Minatti, E.; Zanette, D. Sodium Dodecyl Sulfate Promoting a Cooperative Association Process of Sodium Cholate on the Bovine Serum Albumin(aceito). Journal of Colloid and Interface Science, v. 298, p. 457-466, 2006.

9. Dal-Bó, A. G.; Felippe, A. C.; Schweitzer, B.; Lindman, B.; Zanette, D. . Ethyl(hydroxyethyl)cellulose-Sodium Dodecanoate Interaction Investigated by Surface Tension and Electrical Conductivity Techniques In;. Colloids and Surfaces. A, Physicochemical and Engineering Aspects, v. 256, p. 171-180, 2005.

10. Felippe, A. C.; Dal-Bó, A. G.; Schweitzer, B.; Zanette, D. Competitive Process of Binding between the Anionic Surfactants Sodium Dodecyl Sulfate and Bile Salts on the Bovine Serum Albumin. Macromolecular Symposia, v. 229, p. 208-216, 2005.

To be submitted

Dal-Bó, A. G.; Soldi, V.; Giacomelli, F. C.; Bruno, J.; Pignot-Paintrand, I.; Borsali, R.; Fort, S. Synthesis and self-assembly of carbohydrate-clicked rod-coil amphiphiles. Langmuir, in prep. 2011.